Theory of electron transport through molecular-scale nanostructures

Ghazwan Eid Alshammari

PhD Thesis in Physics

Department of Physics, Lancaster University, UK

This Thesis is submitted in partial fulfilment of the requirements for degree of Doctor of Philosophy

2025

Declaration

This thesis has not been submitted to support an application for another degree at this or any other university. This thesis documents work carried out between April 2021 and January 2025 at Lancaster University UK, under the supervision of Prof. Colin J. Lambert, funded by the Ministry of Education Saudi Arabia and Aljouf University, KSA

Ghazwan Alshammari

January 2025

Acknowledgment

My great thanks to ALLAH for his mercy and blessing. I could not have achieved what I have done without ALLAH.

I would like to express my deepest gratitude to Prof. Colin John Lambert for the excellent supervision and guidance I received. This thesis would never completed without his enormous support and excellent guidance.

I would also like to express my grateful admiration to Dr Songjun Hou, none of this work would have been accomplished without his insightful comments and suggestions, dedicated time, and guidance.

I would like also to thank my sponsor, the Ministry of Education-KSA, and my University in Saudi Arabia Aljouf University, for giving me this great opportunity to study for a Ph.D. in the United Kingdom

Also, many thanks to the theory of molecular-scale groups and the collaborating experimental groups. I would like to thank all my friends and colleagues in Colin's group

I would like to thank my dear family: my parents, sister, and brothers for showing their constant care, love, and support. I also express my deepest gratitude to my supportive wife and my daughter Raghad for giving me courage and hope throughout my studies.

Abstract

Molecular electronics is a useful method for exploring nanoscale and discovering new organic materials that are both low-cost and environmentally friendly. This thesis presents the theoretical methods employed to support this process, starting in chapters 2 and 3, accordingly. I have discussed the fundamental equations and methods that underpin my work, such as the Schrodinger equation, density functional theory (DFT), and the SIESTA program, which is responsible for implementing DFT and solving the equations that are underlying it. In addition, I present an explanation of the single particle transport theory, which is based on the Hamiltonian and Green's functions, as well as some examples of how it might be used.

Chapter 4. This chapter mainly discusses the influence of heteroatom including which position will alleviate destructive quantum interference (DQI), and which position will not. In addition, if we change linkers, the influence of heteroatom will change. These results are supported by my calculations.

Chapter 5. This chapter discusses the transport properties of stable organic radicals for electronic devices due to their half-filled orbitals near the Fermi energy. Also, see the systematic changes when we remove the hydrogen from the OH groups to produce the radicals, and how that affects the electrical conductance.

List of Publications

1. **Quantum Interference in Molecules (In preparation)**

2. **Single-Molecule Conductance Enhancement in a Stable Diradical (In preparation)**

Contents

Chapter 1 ……..**9**

Molecular Electronics……..…….**9**

1.1 Introduction……..….**9**

1.2 Thesis Outline ……....**12**

1.3 Bibliography ……..**14**

Chapter 2 ……...**19**

Theory of Density Functional ……....**19**

2.1 introduction ……....**19**

2.2 The Principle of Variation and the Schrödinger Equation …….....**20**

2.3 The Theorems of Hohenberg-Kohn ……...**25**

2.4 The Theorems of Kohn-Sham …….....**27**

2.5 The Exchange Correlation Functions ……**28**

2.5.1 LDA (local density approximation) ……....**29**

2.5.2 Generalized Gradient Approximation (GGA) ……....**29**

2.6 Pseudoptentials …… ..**30**

2.7 Basis Sets …….....**31**

2.8 Summary …….....**33**

2.9 Bibliography ……...**34**

Chapter 3 ……38

Phase Coherent Electron transport…….....38

3.1 Introduction ……38

3.2 The Landauer Formula …….....38

3.3 The Theory of Scattering in One Dimension…….....41

3.3.1 Perfect One-Dimensional lattice ……42

3.3.2 Scattering in One Dimension…….....46

3.4 Generalization of the Scattering Formalism …….....50

3.4.1 Green's Function of the Leads and Hamiltonian……50

3.5 Summary ……61

3.6 Bibliography ……...62

Chapter 4……64

Quantum interference in molecules…….....64

4.1 Introduction…….....64

4.2 Tight binding calculation and DFTcalculation…..65

4.3 Examples of conjugate π *z* systems……68

4.4 An example of connectivity table (C) and the magic number theory table (M)

of benzene ring…….....69

4.5 The effect of introducing a single heteroatom……71

4.6 Studied Molecules……...73

4.7 Transmission coefficient……74

4.8 Transmission coefficients for the benzene with different linkers connected to gold

electrodes and an increasing number of central rings (naphthalene and anthracene) and the tight binding model results **……...74**

4.9 Wave functions for meta, metaN1, metaN2 and metaN3 with anchor groups of the benzene ring**……....77**

4.10 Examples of conjugated π_Z and π_Y systems**……...81**

4.11 Wave functions for meta, metaN1, metaN2 and metaN3 with triple bombs of the benzene ring**……82**

4.12 An example of connectivity table (C) and the magic number theory table (M) of naphthalene rings**……85**

4.13 Wave functions for meta, metaN1, metaN2 and metaN3 with anchor groups of naphthalene **……88**

4.14 Wave functions for meta, metaN1, metaN2 and metaN3 with triple bombs of naphthalene **……...91**

4.15 Wave functions for meta, metaN1 and metaN2 with triple bombs of anthracene**……..95**

4.16 Summary**…….....97**

4.17 Bibliography **…….....98**

Chapter 5……..99

Single-Molecule Conductance Enhancement in a Stable Diradical**……..99**

5.1 Introduction**……..…...99**

5.2 Studied molecules **……100**

5. 3 Results and discussion**……..101**

5.3.1 CQI case ……..101

5.3.2 DQI 1 case ……105

5.3.3 DQI 2 case ……109

5.4 Summary ……...114

5.5 References ……115

Chapter 6……117

Conclusion and Future Work……117

6.1 Conclusion……117

6.2. Future work……..118

Appendices ……119

Appendix 1: Correction for Basis Set Superposition Error (BSSE) and Counterpoise Correction (CP)……119

Appendix 2: The coefficients of thermoelectricity S……...121

Chapter 1

Molecular Electronics

1.1 Introduction

As shown in Figure 1, electronic components, such as semiconductors, have become smaller and smaller at an exponential rate, according to a historical tendency that Gordon Moore predicted in 1965. A great number of investigations have been carried out to discover ways that can continue this historical trend, and these investigations are now approaching the nano- or molecular scale [1]. At the nanoscale, a range of device concepts have been proposed, and used to demonstrate fundamental phenomena associated with electron transport, including nanoscale superconducting devices [2-4], devices based on carbon nanotubes [5-7], and sensors based on nanopores in graphene [8-12] or silicene [13]. Many of these concepts carry over to molecular-scale structures.

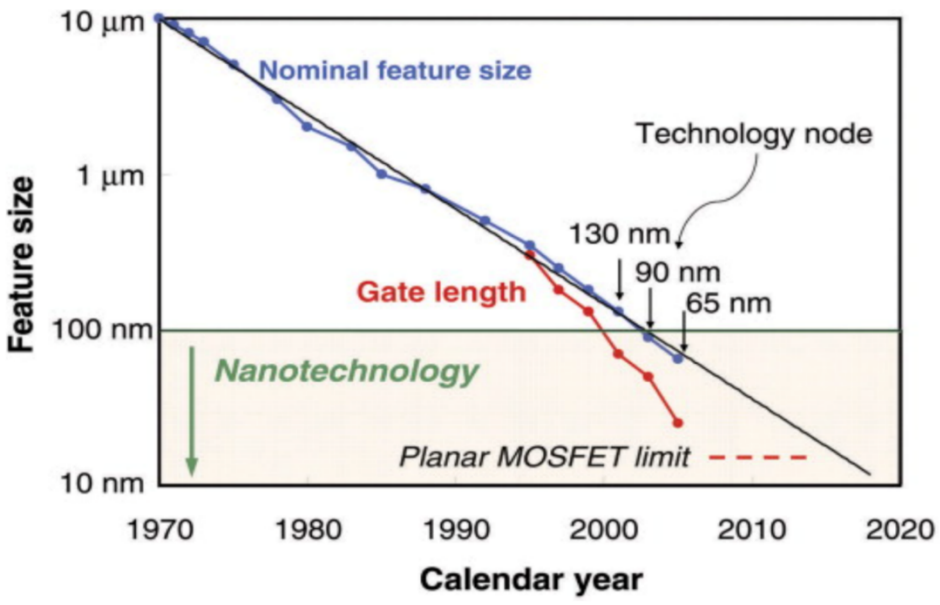

Figure 1.1: This chart shows that the size of a transistor on a silicon chip has decreased steadily, indeed exponentially with time according to Moore's law[1].

Molecular electronics (ME) is the field of science that analyses the electrical and thermal transport properties of circuits constructed with individual molecules (or groups of them) as their fundamental components. In 1974, Aviram and Ratner provided the initial concept for the molecular current rectifier [14]. Since that time, a range of single-molecule electrical devices have been proposed as transistors [15], rectifiers [16,17] and switches [18, 19] and a variety of methods for controlling electron transport through molecules have been proposed, including controlling their molecular conformation [20], controlling their orientation within a junction [21] and controlling their frontier-orbital energy levels relative to the Fermi energy of electrodes [22].

The right of Figure 1.2 shows the anatomy of a single-molecule junction and helps to conceptualise how electron transport can be controlled, by varying the anchor groups, varying the molecular core, attaching pendant groups to the core and varying the linkages to anchor groups. In contrast with the 1974 work of Aviram and Ratner [14], which assumed that electron transport through single molecules takes place in an incoherent manner, one of the great discoveries during the past decade or so is that electron transport through single molecules can remain phase coherent, even at room temperature. This phase coherence means that a range of quantum interference effects are possible and that these can be used to control the electrical and thermal transport properties of molecular junctions. Manifestations of such interference effects include conductance oscillations in atomic wires [23] and Seebeck oscillations in π-stacked molecular junctions [24]. In addition, since molecules can be attached to electrodes via anchor groups, and the anchor groups can be connected to a molecular core with atomic accuracy, a range of connectivity-dependent quantum interference (QI) effects can be observed [25-27]. This ability to control connectivity to electrodes is illustrated on the left of Figure 1.2, where the triple

bonds are anchored to gold electrodes and connect to the pyrene molecular core at specific atomic sites.

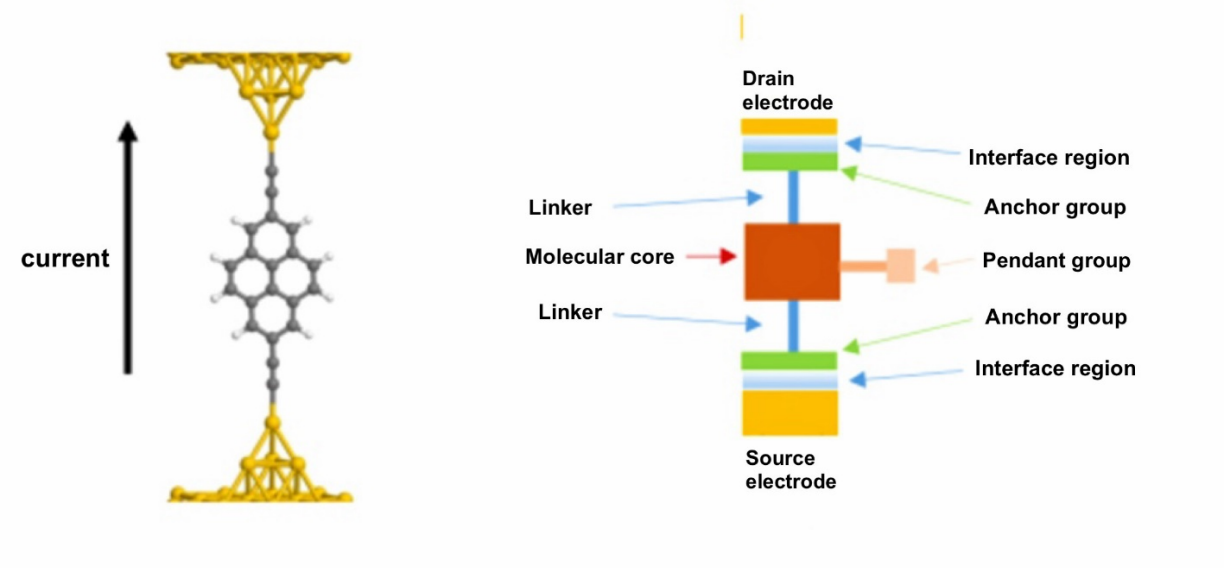

Figure 1.2: This figure illustrates a molecular junction on the left side. It consists of a molecule that is attached by two electrodes. On the right side, it illustrates the physicist's concept of a molecular junction.

In the molecule on the left in Figure 1.2, the molecule is anchored to the electrodes via direct carbon-gold bonds. Many other anchor groups have been tested in the literature and correlations between the binding energy of the anchor to the electrodes and the magnitude of the electrical conductance have been demonstrated [28,29]. Gold is the most commonly used electrode material, but since it is not complementary metal-oxide semiconductor CMOS compatible other electrodes materials such as graphene [30-32] have also been explored.

Remarkably, many of the quantum interference effects discovered in single-molecule junctions have been shown to persist in materials formed from self-assembled molecular layers [33,34]. This is important, because if organic molecules are to be utilised in scalable devices, such as

cross-bar architectures, the finite cross-section electrodes will inevitably make contact to a film of many molecules in parallel.

To close this introduction, it is also worth noting that the above interference effects derive from the wave nature of electrons passing through a molecule from one electrode to another. Since heat is mediated by vibrational waves and minimisation of thermal conductance is highly desirable for thermoelectric applications, it is of interest to determine f phonon interference effects can be used to control thermal conductance. This question has been explored by adapting techniques originally developed to model lattice dynamics is nanostructures [35] to model phonon transport through single-molecule junctions [36,37].

1.2 Thesis Outline

The aim of this thesis is to explore some of the above concepts using the equilibrium Green's function formalism of transportation theory, which is implemented by combining the Gollum quantum transport code [22], with the density functional theory (DFT), code SIESTA code [23].

Chapter 2 provides a brief description of density functional theory (DFT), for studying and understanding the electrical properties of single-molecule junctions. The theory of single-electron quantum transport is described in Chapter 3. This chapter discusses the Landauer formula, Green's functions for different types of transport regimes, scattering theory and methods for calculating transmission coefficients for different systems using the Hamiltonian and Green's functions. Two original theory projects are presented in chapters 4 and 5. In chapter 4, I studied charge transport through molecular cores connected to electrodes by linkers with conjugated π systems are formed from both π_z and π_y orbitals. I found that DQI dips in transport though the π_z

system can be hidden, because the π_y orbitals of the linkers can couple to the sigma system of the core and create a parallel conductance channel. Although this channel makes only a small contribution, it becomes dominate when DQI suppresses transport through the π_z system. This mechanism was demonstrated by increasing the size of the core from benzene to naphthalene and then anthracene, which successively suppresses transport through the sigma system and for the largest core allows the DQI transport dips to become visible. This points to an important design principle for future molecular electronic devices, since if one plans to use DQI to control transport through molecules, it would be wise to avoid links with more than one π system.

In chapter 5 I explore molecular junctions containing stable organic radicals, which have half-filled orbitals at the Fermi energy, making them promising candidates for electrical devices. Due to the possibility that all-organic conjugated radical species with unpaired electrons would give rise to new quantum phenomena, these species have generated a great deal of interest in single-molecule electronics research. To explore whether organic radicals can improve electrical conductivity I investigate the effects of diradicals on the charge transport of different systems exhibiting either constructive quantum interference or destructive quantum interference. In both cases, I find that the presence of diradical causes and increase in electrical conductance.

1.3 Bibliography

[1] R. Reichardt, Moore's Law and the Pace of Change, Internet Reference Services Quarterly, 11 117-124 (2006).

[2] Theory of Andreev resonances in quantum dots. NR Claughton, M Leadbeater, CJ Lambert, Journal of Physics: Condensed Matter 7 (46), 8757 (1995)

[3] Quantum Interference from superconducting islands in a mesoscopic solid. CJ Lambert J. Phys. Condens. Matter 5, 707 (1993)

[4] Boundary conditions for quasiclassical equations in the theory of superconductivity. CJ Lambert, R Raimondi, V Sweeney, AF Volkov, Physical Review B 55 (9), 6015 (1997)

[5] Single- and multi-wall carbon nanotube field-effect transistors. R. Martel, T. Schmidt, H. R. Shea, T. Hertel, and Ph. Avouris,, Applied Physics Letters, 73, (17), 2447–2449, (1998)

[6] Electron transport in carbon nanotube shuttles and telescopes. IM Grace, SW Bailey, CJ Lambert, Physical Review B—Condensed Matter and Materials Physics 70 (15), 153405 (2004)

[7] Tuning the electrical conductivity of nanotube-encapsulated metallocene wires. VM García-Suárez, J Ferrer, CJ Lambert, Physical review letters 96 (10), 106804 (2006)

[8] Stable and robust discriminative sensing of illicit drug molecules utilizing a specific geometry of nanotubes. LA Algharagholy, VM García-Suárez, HA Dhahi, Nano-Structures & Nano-Objects 39, 101281 (2024)

[9] Selective Sensing of DNA Nucleobases with Angular Discrimination. LA Algharagholy, VM García-Suárez, SS Abaas, ACS omega 9 (3), 3240-3249 (2024)

[10], Robust nanotube-based nanosensor designed for the detection of explosive molecules. LA Algharagholy, VM García-Suárez, KH Bardan Nanoscale Advances 6 (14), 3553-3565 (2024)

[11] Effects of antidots on the transport properties of graphene nanoribbons. XH Zheng, GR Zhang, Z Zeng, VM García-Suárez, CJ Lambert, Physical Review B—Condensed Matter and Materials Physics 80 (7), 075413 (2009)

[12] Graphene sculpturene nanopores for DNA nucleobase sensing. H Sadeghi, L Algharagholy, T Pope, S Bailey, D Visontai, D Manrique, J Ferrer, V Garcia-Suarez, S Sangtarash, C J Lambert, The Journal of Physical Chemistry B 118 (24), 6908-6914 (2024)

[13] Silicene-based DNA nucleobase sensing. H Sadeghi, S Bailey, CJ Lambert, Applied Physics Letters 104 (10) (2014)

[14] Molecular rectifiers. A. Aviram and M. Ratner, Chemical Physics Letters 29, 2, 15 277-283 (1974)

[15] Single-molecule transistors. M. L. Perrin, E. Burzurí, and H. S. J. van der Zant, Chem. Soc. Rev., 44 (4) 902 (2015)

[16] High degree of current rectification at nanoscale level, M. Saha and S. K. Maiti, Physica E: Low-dimensional Systems and Nanostructures, 93. 275 (2017).

[17] Tuning rectification in single-molecular diodes. Batra, A., Darancet, P., Chen, Q., Meisner, J. S., Widawsky, J. R., Neaton, J. B., … Venkataraman, L. Nano Letters, 13 (12), 6233 (2013).

[18] Charge transport through molecular switches. S. Jan Van Der Molen and P. Liljeroth, J. Phys.: Condens. Matter, 22, (13) 133001 (2010)

[19] Assembly, structure and thermoelectric properties of 1,1′-dialkynylferrocene ‘hinges.’ Wilkinson, L. A., Bennett, T. L., Grace, I. M., Hamill, J., Wang, X., Au-Yong, S., … Long, N. J. Chemical Science, 13(28), 8380–8387 (2022).

[20] Conformation dependence of molecular conductance: chemistry versus geometry. CM Finch, S Sirichantaropass, SW Bailey, IM Grace, VM Garcia-Suarez, C. J. Lambert, Journal of Physics: Condensed Matter 20 (2), 022203 (2007)

[21] Orientation-controlled single-molecule junctions. S. Afsari, Z. Li, and E. Borguet, Angew Chem Int Ed Engl, 53 (37), 9771 (2014)

[22] Charge transfer complexation boosts molecular conductance through Fermi level pinning. Kun Wang, Andrea Vezzoli, Iain M. Grace, Maeve McLaughlin, Richard J. Nichols, Bingqian Xu, Colin J. Lambert and Simon J. Higgins, Chem. Sci. 10 2396 (2019)

[23] Conductance oscillations in zigzag platinum chains. VM García-Suárez, AR Rocha, SW Bailey, CJ Lambert, S Sanvito, J Ferrer, Physical Review Letters 95 (25), 256804 (2005)

[24] Oscillating Seebeck coefficient in π-stacked molecular junctions. Mohsin K. Al-Khaykanee, Iain Grace and Colin Lambert, RSC Advances 8 (44), 24711-24715 (2018)

[25] Quantum Transport in Nanostructures and Molecules. An introduction to molecular electronics. Colin J. Lambert, IoP Publishing (2021)

[26] Signatures of room-temperature quantum interference in molecular junctions. Shi-Xia Liu, Ali Ismael, Alaa Al-Jobory, Colin J. Lambert, Accounts of Chemical Research 322-331 (2023)

[27] Heteroatom-induced molecular asymmetry tunes quantum interference in charge transport through single-molecule junctions. Y Yang, M Gantenbein, A Alqorashi, J Wei, S Sangtarash, D Hu, H Sadeghi, R Zhang, J Pi, L Chen, X Huang, R Li, J Liu, J Shi, W Hong, C J Lambert, M R Bryce, The Journal of Physical Chemistry C 122 (26), 14965-14970 (2018)

[28] K Yoshida, IV Pobelov, DZ Manrique, T Pope, G Mészáros, M Gulcur, MR Bryce, CJ Lambert, T Wandlowski, Correlation of breaking forces, conductances and geometries of molecular junctions. Scientific reports 5 (1), 9002 (2015)

[29] Single-Molecule Conductance Studies of Organometallic Complexes Bearing 3-Thienyl Contacting Groups. S Bock, OA Al-Owaedi, SG Eaves, DC Milan, M Lemmer, BW Skelton, H M Osorio, R J Nichols, S J Higgins, P Cea, N J Long, T Albrecht, S Martín, C J Lambert, P J Low, Chemistry–A European Journal 23 (9), 2133-2143 (2017)

[30] Robust graphene-based molecular devices. M El Abbassi, S Sangtarash, X Liu, ML Perrin, O Braun, C Lambert, H Sjoerd, J van der Zant, S Yitzchaik, S Decurtins, S-X Liu, H Sadeghi, M Calame, Nature nanotechnology 14 (10), 957-961 (2019)

[31] Controlled quantum dot formation in atomically engineered graphene nanoribbon field-effect transistors. M El Abbassi, ML Perrin, GB Barin, S Sangtarash, J Overbeck, O Braun, C J Lambert, Q Sun, T Prechtl, A Narita, K Müllen, P Ruffieux, H Sadeghi, R Fasel, M Calame, ACS nano 14 (5), 5754-5762 (2020)

[32] Planar aromatic anchors control the electrical conductance of gold-molecule-graphene junctions.Luke J. O'Driscoll, Michael Jay, Benjamin J. Robinson, Hatef Sadeghi, Xintai Wang, Martin R. Bryce, and Colin J. Lambert, Nanoscale Advances 5 2299-2306 (2023)

[33] Self-assembled molecular-electronic films controlled by room temperature quantum interference. M Famili, C Jia, X Liu, P Wang, IM Grace, J Guo, Y Liu, Z Feng, Y Wang, Z Zhao, S Decurtins, R Häner, Y Huang, S-X Liu, C J Lambert, X Duan, Chem 5 (2), 474-484 (2019)

[34] Scale-up of room-temperature constructive quantum interference from single molecules to self-assembled molecular-electronic films. X Wang, TLR Bennett, A Ismael, LA Wilkinson, J

Hamill, AJP White, I M Grace, O V Kolosov, T Albrecht, B J Robinson, N J Long, LF Cohen, J Lambert, Journal of the American Chemical Society 142 (19), 8555-8560 (2020)

[35] Lattice dynamics of a disordered solid-solid interface. G Fagas, AG Kozorezov, CJ Lambert, JK Wigmore, A Peacock, A Poelaert, R Den Hartog, Physical review b 60 (9), 6459 (1999)

[36] Thermal transport through single-molecule junctions. N Mosso, H Sadeghi, A Gemma, S Sangtarash, U Drechsler, CJ Lambert, B. Gotsmann, Nano letters 19 (11), 7614-7622 (2019)

[37] Suppression of phonon transport in molecular Christmas trees. M Famili, I Grace, H Sadeghi and CJ Lambert, ChemPhysChem 18 1234-1241 (2017)

[38] GOLLUM: a next-generation simulation tool for electron, thermal and spin transport, Ferrer, J.; Lambert, C. J.; García-Suárez, V. M.; Manrique, D. Z.; Visontai, D.; Oroszlany, L.; Rodríguez-Ferradás, R.; Grace, I.; Bailey, S. W. D.; Gillemot, K.; Sadeghi, K. H.; Algharagholy, L. A., New Journal of Physics 16 093029-093095 (2014)

[39] The SIESTA method for ab initio order-N materials simulation. M. Soler., Artacho, E., Gale, J. D., García, A., Junquera, J., Ordejón, P., & Sánchez-Portal, D, J. Phys.: Condens. Matter, 14 (11) 2745, (2002)

Chapter 2

Density Functional Theory

This chapter introduces the density functional theory (DFT) and the SIESTA code, which are used in this thesis's electronic structure computations. The first step in finding the molecule's electron transport properties is to generate a mean-field Hamiltonian using DFT.

2.1 Introduction

Molecular electronic device behaviour can be explained with the use of a reliable source of electronic and structural data. I will provide a brief overview of density functional theory (DFT) and the SIESTA (Spanish Initiative for Electronic Simulations with Thousands of Atoms) code [1] in this chapter. During my PhD studies, I made extensive use of DFT as a theoretical tool to investigate the architectures of molecules, charge densities, and band structures in both qualitative and quantitative ways. SIESTA is a set of algorithms and a fully functional programme designed to expedite DFT computations on many atoms in a few hours, days, or weeks. DFT is based on the fundamental idea that the ground state density of a complex system, which is made up of several interacting particles, may be used to describe every physical property of the system. In 1964, Hohenberg and Kohn [2] provided the first evidence for the existence of such a function. On the other hand, the proof gives us no information on the functional's shape. But applications for realistic physical systems were possible due to an ansatz, presented by Kohn and Sham [3]. Since then, DFT has been a widely used method in molecular chemistry and theoretical physics. An introduction to DFT's concepts and all of its numerical applications will be provided in this chapter. The literature covers the subject in great detail and covers a wide range of topics [4-7]. I will start by summarizing the several different approaches

to the many-body problem. I will then show the Hohenberg-Kohn theorems and the Hartree-Fock technique. Finally, I will show the Kohn-Sham ansatz. Then, I distil the most popular functional forms, which are essential for practical numerical analysis. In this thesis, I also provide special attention to localised basis sets, pseudo-atomic orbits that define the number space of the Hilbert calculations, Basis Set Superposition Error Correction (BSSE), and Counterpoise Correction (CP).

2.2 The Principle of Variation and the Schrödinger Equation

Any nonrelativistic multi-particle system can be described by the time-independent, non-relativistic Schrödinger equation:

$$\mathrm{H}\psi_i(\vec{r}_1, \vec{r}_2, \dots, \vec{r}_N, \vec{R}_1, \vec{R}_2, \dots, \vec{R}_M = E_i\psi_i(\vec{r}_1, \vec{r}_2, \dots, \vec{r}_N, \vec{R}_1, \vec{R}_2, \dots, \vec{R}_M) \quad (2.1)$$

where E_i is the numerical value of the energy of the state represented by $\psi_i$and ψ_i is the wavefunction of the system's i^{th}state. This is the Hamiltonian operator of a system made up of M and N nuclei and electrons, which describes how particles interact with one another. For such a system, the Hamiltonian operator can be given as the sum of the five terms [2, 3, 8–12]:

$$= \overbrace{-\frac{\hbar^2}{2m_e}\sum_{i=1}^{N}\nabla_i^2}^{T_e} \overbrace{-\frac{\hbar^2}{2m_n}\sum_{n=1}^{M}\nabla_n^2}^{T_n} \overbrace{-\frac{1}{4\pi\varepsilon_o}\sum_{i=1}^{N}\sum_{n=1}^{M}\frac{1}{\left|\vec{r}_i-\vec{R}_n\right|}Z_n e^2}^{U_{en}}$$

$$+\frac{1}{8\pi\varepsilon_o}\overbrace{\sum_{i=1}^{N}\sum_{i\neq j}^{N}\frac{e^2}{\left|\vec{r}_i-\vec{r}_j\right|}}^{U_{ee}} + \overbrace{\frac{1}{8\pi\varepsilon_o}\sum_{n=1}^{M}\sum_{n\neq n'}^{M}\frac{Z_n Z_{n'} e^2}{\left|\vec{R}_n-\vec{R}_{n'}\right|}}^{U_{nn}} \quad (2.2)$$

Where n and ń run over the M-nuclei in the system, while i and j represent the N-electrons; e and Ze represent the electron and nuclear charge, respectively; and m_e and m_n are the masses of the electron and nucleus, respectively. $\vec{r_i}$ and $\vec{R}_n$, respectively, represent the positions of the electrons and nuclei, while ∇^2 is the Laplacian operator, which has the following definition in Cartesian coordinates:

$$\nabla_i^2 = \frac{\partial^2}{\partial x_i^2} + \frac{\partial^2}{\partial y_i^2} + \frac{\partial^2}{\partial z_i^2}$$

The kinetic energy of the system's nuclei is indicated by the term T_n whereas the kinetic energy of the electrons is represented by the term T_e as shown in equation (2.2). The term U_{en}denotes the attractive electrostatic interaction between nuclei and electrons in the system; the remaining three terms additionally define the potential part of the Hamiltonian. Accordingly, the repulsive parts of the potential are the electron-electron (U_{ee}) and nuclear-nuclear (U_{nn}) [1, 3, 4, 9, 11].

The nucleus of an atom contains around 99.9% of its mass, hence the Born-Oppenheimer approximation, often referred to as the clamped nuclei approximation, can be used in the analysis since the nuclei in the system can be thought of as fixed about the electrons. This suggests, for example, that the mass concentration of a hydrogen atom is indicated by the fact that the nucleus weighs approximately 1800 times more than the electron. The resulting kinetic energy accumulates to zero if the treated atoms' nuclei are kept stable, suggesting that they are no longer contributing to the entire wave function. Due to the previous assumption, the Hamiltonian expression for the electron system reduces the Hamiltonian to a different figure; as well, the electronic Hamiltonian H_{ele}, which in a constant nuclear representation may very well be given by [3, 4, 9, 11]:

$$\mathrm{H}_{ele} = \overbrace{-\frac{\hbar^2}{2m_e}\sum_{i=1}^{N}\nabla_i^2}^{T_e} - \overbrace{\frac{1}{4\pi\varepsilon_o}\sum_{i=1}^{N}\sum_{n=1}^{M}\frac{1}{|\vec{r}_i-\vec{R}_n|}Z_n e^2}^{U_{en}}$$

$$+\overbrace{\frac{1}{4\pi\varepsilon_o}\frac{1}{2}\sum_{i=1}^{N}\sum_{i\neq j}^{N}\frac{e^2}{|\vec{r}_i-\vec{r}_j|}}^{U_{ee}}+$$

$$\overbrace{\frac{1}{4\pi\varepsilon_o}\frac{1}{2}\sum_{i=1}^{M}\sum_{n\neq n'}^{M}\frac{Z_n Z_{n'} e^2}{|\vec{R}_n-\vec{R}_{n'}|}}^{U_{nn}} \qquad (2.3)$$

Where, U_{nn} is the system's obtained constant. The following represents the Schrödinger equation for 'clamped nuclei':

$$\mathrm{H}_{ele}\psi_{ele} = E_{ele}\psi_{ele} \qquad (2.4)$$

Whereas the nuclear component enters only dimensionally and is not clearly visible in ψ_{ele} and ψ_{ele} depends on the electron coordinates for the system.

Total energy E_{total} is defined as the sum of E_{ele}ele and the system's constant nuclear repulsion term, which is written the following:

$$E_{total} = E_{ele} + U_{nn} \qquad (2.5)$$

The wave-function of a system is not measurable; its squared modulus can be expressed as following:

$$|\psi(\vec{r}_1, \vec{r}_2, \dots, \vec{r}_N)|^2 d\vec{r}_1\, d\vec{r}_2 \dots d\vec{r}_N \tag{2.6}$$

The probability that electrons 1, 2…, N are found in the volume elements $d\vec{r}_1\, d\vec{r}_2 \dots\dots d\vec{r}_N$, is represented by the above expression. This is because electrons are indistinguishable, and this probability remains unchanged even if the coordinates of any two electrons (i and j) are switched [15]:

$$\left|\psi(\vec{r}_1, \vec{r}_2, \dots \vec{r}_i, \vec{r}_j, \dots, \vec{r}_N)\right|^2 = \left|\psi(\vec{r}_1, \vec{r}_2, \dots \vec{r}_j, \vec{r}_i, \dots, \vec{r}_N)\right|^2 \tag{2.7}$$

The value of ψ in any pair of electrons must be anti-symmetric with respect to the interchange of the spatial and spin coordinates as well since electrons are fermions with half-spins:

$$\psi(\vec{r}_1, \vec{r}_2, \dots \vec{r}_i, \vec{r}_j, \dots, \vec{r}_N) = -\psi(\vec{r}_1, \vec{r}_2, \dots \vec{r}_i, \vec{r}_j, \dots, \vec{r}_N) \tag{2.8}$$

The logical result of the wave-functions probability interpretation format is that the integral of equation 2.6 over the whole range of all variables provides a value of one. This means that the chance of discovering an N-electron at any point in space must be exactly one,

$$\int \dots \int |\psi(\vec{r}_1, \vec{r}_2, \dots, \vec{r}_N)|^2\, d\vec{r}_1\, d\vec{r}_2 \dots d\vec{r}_N = 1 \tag{2.9}$$

A normalized wave-function meets the conditions given in equation (2.9).

Several theories, including Hartree and Hartree-Fock, have been developed to achieve this objective as the Schrödinger wave equation needs an exact solution. An important theoretical idea known as the variational principle of the wave function served as the foundation for many of these theories. It instructs analysts on how to find answers by using suitable trial wave-functions ψ_{Tri} [11]. The previous principle is useful in studying the ground state; however, it is not very useful in studying excited states. When a system is in the state ψ_{Tri}, the following expression represents the energy's expected value:

$$\langle E_{Tri} \rangle = \frac{\int \psi_{Tri} \mathrm{H}\, \psi^*_{Tri}\, d\vec{r}}{\int \psi_{Tri}\, \psi^*_{Tri}\, d\vec{r}} \tag{2.10}$$

Equation 2.10, which presents the variational principle, suggests that the energy can be computed as the expectation value of the Hamiltonian operator from any ψ_{Tri} , which represents an upper bound on the true ground-state energy ψ_{GS}. Assume that ψ_{Tri} is normalised using equation 2.9, and that ψ_{Tri} then equals to the ground state ($\psi_{\mathrm{Tri}} = \psi_{\mathrm{GS}}$). This means that entity E_{Tri} is equal to the exact ground state energy E_{GS}, also, we can rewrite equation 2.10 for the ground state as the following:

$$\langle E_{GS} \rangle = \int \psi_{GS}\, \mathrm{H}\, \psi^*_{GS}\, d\vec{r} \tag{2.11}$$

We can see from the normalized ψ_{Tri} that $E_{Tri} > E_{GS}$ or $E_{Tri} = E_{GS}$.The best option for $E_{Tri}$is this means the one in which E_{Tri} gets reduced [3].

2.3 The Theorems of Hohenberg-Kohn

The ground state energy and the density, ρ(r), of an interacting electron system are related, as P. Hohenberg and W. Kohn showed in 1964 [2]. The Hohenberg-Kohn theorems consist of two simple but important statements:

a) V_{ext} the exterior potential, is a functional (r) that is particular to density. V_{ext}fixes the Hamiltonian (H) of the system, so the full many-body ground state is a unique functional of ρ(r).

b) A ground state density of ρ(r) is the ground state, given by E_{HK}.

It is a simple matter of reduction ad absurdum to demonstrate the validity of the first theorem provided above. Suppose we have two external potentials with a constant variation,(V_{ext}^{1}) and (V_{ext}^{2}).

Suppose that both external potentials have the same ground-state density ρ (r). The Hamiltonians of each system are denoted by $H^{(1)}$ and $H^{(2)}$, and because they change, they will have different ground-state wavefunctions, , $\psi^{(1)}$ and $\psi^{(2)}$. We have $\psi^{(2)}$,and because it is not a ground state of $H^{(1)}$, so we have:

$$E^{(1)} = \langle\psi^{(1)}|H^{(1)}|\psi^{(1)}\rangle < \langle\psi^{(2)}|H^{(1)}|\psi^{(2)}\rangle \quad (2.12)$$

$$E^{(2)} = \langle\psi^{(2)}|H^{(2)}|\psi^{(2)}\rangle < \langle\psi^{(1)}|H^{(1)}|\psi^{(1)}\rangle \quad (2.13)$$

Our ground states are non-degenerate, according to the simplified assumption. The problem has been made to include degeneracies in the literature [10, 17]. Equation 2.13 can be rewritten as following:

$$\langle\psi^{(2)}\big|H^{(1)}\big|\psi^{(2)}\rangle = \langle\psi\big|H^{(2)}\big|\psi^{(2)}\rangle\langle\psi^{(2)}\big|H^{(1)} - H^{(2)}\big|\psi^{(2)}\rangle$$
$$= E^{(2)} + \int dr\left(V_{ext}^{(1)}(r) - V_{ext}^{(2)}(r)\right)\rho_o(r) \quad (2.14)$$

And equation 2.14:

$$\langle\psi^{(2)}\big|H^{(1)}\big|\psi^{(2)}\rangle = E^{(2)} + \int dr\left(V_{ext}^{(1)}(r) - V_{ext}^{(2)}(r)\right)\rho o\ (r) \quad (2.15)$$

Combining equations 2.13 and 2.14, and the result in the following contradiction:

$$E^{(1)} + E^{(2)} < E^{(1)} + E^{(2)}$$

Two or more potentials can differ by no more than a constant and create the same ground-state density, hence there can't be two of them.

The second theorem is just as simple to demonstrate as the first. Consider the following equation for the total energy E of the system:

$$E(\rho) = T(\rho) + E_{int}(\rho) + \int drV_{ext}(\rho)(r) \quad (2.16)$$

T, the kinetic term, and E_{int}, the internal interaction of electrons, are, by definition, universal. Assume that the system with a ground-state density of ρ_o , an external potential of V_{ext} , and a wavefunction of ψ_0 . Based on the first theorem, the Hamiltonian is determined by $\rho_o$so, for any density and wavefunction ψ, other than the ground state, we get:

$$E_o = \langle\psi_0|H|\psi_0\rangle < \langle\psi|H|\psi\rangle = E \quad (2.17)$$

This decreases the functional density of the ground, ρ_o, in the equation.

2.17. As a result, by minimising equation 2.18, we may extract the ground-state of the system and compute all ground-state attributes if we know the functional: $T(\rho) + E_{int}(\rho)$.

2.4 The Theorems of Kohn-Sham

We have already demonstrated that obtaining the ground-state density allows us to calculate the ground-state energy, and it is possible to compute the ground-state energy by obtaining the ground-state density. The actual form of the functional denoted in equation 2.18, however, is unknown. The kinetic term and internal energy of interacting particles cannot be expressed as a function of density in general. The solution was proposed by Kohn and Sham in 1965 [3]. According to Kohn and Sham, the original Hamiltonian can be replaced by an effective Hamiltonian of non-interacting particles, with a real external potential that has the same ground-state density as the original system. Because this is not a stated recipe, it is only an ansatz, but a non-interacting problem is significantly easier to solve. In contrast to equation 2.17, the functional energy of the ansatz Kohn-Sham will be the formula:

$$E_{KS}(\rho) = T_{KS}(\rho) + + \int drV_{ext}(r)\rho(r) + E_H(\rho) + E_{xc}(\rho) \qquad (2.18)$$

T_{KS} represents the kinetic energy of the non-interacting system. In equation 2.17, the kinetic energy of the interacting system was used. T the distinction is referred to as the eexchange-correlation functional, E_{xc} , in equation 2.20.

The Hartree functional, E_H, represents the electron-electron interaction using the Hatree-Fock technique, and it takes the following form:

$$E_H(\rho) = \frac{1}{2}\int \frac{\rho(r)\rho(r')}{|r-r\prime|}\, drdr' \tag{2.19}$$

This is an approximate E_{int} version, as previously defined. Again, E_{xc} represents the difference. As a result, the eexchange-correlation functional E_{xc} , shows the difference between the exact and approximate solutions to the kinetic energy and electron-electron interaction terms. Its definition is given below:

$$E_{xc}(\rho) = \big(E_{int}(\rho) - E_H(\rho)\big) + \big(T(\rho) - T_{KS}(\rho)\big) \tag{2.20}$$

However, the first three functionals of equation 2.18 are easy and account for the majority of the contribution to ground-state energy. In comparison, the exchange-correlation function gives a small contribution. Despite decades of research, there is no exact solution. The following section describes several great approximations that have been developed.

2.5 The Exchange Correlation Functions

Several changes to the exchange and correlation energies have been reported in the literature. The first successful form was the Local Density Approximation (LDA) [26, 27], which is only dependent on density and thus functional locally. The next step was the Generalized Gradient Approximation (GGA) [17-20], which contains the density derivative as well as neighbourhood information, making it semi-local. LDA and GGA are two of the most common approximations used in density functional theory. LDA and GGA cannot be considered the only functional possibilities. Some of these functionals correspond to the special needs of the basis sets used in

solving the Kohn-Sham equations, equation 2.11, and a big category is the so-called hybrid functionals (e.g., B3LYP [3], HSE [30], and Meta hybrid GGA [29, 31]), which combine the LDA and GGA forms. One of the most recent and universal characteristics, the Van der Waals density functional (vdW-DF) [32], includes non-local terms and has proven to be quite accurate in systems where dispersion forces are significant [33, 34]. The next sections will provide an overview of the Local Density Approximation and the Generalized Gradient Approximation.

2.5.1 LDA (local density approximation)

In LDA, the exchange-correlation function depends on the local density. This approximation is expected to provide good results for systems where the density doesn't change fast. In some ways, the LDA represents the most fundamental aspect of exchange and correlation energy. It is a basic yet effective function that is correct for graphene and carbon nanotubes, as well as where electron density does not change rapidly. For example, atoms with d and f-type orbits are expected to have more inaccuracy. However, LDA has several limitations, including the fact that the band gap in semiconductors and insulators is sometimes underestimated with significant inaccuracy (up to 10-30%). So, it is best to try to increase your functionality.

2.5.2 Generalized Gradient Approximation (GGA)

When derivatives are added to the functional form of exchange and correlation energies, the GGA is formed. There is no closed form for the functional exchange in this condition, hence the corresponding contributions must have been calculated using analytical solutions.

As with the LDA, there are numerous parameterizations for the exchange and correlation energy in GG [17-19, 35]. LDA and GGA are two of the most commonly used methods for

approximating exchange-correlation energy in the DFT. In addition to LDA and GGA, several functionalities are available. Overall, the validity of these functions is not a plausible theory. Tests are performed on a variety of materials to determine functional qualities for a wide range of systems, followed by statistical comparisons to establish credible results.

2.6 Pseudopotentials

I used Kohn Sham formalism and an exchange-correlation function to transform a large interacting problem into an effective non-interacting problem. This significantly simplifies the situation in terms of physical aspects. When molecules with a large number of atoms are involved, the calculation becomes too huge and computationally intensive to use. By using pseudopotentials, the number of core electrons in an atom can be decreased. Fermi suggested pseudopotentials in 1934 [19, 20], and methods have progressed, since then from constructing not-so-realistic empirical pseudopotentials [21, 22] to more realistic ab initio pseudopotentials [22-24].

Electrons, which are present in the nucleus of an atom, are divided into two types: core and valence. Core electrons are present in the nucleus, whereas valence electrons are found in partially filled atomic shells. When atoms are brought together and core electrons are limited around the nucleus, the only valence electron states overlap. This allows the core electron to be removed and replaced with a pseudopotential, allowing the valence electrons to be screened as if the core electrons were still there. This significantly reduces the number of electrons in a system, as well as the time and stored properties of molecules with a large number of electrons.

2.7 Basis Sets

To determine the wavefunctions, the Hamiltonian must be diagonalized. This method involves inverting a large matrix. For effective calculations, the Hamiltonian must be sparse and contain several zeros. SIESTA employs a Linear Atomic Orbital Combination (LCAO) basis set composed of atom orbitals that decay to zero after a specific cut-off radius. As the overlap between basis functions decreases, the former produces the needed sparse form of the Hamiltonian, whilst the latter permits even a small basis set to produce similar features to those of the studied system. As the overlap between basis functions decreases, the former produces the needed sparse form of the Hamiltonian, whilst the latter permits even a small basis set to produce similar features to those of the studied system. A single ξ basis is the most basic atomic basis set for an atom, with a single basis function $\psi_{nlm(r)}$per electron orbital. Each basis function is made up of a radial wavefunction Φ_{nl}^{1} and a spherical harmonic Y_{lm} :

$$\psi_{nlm(r)} = \Phi_{nl}^{1}(r)Y_{lm}(\theta, \Phi) \tag{2.21}$$

Sankey [25] provided a method for determining the radial component of the wavefunction, which involves solving the Schrodinger equation for an atom inside a spherical box. It is constrained to vanish at a cut-off radius r_c. The constraint creates an energy shift δE in the Schrödinger equation, resulting in the eigen function's initial node at r_c:

$$\left[-\frac{d^2}{dr^2} + \frac{l(l+1)}{2r^2} + V_{nl}^{ion}(r)\right]\Phi_{nl}^{1}(r) = (\varepsilon_{nl} + \delta E)\,\Phi_{nl}^{1}(r)) \tag{2.22}$$

For greater accuracy basis sets, each electron orbital might have many radial wavefunctions. A split-valence method is used to calculate the additional radial wavefunctions, Φ_{nl}^{i} for > 1. To

define a split valence cut off for each additional wavefunction, r_s^i, it is split into two piecewise functions: a polynomial below the cut-off and the preceding basis wavefunction above it.

$$\Phi_{nl}^1(r) = \begin{cases} r^l(a_{nl} - b_{nl}r^2) & r < r_s^i \\ \Phi_{nl}^{i-1} & r_s^i < r < r_s^{i-1} \end{cases} \quad (2.23)$$

Additional parameters are found at the point when the wavefunction and its derivative are expected to be continuous.

To get accuracy (multiple-ξ polarized), include wavefunctions that have different angular momenta that correspond to unoccupied orbitals in the atom. This can be done by solving Eq. 2.22 in an electric field such that the orbital is polarized or deformed by the field (see [6] for details), getting another radial function. This has been combined with the appropriate angular dependent spherical harmonic, that increasing the size of the basis. Table 2.1 gives the number of basis orbitals for a specific number of atoms for single- ξ, single- ξ polarised, double- ξ, and double- ξ polarised.

Table 2.1: is an example of the number of radial basis functions per atom that are used in the SIESTA at various degrees of precision.

Atom	**Valence configuration**	**SZ**	**SZP**	**DZ**	**DZP**
H	$1s$	1	4	2	5
C	$(2s^2\ 2P^2)$	4	9	8	13
S	$(3S^2\ 3P^4)$	4	9	8	13
Au	$(6S^1\ 5d^{10})$	6	9	12	15

I have used Double- ξ polarized basis set(DZP) and Double-ξ basis set (DZ). Also, I have used Generalized Gradient Approximation (GGA) and Local Density Approximation (LDA).

2.8 Summary

In conclusion, I have provided an overview of the DFT technique and the SIESTA DFT method, which are used throughout this thesis to compute the electronic structures. The first step in determining a molecule's electron transport properties is to obtain a DFT mean-field Hamiltonian that describes the isolated molecule. The next step is to connect the molecule to semi-infinite leads, which will be discussed in the following chapter.

2.9 Bibliography

[1] The SIESTA method for ab initio order-N materials simulation. JM Soler, E Artacho, JD Gale, A García, J Junquera, P Ordejón, D Sánchez-Portal, *J Phys: Condens Matter*, 14(11), 2745 (2002)

[2] Inhomogeneous Electron Gas. P Hohenberg, W Kohn, *Phys Rev*, 136(3B), B864–B871 (1964)

[3] Self-Consistent Equations Including Exchange and Correlation Effects. W Kohn, LJ Sham, *Phys Rev*, 140(4A), A1133–A1138 (1965)

[4] Many-Particle Theory. EKU Gross, E Runge, O Heinonen, 1st ed., CRC Press, Bristol (1991)

[5] Electronic Structure: Basic Theory and Practical Methods, by Richard M. Martin. M Probert, *Contemporary Physics*, 52(1), 77–77 (2011)

[6] Density Functional Theory. EKU Gross, RM Dreizler, Vol. 337, Springer (1995)

[7] Density-Functional Theory of Atoms and Molecules. RG Parr, Y Weitao, Oxford University Press (1989)

[8] On the Quantum Theory of Molecules. M Born, JR Oppenheimer, (1927)

[9] The Constrained Search Formulation of Density Functional Theory. M Levy, JP Perdew, in *Density Functional Methods In Physics*, RM Dreizler, J da Providência, Eds., Springer, Boston, 11–30 (1985)

[10] Electron densities in search of Hamiltonians. M Levy, *Phys Rev A*, 26(3), 1200–1208 (1982)

[11] Electronic Structure: Basic Theory and Practical Methods. RM Martin, 2nd ed., Cambridge University Press (2020)

[12] Introduction to Quantum Mechanics. DJ Griffiths, Pearson Prentice Hall (2005)

[13] Sopra lo Spostamento per Pressione delle Righe Elevate delle Serie Spettrali. E Fermi,

Nuovo Cim, 11(3), 157–166 (1934)

[14] Motion of neutrons in hydrogenous substances. E Fermi, *Ricerca Scientifica*, 7(2), 13–15 (1936)

[15] Universal variational functionals of electron densities, first-order density matrices, and natural spin-orbitals. M Levy, *Proc Natl Acad Sci*, 76(12), 6062–6065 (1979)

[16] Density Functional Methods in Physics. The Inhomogeneous Electron Gas. M Levy, 32–94 (1985)

[17] Density-functional exchange-energy approximation with correct asymptotic behavior. AD Becke, *Phys Rev A*, 38(6), 3098–3100 (1988)

[18] Improved adsorption energetics within density-functional theory using revised Perdew-Burke-Ernzerhof functionals. B Hammer, LB Hansen, JK Nørskov, *Phys Rev B*, 59(11), 7413–7421 (1999)

[19] Generalized Gradient Approximation Made Simple. JP Perdew, K Burke, M Ernzerhof, *Phys Rev Lett*, 77(18), 3865–3868 (1996)

[20] Tuning the thermoelectrical properties of anthracene-based self-assembled monolayers. A Ismael, X Wang, T Bennett, L Wilkinson, B Robinson, N Long, L Cohen, CJ Lambert, *Chem Sci*, 11(26), 6836–6841 (2020)

[21] Discriminating single-molecule sensing by crown-ether-based molecular junctions. AK Ismael, A Al-Jobory, I Grace, CJ Lambert, *J Chem Phys*, 146(6), 064704 (2017)

[22] Density functionals for Coulomb systems. EH Lieb, in *Physics as Natural Philosophy: Essays in Honor of Laszlo Tisza*, MIT Press, 111 (1982)

[23] First-principles nonlocal-pseudopotential approach in the density-functional formalism. A Zunger, ML Cohen, *Phys Rev B*, 18(10), 5449–5472 (1978)

[24] Norm-Conserving Pseudopotentials. DR Hamann, M Schlüter, C Chiang, *Phys Rev Lett*, 43(20), 1494–1497 (1979)

[25] The calculation of small molecular interactions by the differences of separate total energies. SF Boys, F Bernardi, *Mol Phys*, 19(4), 553–566 (1970)

[26] Elimination of basis set superposition error in linear-scaling density-functional calculations. PD Haynes, C-K Skylaris, AA Mostofi, MC Payne, *Chem Phys Lett*, 422(4–6), 345–349 (2006)

[27] Exchange-correlation energy of a metallic surface: Wave-vector analysis. DC Langreth, JP Perdew, *Phys Rev B*, 15(6), 2884–2901 (1977)

[28] Intramolecular basis set superposition errors. ML Senent, S Wilson, *Int J Quantum Chem*, 82(6), 282–292 (2001)

[29] Basis set superposition error in N-body clusters. K Mierzwicki, Z Latajka, *Chem Phys Lett*, 380(5–6), 654–664 (2003)

[30] Hybrid functionals based on a screened Coulomb potential. J Heyd, GE Scuseria, M Ernzerhof, *J Chem Phys*, 118(18), 8207–8215 (2003)

[31] Applications and validations of the Minnesota density functionals. Y Zhao, DG Truhlar, *Chem Phys Lett*, 502(1), 1–13 (2011)

[32] Van der Waals Density Functional for General Geometries. M Dion, H Rydberg, E Schröder, DC Langreth, BI Lundqvist, *Phys Rev Lett*, 92(24), 246401 (2004)

[33] Van der Waals density functionals applied to solids. J Klimeš, DR Bowler, A Michaelides, *Phys Rev B*, 83(19), 195131 (2011)

[34] Quantum interference and heteroaromaticity of para- and meta-linked bridged biphenyl units. M Gantenbein et al., *Sci Rep*, 7(1), 1794 (2017)

[35] Effects of counterpoise correction and basis set extrapolation. A Boese, G Jansen, M

Torheyden, S Höfener, W Klopper, *Phys Chem Chem Phys*, 13, 1230–1238 (2011)

[36] Development of the Colle-Salvetti correlation-energy formula. C Lee, W Yang, RG Parr, *Phys Rev B*, 37(2), 785–789 (1988)

[37] Ground State of the Electron Gas by a Stochastic Method. DM Ceperley, BJ Alder, *Phys Rev Lett*, 45(7), 566–569 (1980)

[38] Basis set superposition error-counterpoise corrected potential energy surfaces. MC Daza et al., *J Chem Phys*, 110(24), 11806–11813 (1999)

Chapter 3

Phase Coherent Electron Transport

Chapter 2 covered density functional theory, a method for determining the electrical structure of an isolated molecule. The next step involves connecting this isolated molecule to semi-infinite leads and calculating the transmission coefficient across the system. This process is carried out using the Green's function scattering formalism, which is the focus of this chapter and is utilized throughout the thesis. The electrical properties of nanoscale systems situated between several macroscopic metal electrodes are explained using scattering theory and the Green's function techniques.

3.1 Introduction

In this chapter, I start with a brief summary of the Landauer formula. Following that, I present the most basic form of a retarded Green's function for Scattering Theory in a one-dimensional tight-binding chain. After that, I break the lattice's periodicity at one connection and demonstrate that Green's function is directly related to the transmission coefficient across the scattering area. The methods applied to these simple systems are going to be used to calculate the transmission coefficient of mesoscopic conductors with arbitrarily complex geometry. The methods provided here assume negligible interaction between carriers, the absence of inelastic processes, and zero temperature.

3.2 The Landauer Formula

The Landauer formula [1, 6] describes electron transport in mesoscopic systems and is also appropriate to describe phase-coherent systems in the absence of inelastic scattering. It relates a mesoscopic sample's conductance to the transmission qualities of electrons that pass through it. The method used for calculating the transmission qualities will be covered later in this chapter.

Figure 3.1: A mesoscopic scatterer connected to contacts with ballistic leads. μ_L and μ_R indicate the left and right contacts' chemical potentials, respectively.

A mesoscopic scattering area that is connected to contacts via ballistic leads. The chemical potentials in the contacts are μ_L and μ_R. When an incident wave packet reaches the scattering region from the left, it is transmitted with probability $T = tt^*$ and reflected with probability $R = rr^*$. Charge conservation requires that T + R = 1.

To begin, consider a mesoscopic scatter linked to two contacts that behave as electron reservoirs via two perfect ballistic leads as shown in figure 3.1. All inelastic relaxation processes have limitations to the reservoirs [1]. The reservoirs have slightly different chemical potentials μ_L and μ_R resulting in a tiny $\mu_L - \mu_R$ difference. We are using the notation $\mu_L - \mu_R = \delta E = e\delta V > 0$ to drive electrons from the left to the right reservoir. Initially, I will present the solution for a single open channel (where only one electron can flow in a given direction). The incident current travelling through the system from the left to the right reservoir is:

$$\delta \mathrm{I\ in} = \mathrm{e}v\left(\frac{\partial \mathrm{n}}{\partial \mathrm{E}}\right)(\mu_L - \mu_R) \qquad (3.1)$$

whereas e is the electronic charge, v is the group velocity, and $\frac{\partial \mathrm{n}}{\partial \mathrm{E}}$is the density of states per unit length in the lead within the energy window determined by the chemical potentials of the contacts.

$$\frac{\partial \mathrm{n}}{\partial \mathrm{E}} = \frac{\partial \mathrm{n}}{\partial \mathrm{k}}\frac{\partial \mathrm{k}}{\partial \mathrm{E}} = \frac{\partial \mathrm{n}}{\partial \mathrm{k}}\frac{1}{v\hbar} \qquad (3.2)$$

After adding a factor of 2 for spin dependency, $\frac{\partial \mathrm{n}}{\partial \mathrm{k}} = \frac{1}{2\pi}$ putting this into Equation 3.2, we get $\frac{\partial \mathrm{k}}{\partial \mathrm{E}} = \frac{1}{v\hbar}$. This reduces Equation 3.1 as follows:

$$\delta I = \frac{2e}{h}(\mu_L - \mu_R) = \frac{2e^2}{h}\delta V \qquad (3.3)$$

δV represents the voltage created by the chemical potential mismatch. Equation 3.3 shows that in the absence of a scattering area, the conductance of a quantum wire with one open channel is $\frac{2e^2}{h}$, which is about 77.5μS (or resistance of 12.9 kΩ). This is a common number that appears on the circuit boards of daily electrical products. If we assume a scattering region, the current collected in the correct contacts will be:

$$\delta \mathrm{I\ out} = \frac{2e^2}{h}\,T\delta V \rightarrow \frac{\delta I}{\delta V} = G = \frac{2e^2}{h}\,T \qquad (3.4)$$

This is the well-known Landauer formula, which relates the conductivity, G, of a mesoscopic scatterer to the transmission probability, T, of electrons passing through it. It represents the linear response conductance, so it only applies to small bias voltages (δV = 0).

Buttiker generalised the Landauer formula for the case of several open channels [3]. In this situation, the transmission coefficient is replaced by the sum of all transmission amplitudes

representing electrons that come from the left contact and arrive at the right contact. For several open channels, equation 3.3 of the Landauer formula becomes:

$$\frac{\text{Iout}}{V} = G = \frac{2e^2}{h}\sum_{i,j}|t_{i,j}|^2 = \frac{2e^2}{h}Trace(tt^{\dagger}) \qquad (3.5)$$

The transmission amplitude t_{ij} represents scattering from the j^{th}channel of the left lead to the i^{th}channel of the right lead. In addition to transmission amplitudes, reflection amplitudes r_{ij}that represent particle scattering from the j^{th}channel of the left lead to the i^{th} channel of the same lead. The S matrix, which connects states from the left to the right lead and vice versa, can be defined by combining reflection and transmission amplitudes.

$$S = \begin{pmatrix} r & \mathrm{t}' \\ t & \mathrm{r}' \end{pmatrix} \qquad (3.6)$$

In this case, r and t indicate electrons r coming from the left, whereas t' and r' represent electrons coming from the right. Equation 3.6 indicates that $r, t, \acute{r}$ and t' are matrices for many channels, which may be complex in the presence of a magnetic field. However, charge conservation requires that the S matrix be unitary: $SS^{+}=I$. The S matrix is an important part of scattering theory. This method is not only helpful in defining transport in the linear response regime, but it is also useful in other applications, such as adiabatic pumping.

3.3 The Theory of Scattering in One Dimension:

Before going over the extended methods, it's helpful to figure out the scattering matrix for a simple one-dimensional system. This will give a full explanation of the method used. Before moving on to the next step, which is calculating the scattering matrix of a one-dimensional scattered section 3.4.2, I will first go over the form of the Green's function for a simple one-

dimensional discretized lattice section 3.4.1. This is because the Green's functions will be utilised in the derivation.

3.3.1 Perfect One-Dimensional Lattice

In this part, I will analyse the structure of the Green's function for a simple one-dimensional lattice with on-site energies ε_o and real hopping parameters -γ, as illustrated in Figure 3.2.

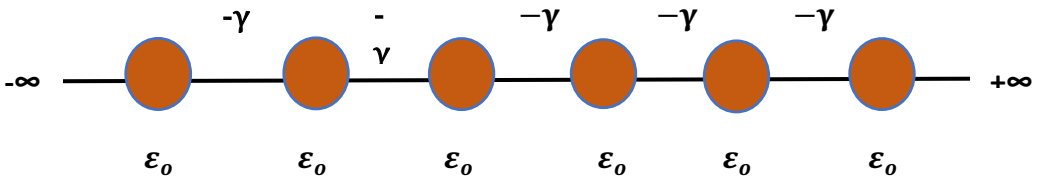

Figure 3.2: shows the tight-binding approximation of a periodic one-dimensional lattice with one site energies $\boldsymbol{\varepsilon_o}$ and coupling $\boldsymbol{\gamma}$.

The Hamiltonian's matrix form is simple to write:

$$H = \begin{pmatrix} -\infty & . & . & . & . & . & . & . & . \\ . & . & . & . & . & . & . & . & . \\ . & . & \varepsilon_o & -\gamma & 0 & 0 & 0 & . & . \\ . & . & -\gamma & \varepsilon_o & -\gamma & 0 & 0 & . & . \\ . & . & 0 & -\gamma & \varepsilon_o & -\gamma & 0 & . & . \\ . & . & 0 & 0 & -\gamma & \varepsilon_o & -\gamma & . & . \\ . & . & 0 & 0 & 0 & -\gamma & \varepsilon_o & . & . \\ . & . & . & . & . & 0 & -\gamma & . & . \\ . & . & . & . & . & . & . & . & +\infty \end{pmatrix} \quad (3.7)$$

Using the tight-binding approximation, we may expand the Schrödinger equation (Equation 3.8) at a specific lattice site z in terms of the energy and wavefunction ψ_z (Equation 3.9).

$$(E - H)\psi = 0 \tag{3.8}$$

$$\varepsilon_o \psi_z - \gamma \psi_z + 1 - \gamma \psi_z - 1 = E\psi_z \tag{3.9}$$

The wavefunction for this ideal lattice is described by a propagating Bloch state equation 3.10, which is normalised by its group velocity v to ensure that it carries a unit current flux. By substituting this into equation 3.9, we obtain the well-known one-dimensional dispersion relation equation 3.11.

$$\psi_z = \frac{1}{\sqrt{v}} e^{ikZ} \qquad (3.10)$$

$$E = \varepsilon_0 - 2\gamma \cos(\mathrm{k}) \qquad (3.11)$$

In this section, we presented the quantum number, k, which is also generally known as the wavenumber. In fact, the retarded Greens function g (z, ź) is the solution to an equation that is very similar to the Schrodinger equation. This gives it a close relationship with the wave function.

$$(E - H)\, g(z, z') = \delta_{(z,z')} \qquad (3.12)$$

On a physical level, the retarded Green's function, g (z, z'), represents the reaction of a system at a point z in response to a source at a point z'. As shown in Figure 3.3, we would expect this kind of excitation to cause two waves to move away from the point of excitation. These waves would have amplitudes A^+ and A^-.

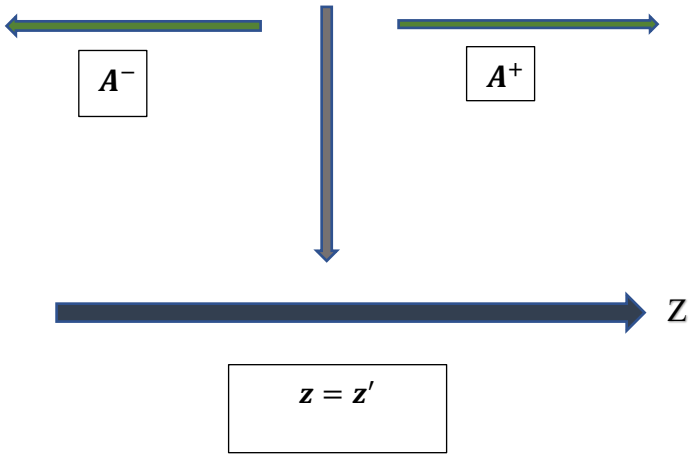

Figure 3.3: The configuration of an infinite one-dimensional lattice's retarded green's function. As a result of the excitation at z = z′, the waves go to the left and right with amplitudes $\boldsymbol{A}^{+}$ and $\boldsymbol{A}^{-}$ respectively.

Here is a simplified way to represent these waves:

$$g(z,z') = \begin{cases} A^{+}\, e^{ikz}, & z \geq z' \\ A^{-}\, e^{-ikz}, & z \leq z' \end{cases} \qquad (3.13)$$

This solution satisfies equation 3.12 at all points except z = ź. To solve this, the Green's function has to be continuous in equation 3.14, therefore, we can equate the two at $z = \acute{z}$

$$A^{+}\, e^{ikz'} = A^{-}\, e^{-ik\acute{z}} \qquad (3.14)$$

$$A^{+}\, e^{2ikz'} = A^{-} \qquad (3.15)$$

When equation 3.15 is substituted into equation 3.13 of the Green's functions, we get:

$$g(z,z') = A^{+} e^{ikz'} e^{ik(z-z')} \quad z' > z$$

$$g(z,z') = A^{+} e^{ikz'} e^{ik(z'-z)} \quad z' < z \qquad (3.16)$$

Clearly, this may be expressed as:

$$g(z,z') = A^{+} e^{ikz'} e^{ik\,|z-z'|} \qquad (3.17)$$

Whereas

$$A^{+} = \frac{e^{-iKź}}{i\hbar v} \tag{3.18}$$

$$g(z, z') = \frac{e^{ik|z-z'|}}{i\hbar v} \tag{3.19}$$

$$v = \frac{dE(k)}{\hbar dk} = \frac{2\gamma sin(k)}{\hbar} \tag{3.20}$$

A more detailed derivation can be found in the literature [6–8].

3.3.2 Scattering in One Dimension

I study two single-axis, half-infinite leads that are connected by a coupling element -α. Figure 3.4 shows that both leads have the same on-site potentials, ε_o, and hopping elements (-γ). The analytical solutions for transmission and reflection coefficients are simple to calculate.

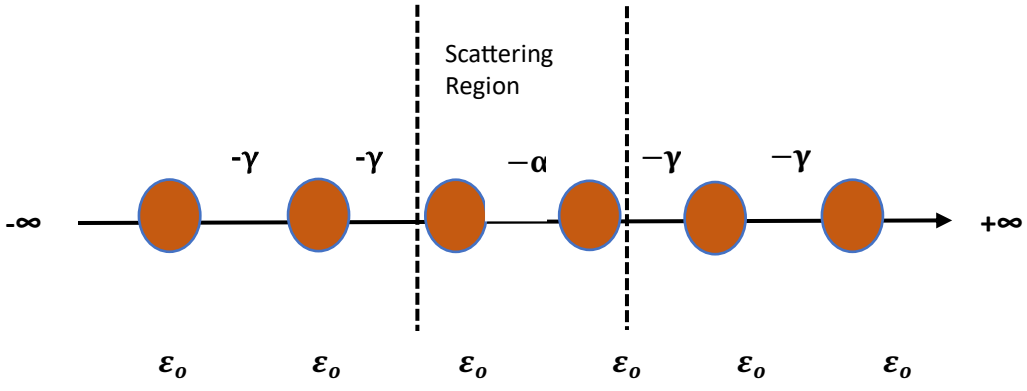

Figure 3.4: shows a simple tight-binding model for a one-dimensional scatterer attached to one-dimensional leads.

We have to define a Hamiltonian, that is represented by an infinite matrix.

$$H = \begin{pmatrix} \ddots & . & . & . & . & . & . & . & . \\ . & . & . & . & . & . & . & . & . \\ . & . & \varepsilon_o & -\gamma & 0 & 0 & 0 & . & . \\ . & . & -\gamma & \varepsilon_o & -\gamma & 0 & 0 & . & . \\ . & . & 0 & -\gamma & \varepsilon_o & -\alpha & 0 & . & . \\ . & . & 0 & 0 & -\alpha & \varepsilon_o & -\gamma & . & . \\ . & . & 0 & 0 & 0 & -\gamma & \varepsilon_o & . & . \\ . & . & . & . & . & 0 & -\gamma & . & . \\ . & . & . & . & . & . & . & . & \ddots \end{pmatrix} \quad (3.21)$$

Equation 3.11 provided the dispersion relation for real γ that corresponds to the leads mentioned before, while equation 3.20 provided the group velocity.

$$E(k) = \varepsilon_0 - 2\gamma \cos(\mathrm{k}) \quad (3.22)$$

$$v = \frac{1}{\hbar}\frac{dE}{dk} \quad (3.23)$$

To get the scattering amplitudes, we have to determine the system's Green's function. The formal solution to equation 3.12 may be expressed as:

$$G = (E - H)^{-1} \quad (3.24)$$

Equation 3.24 exhibits singularity when the energy E equals to the eigenvalues of the Hamiltonian H. In order to overcome this issue, it is advisable to consider the limit.

$$G_{\pm} = \lim_{\eta \to 0}(E - H \pm i\eta)^{-1} \tag{3.25}$$

The retarded (advanced) Green's function is represented by G_+, G_- , where η is a positive number. In this thesis, I will just use retarded Green's functions, therefore I have chosen the + sign. Equation 3.19 defines the retarded Green's function for an infinite, one-dimensional chain with equal parameters.

$$g^{\infty}(j,l) = \frac{e^{ik|j-l|}}{i\hbar v} \tag{3.26}$$

The labels of the chain's sites are j *and* l. The Green's function of a semi-infinite lead can be obtained by introducing the correct boundary conditions. Because the lattice is semi-infinite, the chain has to terminate at a given point i_0. Otherwise, all points with $i \geq i_0$ are missing. To illustrate this condition mathematically, a wave function is added to the Green's function. Here, the wavefunction is as follows:

$$\psi_{j,l}^{i_0} = \frac{-e^{ik(2i_0-l-j)}}{i\hbar v} \tag{3.27}$$

At the boundary $j = l = i_0 - 1$, the Green's function $g(j,l) = g_{j,l}^{\infty} + \psi_{j,l}^{i_0}$ will take the following simplified form:

$$g\,(i_0 - 1, i_0 - 1) = -\frac{e^{ik}}{\gamma} \tag{3.28}$$

If we assume that the leads are decoupled, meaning that α = 0, then the total Green's function of the system can be expressed as the decoupled Green's function.

$$g = \begin{pmatrix} -\frac{e^{ik}}{\gamma} & 0 \\ 0 & -\frac{e^{ik}}{\gamma} \end{pmatrix} = \begin{pmatrix} g_L & 0 \\ 0 & g_R \end{pmatrix} \quad (3.29)$$

We need to apply Dyson's equation to get Green's function of the coupled system G if we turn on the interaction presently.

$$G = (g^{-1} - V)^{-1} \quad (3.30)$$

In this case, the operator V characterising the relationship between the two leads will have the form:

$$V = \begin{pmatrix} 0 & V_c \\ V_c^{\dagger} & 0 \end{pmatrix} = \begin{pmatrix} 0 & \alpha \\ \alpha^* & 0 \end{pmatrix} \quad (3.31)$$

Get the solution to Dyson's equation by substituting equations 3.47 and 3.49 into equation 3.48:

$$G = \frac{1}{|\alpha|^2 - \gamma^2 e^{-2ik}} \begin{pmatrix} \gamma e^{-ik} & \alpha \\ \alpha^* & \gamma e^{-ik} \end{pmatrix} \quad (3.32)$$

Finding the amplitudes of transmission (t) and reflection (r) using the Green's function equation 3.32 is the only remaining step. This is achieved by applying the Fisher-Lee relation [4, 6], which creates a relationship between the scattering amplitudes and the Green's function of the scattering problem. Here, the Fisher-Lee relations take the following form:

$$r = i\hbar\, v_L G_{00} - 1 \quad (3.33)$$

$$t = i\hbar\sqrt{v_R v_L}\, G_{10} \tag{3.34}$$

These amplitudes are corresponding to particles that are coming from the left. When particles come from the right, similar formulas can be obtained for the transmission ($\acute{t}$) and reflection ($\acute{r}$) amplitudes.

Now that we have obtained the whole scattering matrix, we are able to use equation 3.4 of the Landauer formula to determine the conductance at zero bias.

3.4 Generalization of the Scattering Formalism

In this part, I give a generalized approach to transport calculations based on Lambert's derivation, as presented in [2]. This is similar to the earlier method. A generalisation of the Fisher-Lee relation is used to recover the scattering amplitudes once the surface Green's function of crystalline leads is determined.

3.4.1 Green's Function of the Leads and Hamiltonian

We study a basic semi-infinite crystalline electrode with any level of complexity. Due to the crystalline form of the leads, the structure of the Hamiltonian can be considered as an extension of the one-dimensional electrode Hamiltonian. Figure 3.5 illustrates the overall system structure. Instead of considering the energies of the sites, we use Hamiltonians to represent each repeated layer of the bulk electrode, given as H_0. Additionally, we use a coupling matrix to characterise the hopping parameters between these layers H_1.

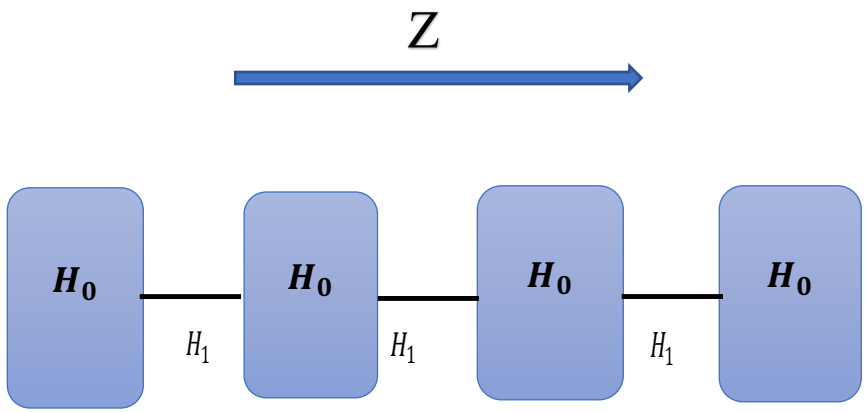

Figure 3.5: illustrates a diagrammatic representation of a semi-infinite generalized lead. The states defined by the Hamiltonian H_0 are linked together through a generalized hopping matrix H_1. The direction z is defined as being parallel to the axis of the chain. Each slice can be assigned a label z.

The Hamiltonian for this system is expressed in the following form:

$$H = \begin{pmatrix} \bullet & \bullet & 0 & 0 & 0 & 0 & 0 & 0 \\ \bullet & \bullet & H_1 & 0 & 0 & 0 & 0 & 0 \\ 0 & H_1^\dagger & H_o & H_1 & 0 & 0 & 0 & 0 \\ 0 & 0 & H_1^\dagger & H_o & H_1 & 0 & 0 & 0 \\ 0 & 0 & 0 & H_1^\dagger & H_o & H_1 & 0 & 0 \\ 0 & 0 & 0 & 0 & H_1^\dagger & H_o & H_1 & 0 \\ 0 & 0 & 0 & 0 & 0 & H_1^\dagger & \bullet & \bullet \\ 0 & 0 & 0 & 0 & 0 & 0 & \bullet & \bullet \end{pmatrix} \tag{3.35}$$

In this case, H_o and H_1 are typically complex matrices, and the only condition is that the complete Hamiltonian, represented as H, must be Hermitian. In this part, the first goal is to calculate the Green's function of this kind of lead for general H_1 and H_0. In order to determine

the Green's function, it is necessary to calculate the spectrum of the Hamiltonian by solving the Schrödinger equation for the lead.

$$H_1^\dagger \psi_{z-1} + H_o \psi_z + H_1 \psi_{z+1} = E\psi_z \tag{3.36}$$

Here, the wave function that describes layer z is represented as ψ_z, where z is an integer that is measured in units of inter-layer distance. Assuming that the system is infinitely periodic only in the z direction, we can represent the on-site wavefunction $\psi_{z,}$ using Bloch form. This form consists of a product of a propagating plane wave and a wavefunction, Φ_k, which is perpendicular to the transport direction, z. The layer Hamiltonian, H_0, has dimensions M × M, meaning it consists of M site energies and their respective hopping elements. Therefore, the perpendicular wavefunction, Φ_k, will have M degrees of freedom and can be represented as a $1 \times M$ dimensional vector. Thus, ψ_z, the wave function, has the following form:

$$\psi_z = \sqrt{n_k} e^{ikz} \Phi_k \tag{3.37}$$

here n_k is an arbitrary normalization parameter. Substituting this into the Schrödinger equation (Equation 3.36), we get:

$$\left(H_0 + e^{ik} H_1 + e^{-ik} H_1^\dagger - E\right)\Phi_k = 0 \tag{3.38}$$

In order to determine the band structure for such a problem, one would choose values of k and then calculate the eigenvalues at that point, which would be represented by the equation $E = E_l(k)$, where k =1,2,3,…,M. Where l is the band index. For each k value, there will be M solutions to the eigenvalue issue, and hence M energy values. It is not very difficult to build a

band structure by choosing several different values for the variable k. In a scattering problem, the problem is solved by applying an alternative method. Instead of determining the eigenvalues at a specific k, we determine the values of k at a particular E. In order to accomplish this, a root-finding may have been utilised, but this would have needed an immense computational effort because the wave numbers are generally complex. On the other hand, we may formulate an alternate eigenvalue problem in which energy is the result and wave numbers are the result by introducing the function:

$$v_k = e^{-ikz}\Phi_k \tag{3.39}$$

This is combined with equation 3.38:

$$\begin{pmatrix} -H_1^{-1}(H_o - E) & -H_1^{-1}H_1^{\dagger} \\ I & 0 \end{pmatrix}\begin{pmatrix} \Phi_k \\ v_k \end{pmatrix} = e^{ikz}\begin{pmatrix} \Phi_k \\ v_k \end{pmatrix} \tag{3.40}$$

If we consider a layer Hamiltonian, represented as H_o, with dimensions of M×M, then equation 3.40 will generate 2M eigenvalues, represented as e^{ik_lz},and eigenvectors, represented as Φ_k, of magnitude M. After that, these states can be classified into four separate categories according on whether they are propagating or decaying, as well as whether they are left going or right going. When the value of k_l is real, we suggest that the state is propagating. A wave number with a positive imaginary part is referred to as a left decaying state, while a wave number with a negative imaginary part is referred to as a right decaying state. The propagating states are sorted according to their group velocity, which is provided by:

$$v_{kl} = \frac{1}{\hbar}\frac{\partial E_{k,l}}{\partial k} \tag{3.41}$$

If the state's group velocity, v_{kl}, is positive, then it is a right propagating state; if it is negative, then it is left propagating.

The eigenstates are sorted into left and right propagating or decaying states according to the wave number and group velocity, as shown in Table 3.1.

Category	**Left**	**Right**
Decaying	$Im(k_l) > 0$	$Im(k_l) < 0$
Propagation	$Im(k_l) = 0, v_g^{k_l} < 0$	$Im(k_l) = 0, v_g^{k_l} > 0$

Table 3.1: Sorting the eigenstates into left and right propagating or decaying states according to the wave number and group velocity.

Now, I will represent the wave numbers that belong to the left propagating-decaying set as k_l, whereas the wave numbers that belong to the right propagating-decaying set will simply be denoted as k_r. Therefore, ϕ_{kr} represents a wave function that corresponds to a right state, while ϕ_{kl} represents a wave function that corresponds to a left state. If H_1 is invertible, there must exist an equal number, M, of left and right travelling states. It is obvious that if $H_1$is singular, the matrix in equation 3.59 cannot be built because it depends on the inversion of H_1. In

addition, one of various ways can be used to solve this problem. The first [2, 8, 10] uses the decimation method to get a useful, non-singular H_1. Another option is to populate a solitary H_1 with small values at random, creating a specific numerical mistake. This method is reasonable since the numerical error that is introduced could be as small as the numerical error that is introduced by decimation. A different solution would be to rewrite equation 3.40 without inverting H_1 as follows:

$$\begin{pmatrix} -(H_o - E) & -H_1^{\dagger} \\ I & 0 \end{pmatrix} \begin{pmatrix} \Phi_k \\ v_k \end{pmatrix} = e^{ikz} \begin{pmatrix} H_1 & 0 \\ 0 & I \end{pmatrix} \begin{pmatrix} \Phi_k \\ v_k \end{pmatrix} \tag{3.42}$$

Although, solving this generalized Eigen-problem requires additional computational resources. Any of the previously mentioned solutions are effective in addressing the issue of a solitary H_1 matrix. Additionally, the requirement that there must be an equal number, M, of left and right going states, whether H_1 is singular or not [11-15]. The solutions to the eigenvalue equation 3.38 at a specific wave number, k, will provide a set of basis that are orthogonal. However, the eigenstates, Φ_{k_l}, produced by solving the Eigen problem equation 3.42 at a particular energy, E, will not typically construct a set of states that are orthogonal. This is really important, as we will need to calculate the Green's function in a non-orthogonal method while creating it. As a result, it is important to introduce the duals to, Φ_{k_l}, and, $\Phi_{\bar{k}_l}$, in a method that corresponds to the following:

$$\widetilde{\Phi}^{\dagger}_{(k_i)}\Phi_{k_j} = \widetilde{\Phi}^{\dagger}_{(\bar{k}_i)}\Phi_{\bar{k}_j} = \delta_{ij} \tag{3.43}$$

The result is the generalized completeness relation:

$$\sum_{l=1}^{M} \widetilde{\Phi}^{\dagger}_{(k_l)}\Phi_{(k_l)} = \sum_{l=1}^{M} \widetilde{\Phi}^{\dagger}_{(\bar{k}_l)}\Phi_{(\bar{k}_l)} = I \tag{3.44}$$

Given that we have all the eigenstates at a specific energy, we can first calculate the Green's function for the infinite system. If the appropriate boundary conditions have been satisfied, we can then calculate the Green's function for the semi-infinite leads on their surfaces. By using the fact that the Green's function solves the Schrödinger equation at z=z', we may construct the Green's function by combining the eigenstates Φ_{k_l} and $\Phi_{\bar{k}_l}$:

$$g(z,z') = \begin{cases} \sum_{l=1}^{M} \Phi_{(k_l)} e^{ik_l(z-z')}\, \omega^{\dagger}_{k_l}, & z \geq z' \\ \sum_{l=1}^{M} \Phi_{(\bar{k}_l)} e^{i\bar{k}_l(z-z')}\, \omega^{\dagger}_{\bar{k}_l}, & z \leq z' \end{cases} \tag{3.45}$$

The M-component vectors ω_{k_l} and $\omega_{\bar{k}_l}$ need to be found. It is necessary to see the structural similarity between this equation and equation 3.13, as well as the fact that all the degrees of freedom in the transverse direction are included within the vectors Φ_k and ω_k. The current objective is to get the vectors. According to section 3.4.1, it is required that equation 3.45 is

continuous at z=z' and also satisfies Green's function equation (equation 3.12). The initial condition is expressed as:

$$\sum_{l=1}^{M} \Phi_{(k_l)} \omega_{k_l}^{\dagger} = \sum_{l=1} \Phi_{(\bar{k}_l)} \omega_{\bar{k}_l}^{\dagger} \tag{3.46}$$

Furthermore, the second one:

$$\sum_{l=1}^{M} \left[(E - H_o) \Phi_{(k_l)} \omega_{k_l}^{\dagger} + H_1 e^{ik_l} \omega_{k_l}^{\dagger} + H_1^{\dagger} \Phi_{(\bar{k}_l)} e^{-i\bar{k}_l} \omega_{\bar{k}_l}^{\dagger} \right] = I$$

$$\sum_{l=1}^{M} \left[(E - H_o) \Phi_{(k_l)} \omega_{k_l}^{\dagger} + H_1 \Phi_{(k_l)} e^{ik_l} \omega_{k_l}^{\dagger} + H_1^{\dagger} \Phi_{(\bar{k}_l)} e^{-i\bar{k}_l} \omega_{\bar{k}_l}^{\dagger} + H_1^{\dagger} e^{-ik_l} \omega_{k_l}^{\dagger} - H_1^{\dagger} e^{-ik_l} \omega_{k_l}^{\dagger} \right] = I$$

$$\sum_{l=1}^{N} \left[H_1^{\dagger} \Phi_{(\bar{k}_l)} e^{i\bar{k}_l} \omega_{\bar{k}_l}^{\dagger} - H_1^{\dagger} \Phi_{(k_l)} e^{-ik_l} \omega_{k_l}^{\dagger} \right] + \sum_{l=1}^{M} \left[(E - H_o) + H_1 e^{ik_l} + H_1^{\dagger} e^{-ik_l} \right] \Phi_{(k_l)} \omega_{k_l}^{\dagger} = I$$

That is known as well from the Schrödinger equation.

$$\sum_{l=1}^{M}\left[(E-H_o)+H_1e^{ik_l}+H_1^{\dagger}e^{-ik_l}\right]\Phi_{(k_l)}=0 \tag{3.47}$$

This gives us:

$$\sum_{l=1}^{N}H_1^{\dagger}\left[\Phi_{(\bar{k}_l)}e^{i\bar{k}_l}\omega_{\bar{k}_l}^{\dagger}+\Phi_{(k_l)}e^{-ik_l}\omega_{k_l}^{\dagger}\right]=I \tag{3.48}$$

After that, the dual vectors defined in equation 3.43 are applied. Multiplying equation 3.46 by $\widetilde{\Phi}_{(k_p)}$ results in:

$$\sum_{l=1}^{M}\widetilde{\Phi}_{(k_p)}^{\dagger}\,\Phi_{(\bar{k}_l)}\omega_{\bar{k}_l}^{\dagger}=\omega_{k_p}^{\dagger} \tag{3.49}$$

Similarly, multiplication by $\widetilde{\Phi}_{(\bar{k}_p)}^{\dagger}$results in:

$$\sum_{l=1}^{M}\widetilde{\Phi}_{(\bar{k}_p)}^{\dagger}\,\Phi_{(k_l)}\omega_{k_l}^{\dagger}=\omega_{\bar{k}_p}^{\dagger} \tag{3.50}$$

By applying the continuity equation 3.46 and equations 3.49 and 3.50, the Green's function equation (equation 3.49) can be expressed as:

$$\sum_{l=1}^{M}\sum_{p=1}^{M}H_1^{\dagger}\left(\Phi_{(\bar{k}_l)}e^{-i\bar{k}_l}\widetilde{\Phi}_{(\bar{k}_l)}^{\dagger}-\Phi_{(k_l)}e^{-ik_l}\widetilde{\Phi}_{(k_l)}^{\dagger}\right)\Phi_{(\bar{k}_p)}\omega_{\bar{k}_p}^{\dagger}=I \tag{3.51}$$

Therefore, it follows that:

$$\sum_{l=1}^{M}\left[H_1^{\dagger}\left(\Phi_{(\bar{k}_l)}e^{-i\bar{k}_l}\widetilde{\Phi}_{(\bar{k}_l)}^{\dagger}-\Phi_{(k_l)}e^{-ik_l}\widetilde{\Phi}_{(k_l)}^{\dagger}\right)\right]^{-1} = \sum_{p=1}^{M}\Phi_{(\bar{k}_p)}\omega_{\bar{k}_p}^{\dagger}=\sum_{p=1}^{M}\Phi_{(k_p)}\omega_{k_p}^{\dagger} \tag{3.52}$$

This provides an expression for $\omega_k^{\dagger}$ immediately:

$$\omega_k^{\dagger}=\widetilde{\Phi}_{(k)}^{\dagger}\nu^{-1} \tag{3.53}$$

where the variable v is defined:

$$\nu=\sum_{l=1}^{M}H_1^{\dagger}\left(\Phi_{(\bar{k}_l)}e^{-i\bar{k}_l}\widetilde{\Phi}_{(\bar{k}_l)}^{\dagger}-\Phi_{(k_l)}e^{-ik_l}\widetilde{\Phi}_{(k_l)}^{\dagger}\right) \tag{3.54}$$

Equation 3.53 represents the wave number (k), which represents both left and moving states. By substituting equation 3.53 into equation 3.45, the Green's function of an infinite system is obtained.

$$g_{z,z'}^{\infty}=\begin{cases}\sum_{l=1}^{M}\Phi_{(k_l)}e^{ik_l(z-z')}\widetilde{\Phi}_{(k_l)}^{\dagger}\nu^{-1}, & z\geq z'\\ \sum_{l=1}^{M}\Phi_{(\bar{k}_l)}e^{i\bar{k}_l(z-z')}\widetilde{\Phi}_{(\bar{k}_l)}^{\dagger}\nu^{-1}, & z\leq z'\end{cases} \tag{3.55}$$

In order to obtain the Green's function for a semi-infinite lead, it is necessary to add a wave function into the Green's function. This means the boundary conditions at the edge of the lead are

satisfied, similar to the one-dimensional case. Here, the boundary condition requires that the Green's function disappears at a specific location ($z = z_o$). In order to achieve this.

$$\Delta = -\sum_{l,p=1}^{M} \Phi_{\bar{k}_l} e^{i\bar{k}_l(z-z_o)} \widetilde{\Phi}^{\dagger}_{(\bar{k}_l)} \Phi_{(k_p)} e^{ik_p(z_o-z)} \widetilde{\Phi}^{\dagger}_{(k_p)} \nu^{-1} \tag{3.56}$$

Equation 3.55 for Green's function states that $g = g^{\infty} + \Delta$. This produces the surface Green's function for a semi-infinite lead in the left direction:

$$g_L = \left(I - \sum_{l,p=1}^{M} \Phi_{(\bar{k}_l)} e^{-i\bar{k}_l} \widetilde{\Phi}^{\dagger}_{(\bar{k}_l)} \Phi_{(k_p)} e^{ik_p} \widetilde{\Phi}^{\dagger}_{(k_p)} \right) \nu^{-1} \tag{3.57}$$

and continuing right:

$$g_R = \left(I - \sum_{l,p=1}^{M} \Phi_{(k_l)} e^{ik_l} \widetilde{\Phi}^{\dagger}_{(k_l)} \Phi_{(\bar{k}_p)} e^{-i\bar{k}_p} \widetilde{\Phi}^{\dagger}_{(\bar{k}_p)} \right) \nu^{-1} \tag{3.58}$$

To complete the process, we need to get the Hamiltonian of the scattering region using Density Functional Theory (DFT). Then, we can combine this with the surface Green's functions using Dyson's equation. This will allow us to get the overall Green's function and the transmission amplitude t_{kl} [16].

$$G_{total} = \left[\begin{pmatrix} g_L & 0 \\ 0 & g_R \end{pmatrix} - H_{scattering} \right] \tag{3.59}$$

$$t_{kl} = \widetilde{\Phi}^{\dagger}_{(k_l)} G_{total} v \Phi_{(k_l)} \sqrt{\frac{v_k}{v_l}}\, e^{ik_l} \tag{3.60}$$

3.5 Summary

This chapter explores the Landauer formula, which relates to the electrical conductance G and thermoelectric coefficients to the transmission coefficient. This chapter explains the method of calculating the scattering matrix of a system connected to one-dimensional leads using the Green's function approach within scattering theory. This was generalised to higher-dimensional transport calculations, which provides the basis for the GOLLUM transport code and will be used in the next chapters.

3.6 Bibliography

[1] Spatial Variation of Currents and Fields Due to Localized Scatterers in Metallic Conduction. R. Landauer, *IBM Journal of Research and Development*, 1(3), 223–231, 1957.

[2] Giant Magnetoresistance and Quantum Transport in Magnetic Hybrid Nanostructures. S. Sanvito, PhD Thesis, Lancaster University, Lancaster, 1999. Accessed: May 03, 2024. [Online]. Available: https://eprints.lancs.ac.uk/id/eprint/133492/

[3] Generalized Many-Channel Conductance Formula with Application to Small Rings. M. Büttiker, Y. Imry, R. Landauer, and S. Pinhas, *Phys. Rev. B*, 31(10), 6207–6215, 1985.

[4] Relation Between Conductivity and Transmission Matrix. D. S. Fisher and P. A. Lee, *Phys. Rev. B*, 23(12), 6851–6854, 1981

[5] Conformation Dependence of Molecular Conductance: Chemistry Versus Geometry. C. M. Finch, S. Sirichantaropass, S. W. Bailey, I. M. Grace, V. M. García-Suárez, and C. J. Lambert, *J. Phys.: Condens. Matter*, 20(2), 022203, 2007.

[6] Electronic Transport in Mesoscopic Systems. S. Datta, Cambridge University Press, 1997

[7] Two or More Impurities; Disordered Systems. E. N. Economou, in *Green's Functions in Quantum Physics*, Berlin, Heidelberg: Springer, 128–195 1983

[8] Quantum Transport in Mesoscopic Systems: Complexity and Statistical Fluctuations, a Maximum-Entropy Viewpoint. P. A. Mello and N. Kumar, Oxford University Press, 2004

[9] The Single-Molecule Electrical Conductance of a Rotaxane-Hexayne Supramolecular Assembly. D. C. Milan et al., *Nanoscale*, 9(1), 355–361, 2017.

[10] Some Heteroskedasticity-Consistent Covariance Matrix Estimators with Improved Finite Sample Properties. J. G. MacKinnon and H. White, *Journal of Econometrics*, 29(3), 305–325, 1985.

[11] Conductance of 'Bare-Bones' Tripodal Molecular Wires. R. J. Davidson et al., *RSC Advances*, 8(42), 23585–23590, 2018

[12] Andreev Bound States for a Superconducting-Ferromagnetic Box. J. Koltai, J. Cserti, and C. J. Lambert, *Phys. Rev. B*, 69(9), 092506, Mar. 2004.

[13] Electronic Properties of Hybrid Carbon Nanotubes. S. Athanasopoulos, PhD Thesis, Lancaster University, 2005

[14] Connectivity Dependence of Fano Resonances in Single Molecules. A. K. Ismael, I. Grace, and C. J. Lambert, *Phys. Chem. Chem. Phys.*, 19(9), 6416–6421, Mar. 2017

[15] Andreev Drag Effect via Magnetic Quasiparticle Focusing in Normal-Superconductor Nanojunctions. P. K. Polinák, C. J. Lambert, J. Koltai, and J. Cserti, *Phys. Rev. B*, 74(13), 132508, Oct. 2006.

[16] Quantum Transport in Nanostructures and Molecules. P. C. J. Lambert, Institute of Physics Publishing, 2021

[17] An Understanding of the Electrical Characteristics of Organic Molecular Devices. C. M. Finch, PhD Thesis, Lancaster University, 2008

[18] Electronic Properties of Hybrid Carbon Nanotubes. S. Athanasopoulos, PhD Thesis, Lancaster University, 2005

[19] Thermoelectric Refrigeration. H. Goldsmid, Springer, 2013

Chapter 4

Quantum Interference in Molecules

4.1 Introduction

In the field of molecular electronics, one of the main challenges is to get a more in-depth understanding of the fundamental behaviour of electron transport through single-molecule junctions. In order to increase our understanding, many experimental techniques have been created to make contact with individual molecules. In recent years, it has become clear that the electrical properties of a molecular junction are controlled by the whole system, which includes both the electrodes and the molecule. As mentioned in chapter 1 and shown in Figure 1.2, there are several components that comprise a single-molecule junction including the molecular bridge, the two electrodes, and the two anchors. The anchors are used to connect the molecule to the electrodes. The fundamental characteristics of charge transport in a junction are greatly affected by the electrical connection between its individual components [1]. An isolated molecule has different energy levels, referred to as frontier orbitals (such as the HOMO and LUMO), while metal electrodes have a band structure that includes a continuum of states, with a precisely defined Fermi energy. Once these two components are close to each other, they interact with each other, which leads to different physical effects. Due to the fact that there is a transfer of charge between the two systems, the impact of donating or withdrawing electrons from the molecule has an effect not only on the energy levels of the molecule, but also on the contacts. The highest occupied molecular orbital (HOMO) and the lowest unoccupied molecular orbital (LUMO) may be moved upwards or downwards as a result of this charge transfer. This results in a slope in the transmission function at the Fermi level that is either more pronounced or less

pronounced [2]. Additionally, the position of the molecular orbitals in relation to the Fermi level of the electrodes is influenced by the chemical bonds that are present in the anchor group. These bonds are responsible for the chemical binding of the molecules to the electrodes. As noted in chapter 1, quantum interference (QI) effects have received great interest in the field of charge transport at the individual molecule level due to their remarkable ability to control the flow of charge through molecular materials and devices in experimental investigations, at a phase-coherent level [3-5]. By changing the conductance in molecular systems, it is possible to see a phenomenon called constructive quantum interference (CQI) or destructive quantum interference (DQI), depending on whether the conductance is increased or decreased, respectively [6].

4.2 Tight binding model and density functional theory calculations

A method that is used to compute electronic band structures is known as the tight-binding model (TBM) or the linear combination of atomic orbitals (LCAO) method. This method employs a set of wave functions that are produced from the superposition of wave functions of isolated orbitals that are located at each atomic site.

As noted in chapter 2, DFT is a technique that has the ability to solve the many-body Schrodinger equation by transforming it into a problem with electrons that do not interact with another one. In what follows, computations are carried out on benzene with specific connectivities, to illustrate the role of different kinds of linkers that are located between the benzene core and the anchor groups. DFT calculations were performed using a combination of SIESTA and GOLLUM and detailed comparisons with tight binding model (TBM) calculations are made.

As a typical example, benzene can be connected to lead either via meta connectivity or para connectivity, as shown in Figure 4.1. These are referred to as Meta-Benzene and Para-Benzene for reference. This Figure shows a comparison between TBM and DFT transmission coefficients for the two connectivities.

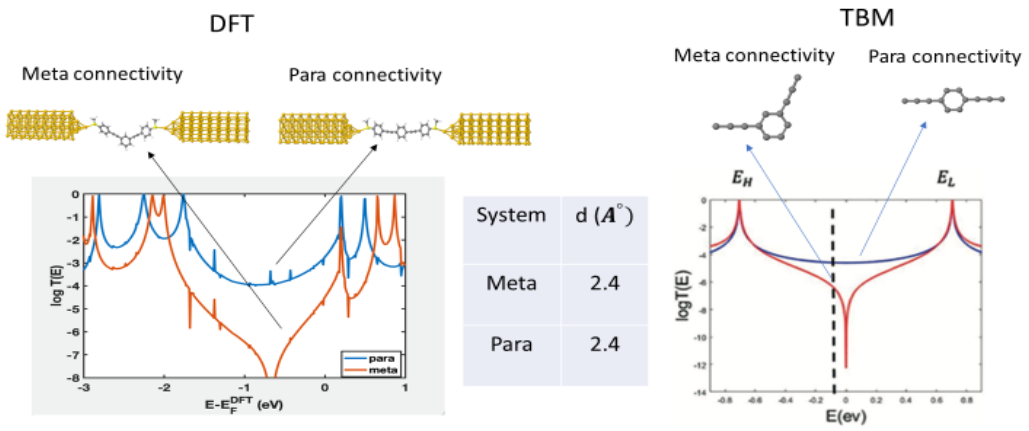

Figure 4.1: The transmission coefficients of Meta-Benzene and Para-Benzene by DFT and TBM respectively.

For both the meta and para connectivities, the right figure shows the transmission coefficients obtained from a tight binding model, where the centre of the HOMO-LUMO gap is located at $E = 0$. For the meta connectivity, the tight binding model clearly predicts destructive quantum interference (DQI), signaled by the presence of a transmission dip at the centre of the HOMO-LUMO gap, whereas for the para connectivity, constructive quantum interference (CQI) is predicted, corresponding to a smooth transmission coefficient near the gap centre.

Clearly these features are shared by the DFT calculation in the left figure, so the simple conceptual TBM on the right predicts the key features of the full DFT calculation on the left. The following figure shows the frontier molecular orbitals of the isolated molecules with meta and para connectivities:

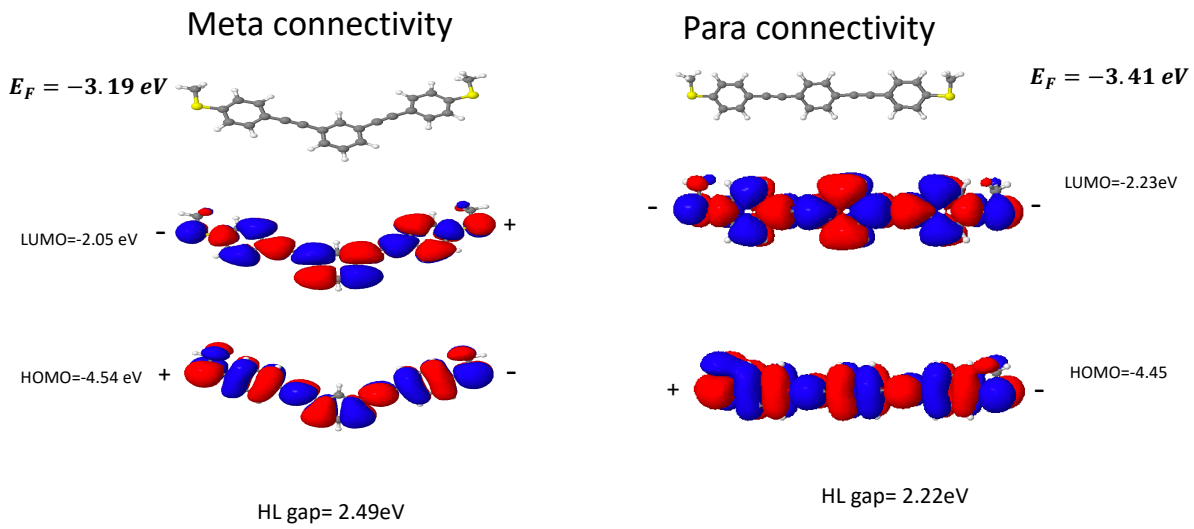

Figure 4.2: Shows meta and para wave functions.

From Figure 4.2, it is interesting that one can predict whether DQI or CQI is likely to occur by looking at the symmetry of the frontier molecular orbitals. The molecular orbitals are real and so the amplitude of the orbital could either be positive or negative. In Figure 4.2 for example, red is positive and blue is negative. Since these molecules are symmetric, their molecular orbitals must be either symmetric or antisymmetric, in agreement with Figure 4.2. This means that if the value of the orbital amplitude at the left end of a molecule is multiplied by the value of the orbital amplitude at the right end of the molecule, then the result 'orbital product' is either positive (eg

for the symmetric LUMO of the molecule on the right of Figure 4.2, the LUMO product is positive) or negative (eg for the antisymmetric HOMO of the molecule on the right the HOMO product is negative and for both the LUMO and HOMO of the molecule on the left the LUMO product and the HOMO product are both negative). According to an 'orbital product rule' [7,8] if the HOMO and LUMO products have opposite signs, as for the para-connected molecule on the right of Figure 4.2, then CQI is expected. On the other hand, if the HOMO and LUMO products have the same sign, as for the meta-connected molecule on the left of Figure 4.2, then DQI is expected. Clearly, this is in agreement with the DFT and TBM transmission curves of Figure 4.1. Finally, it should be noted that if the magnitudes of the HOMO and LUMO product are different, then the DQI dip will be positioned closer in energy to the orbital with the smaller magnitude of the product.

4.3 Examples of conjugated π_z systems

In what follows, I shall explore the occurrence of DQI and CQI in a variety of conjugated π_z systems. Examples of such systems are shown below.

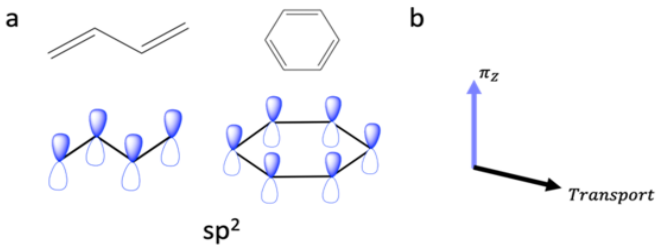

Figure 4.3: The molecular systems with one conjugated π system, namely a collection of π_z orbitals.

A typical conjugated π system consists of an array of coupled π_z orbitals, each located on a carbon atom. Basically, the HOMO and LUMO levels are formed from linear combinations of these π_z orbitals and so that's where all the electron transport takes a place. Since there is only a single π_z orbital on each carbon atom, we can produce a simple tight binding model to describe the key qualitative features. In contrast, as we shall see below, some conjugated π systems are formed from both π_z and π_x or π_y orbitals located on each atom, in which case the TBM model should be generalised to accommodate these extra degrees of freedom. In this case, we shall find that DQI dips that occur when there is a single π_z orbital on each carbon atom can be masked by the presence of additional π_x or π_y orbitals.

4.4 An example of connectivity table (C) and the magic number theory table (M) of the benzene ring

For a conjugated system with a single π_z orbital located on each atom, if the atoms are identical, then the simplest TBM Hamiltonian H is obtained by choosing the site energies to be zero (which corresponds to choose the energy origin to equal the site energies) and choosing the nearest neighbour Hamiltonian matrix elements to equal -1 (which corresponds to choosing the unit of energy equal to the nearest neighbour coupling), with all others equal to zero. With such a choice, find that $H = -C$, where C is a connectivity table, such that $C_{ij} = 1$ if atoms i and j are nearest neighbours and $C_{ij} = 0$ otherwise. As an example, the connectivity table of benzene is shown below. The Greens function for such a molecular core is $g(E) = (E - H)^{-1} = (E + C)^{-1}$ and since the middle of the HOMO=LUMO gap is $E = 0$, the mid-gap greens function, arising at $E = 0$ is $g = C^{-1}$. To make it easy to picture the structure of g, magic number theory introduces a magic number table M, defined to be $M = ag = aC^{-1}$, where a is

any convenient constant. For the benzene core described by the above simple TBM, choosing $a = 2$ yields the magic number table M shown below. (As a check the reader can verify that $MC = 2I$, where I is the unit matrix.)

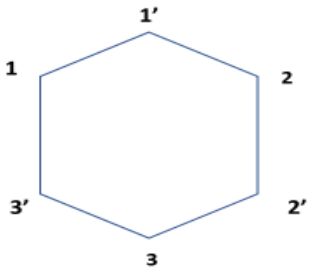

C =

	1	2	3	1`	2`	3`
1	0	0	0	1	0	1
2	0	0	0	1	1	0
3	0	0	0	0	1	1
1`	1	1	0	0	0	0
2`	0	1	1	0	0	0
3`	1	0	1	0	0	0

M=

	1	2	3	1`	2`	3`
1	0	0	0	1	-1	1
2	0	0	0	1	1	-1
3	0	0	0	-1	1	1
1`	1	1	-1	0	0	0
2`	-1	1	1	0	0	0
3`	1	-1	1	0	0	0

Table 4.1. The connectivity table C and magic number table M of benzene.

The magic number theory [7-11] notes that provided the Fermi energy of the electrodes is close to the middle of the HOMO-LUMO gap, then if the linkers connecting the molecular core to the electrodes are connected to sites i and j of the core, the electrical conductance σ_{ij} is proportional to $|g_{ij}|^2 = a^2|M_{ij}|^2$. For benzene, Table 4.1 shows that the magic number table is block off diagonal, so that M_{ij} and σ_{ij} are zero if i and j are both odd or both even. Such connectivities correspond to a meta connected core and therefore magic number theory predicts DQI for meta connected benzene, in agreement with Figure 4.1. On the other hand, if i is odd and j is even, or vice versa, M_{ij} and σ_{ij} are non-zero and therefore for such para or ortho connectivites, magic

number predicts a non-zero mid-gap transmission coefficient, again in agreement with Figure 4.1.

Similarly, for a molecule with the same core, but linkers connected to sites l, m, the electrical conductance σ_{lm} is proportional to $|g_{lm}|^2$. This means that the ratio of the conductance corresponding to the two different connectivities is $\frac{\sigma_{ij}}{\sigma_{lm}} = \frac{|g_{ij}|^2}{|g_{lm}|^2} = \frac{|M_{ij}|^2}{|M_{lm}|^2}$. In the last step, the arbitrary constant a has cancelled, so that the conductance ratio is obtained simply by looking up the numbers M_{ij} and M_{lm} from the magic number table.

4.5 The effect of introducing a single heteroatom

Magic numbers, or equivalently the core mid-gap Greens function g can also be used to predict the effect of introducing a single heteroatom into a 'parent' conjugated π system, for example by substituting a nitrogen atom into for example naphthalene as shown in Figure 4.4. After heteroatom substitution into site l, if the site energy is changed from zero to ϵ_l, then the Green's function G of the resulting 'daughter molecule' can be computed by using Dyson's equation [7], which takes the form

$$G_{ij} = g_{ij} + \frac{g_{il}\,\varepsilon_l g_{lj}}{1 - g_{ll}\varepsilon_l} \qquad (4.1)$$

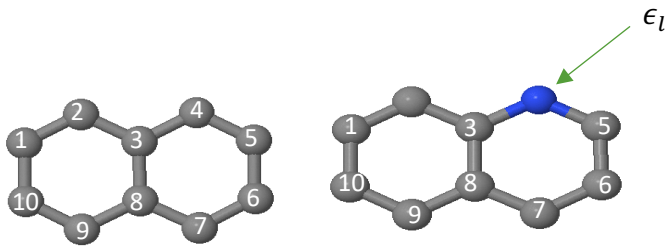

Figure 4.4: In this figure, (Left) A lattice of sites representing the connectivity of naphthalene. (Right) A lattice of sites representing the connectivity of quinoline, in which the site energy of site l = 4 is perturbed by the presence of a nitrogen atom, coloured blue.

From the magic number table of the parent, shown in Table 4.1, $g_{ll} = 0$, so equation (1) simplifies to

$$G_{ij} = g_{ij} + g_{il}\varepsilon_l g_{lj} \qquad (4.2)$$

This equation represents the mid-gap Green's function of the parent in the presence of the heteroatom.

From equation (4.2), this formula predicts that if we place the nitrogen in a certain site, it may have no effect and if we place the nitrogen somewhere else, may have a large effect. For example, if i is odd and j is odd, then$g_{ij} = 0$ and the parent exhibits DQI. In this case, if l is odd, G_{ij} is also zero, DQI persists and the heteroatom as a negligible effect. On the other hand, if l is even, the second term in (4.2) is non-zero. This means that $G_{ij} \neq 0$, DQI is alleviated and the heteroatom causes a large increase in conductance.

For the case where i is odd and j is even or vice versa, $g_{ij} \neq 0$ and the parent exhibit CQI. In this case, $g_{il}\varepsilon_l g_{lj}$ is zero for any choice of l, so the daughter also exhibits CQI and the heteroatom has a negligible effect.

This shows that magic numbers are important for understanding the impact of introducing a heteroatom into a conjugated π system.

4.6 Studied Molecules

In what follows, the aim will be to study CQI and DQI in the following molecules, which have different cores and different linkers to the electrodes. One reason for studying these molecules is that the carbon atoms within the carbon chains possess π_z or π_y orbitals, so that these molecules will reveal the effect on QI of these more complex π systems.

1

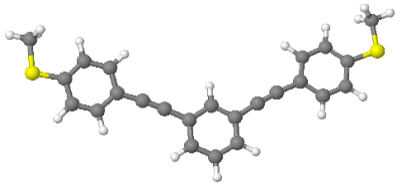

2

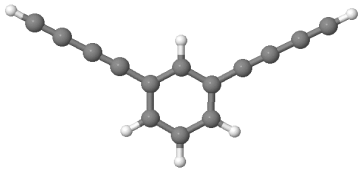

3

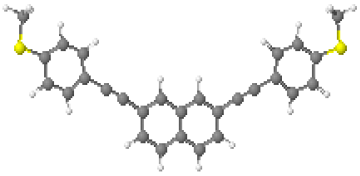

4

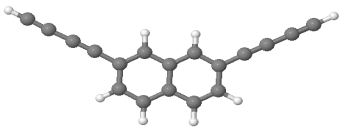

5

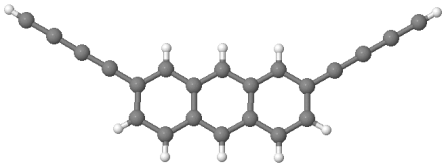

Figure 4.5: Shows the five studied molecules.

4.7 Transmission coefficient

The transmission coefficients $T(E)$ for the above molecules, with various anchors and linkers, are calculated using DFT. Initially, the molecules are relaxed using the SIESTA software program. Finally, the $T(E)$ values are calculated for molecules using different linkers and anchors, and their CQI or DQI characteristics are related to connectivity.

4.8 Transmission coefficients for the benzene with different linkers connected to gold electrodes and an increasing number of central rings (naphthalene and anthracene) and the tight binding model results:

The DFT-based transmission coefficients $T(E)$ for molecule 1, with and without heteroatoms are shown in Figure 4.6, while Figure 4.7 shows their TBM transmission coefficients, along with the bond currents within the molecular core, occurring when electrons are injected at $E = 0$. One questions of interest is whether or not the predictions of section 4.5, which assumes that there is

only a single π orbital per atom, remain correct when both πz or πy orbitals are present in the pairs of carbon atoms within the linkers.

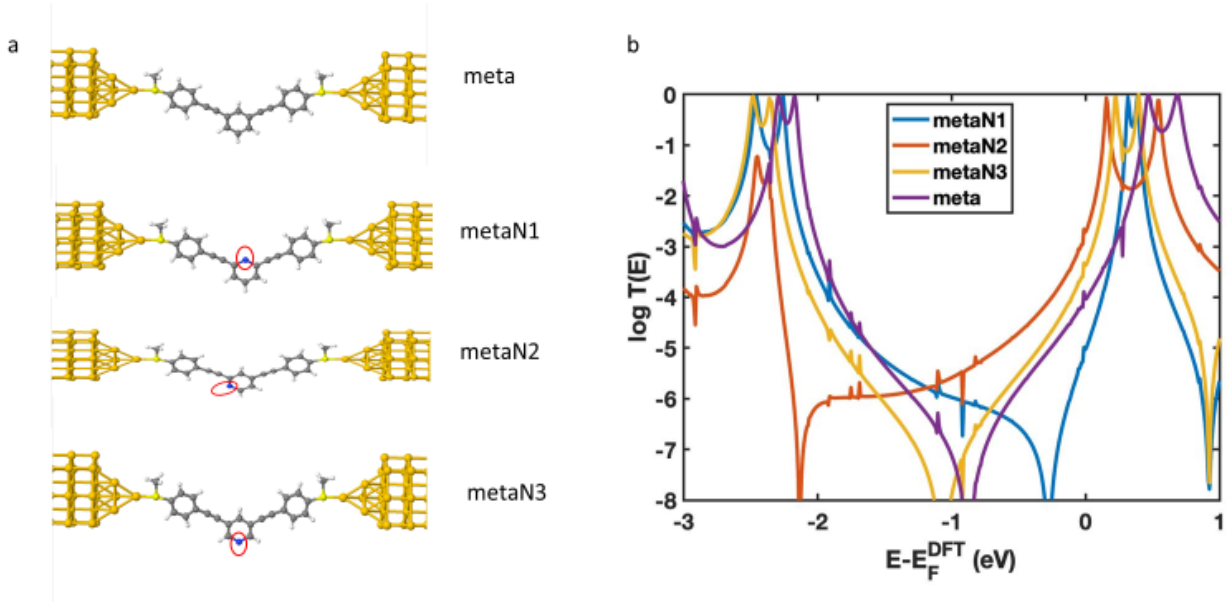

Figure 4.6**:** DFT-based transmission functions for the parent benzene (one phenyl ring) connected to the gold via SMe-anchor at meta connectivity. For the heteroatom-substituted daughters, the N atoms are indicated by red circles.

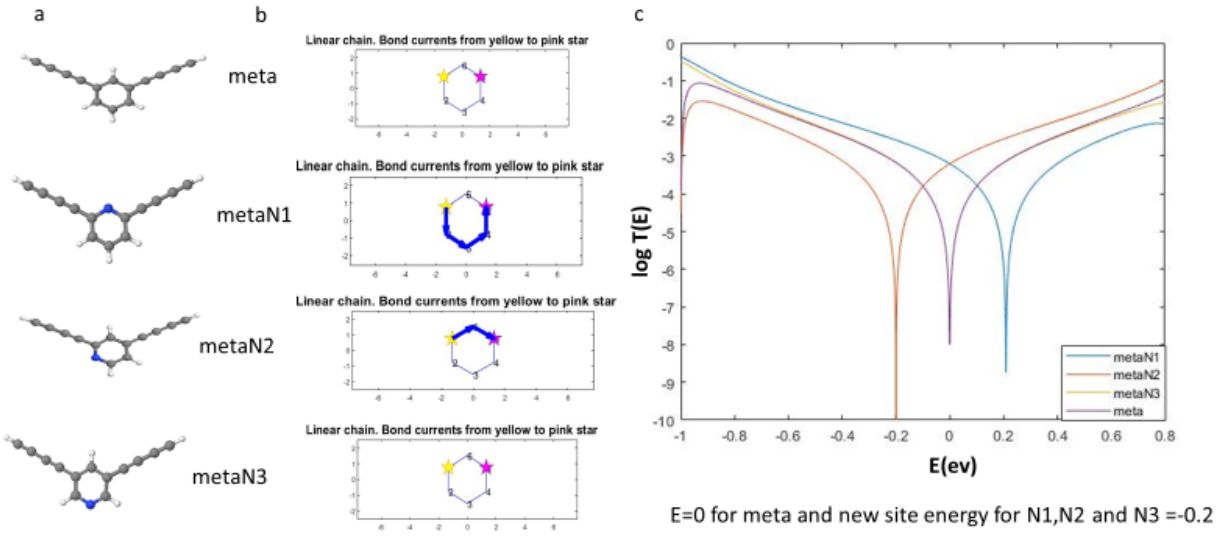

Figure 4.7: TBM results for transmission functions of the parent benzene (one phenyl ring) connected to the gold via SMe-anchor at meta connectivity, along with the heteroatom-substituted daughters.

From Figure 4.6, in the top graph, we see that the core is meta connected to the linkers, and the atoms i and j are both odd. Therefore, for the parent, as expected, a DQI transmission dip is present near the middle of the HOMO-LUMO gap. When a nitrogen heteroatom is inserted into an even numbered site, to yield the daughters metaN2 and metaN1, this alleviates the DQI near the middle of the HOMO LUMO gap, in agreement with the discussion in section 4.5. In contrast, when a nitrogen heteroatom is inserted into an odd numbered site, to yield the daughters metaN3, the DQI dip near the middle of the HOMO LUMO gap persists, again in agreement with the discussion in section 4.5.

If we compare the DFT calculation in Figure 4.6 and the TBM results in Figure 4.7, we find that the tight binding model is in qualitative agreement with the DFT calculations. (In this case the transmission curves of the parent and the daughter metaN3 are identical.) So, the simple conceptual TBM, which assumes only a single π orbital per atom, correctly predicts the key features of the full DFT calculation, even though both π_z or π_y orbitals are present in the pairs of carbon atoms within the linkers.

4.9 Wave functions for meta, metaN1, metaN2 and metaN3 with anchor groups of the benzene

To apply the orbital product rule, the frontier orbitals of both the parent and daughters are shown below.

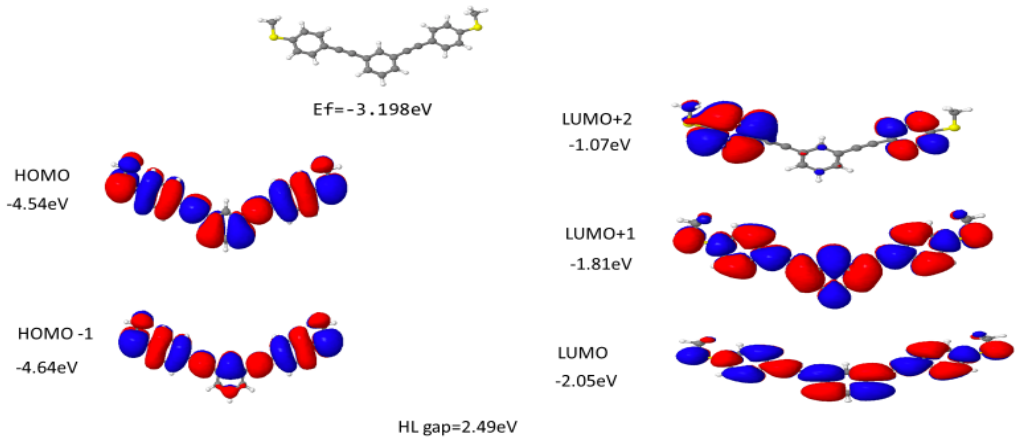

Figure 4.8: Frontier molecular orbitals of a meta-studied molecule with its eigenvalues obtained from DFT, where red represents positive and blue indicates negative regions of the wave functions.

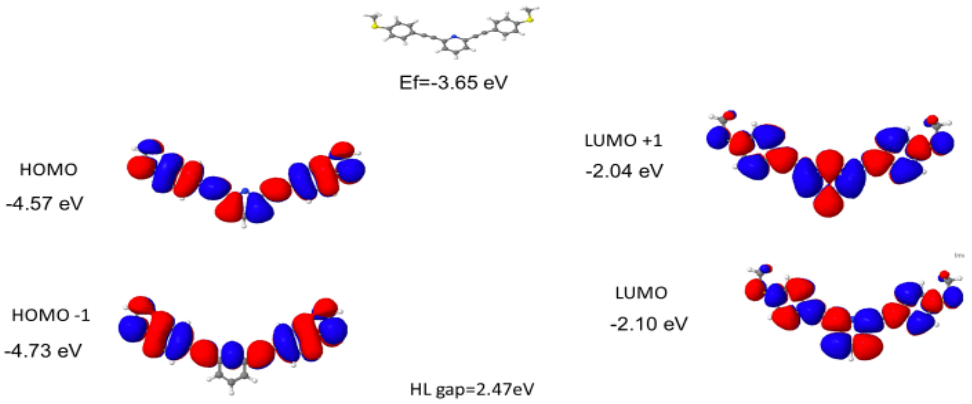

Figure 4.9: Frontier molecular orbitals of metaN1 studied molecule with its eigenvalues obtained from DFT, where red represents positive and blue indicates negative regions of the wave functions.

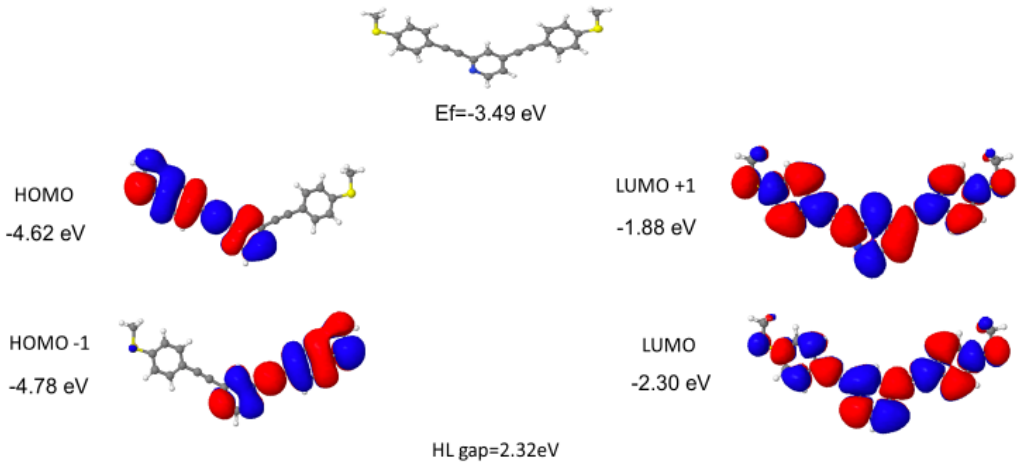

Figure 4.10: Frontier molecular orbitals of metaN2 studied molecule with its eigenvalues obtained from DFT, where red represents positive and blue indicates negative regions of the wave functions.

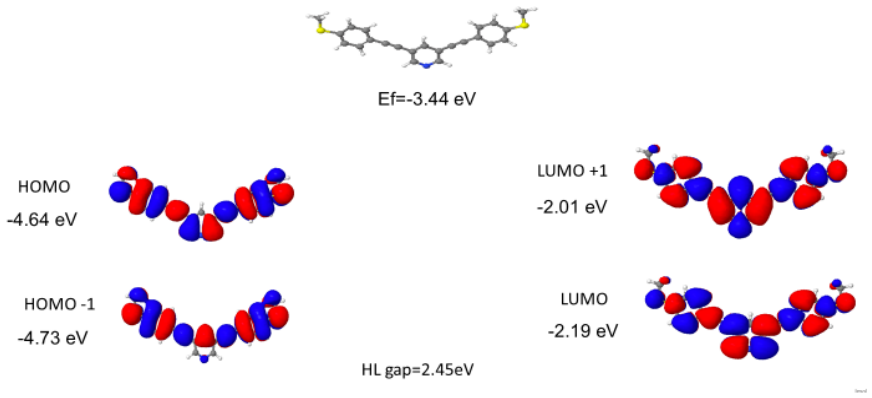

Figure 4.11: Frontier molecular orbitals of metaN3 studied molecule with its eigenvalues obtained from DFT, where red represents positive and blue indicates negative regions of the wave functions.

According to the product rule, if the HOMO product and LUMO product have the same sign, then DQI is expected, whereas if they have different signs, COI is predicted. From Figures 4.8, 4.9 and 4.11, the HOMO and LUMO products have the same sign, so DQI is predicted to occur somewhere within the HOMO-LUMO gap. As noted in section 4.2, if the magnitudes of the HOMO and LUMO product are different, then the DQI dip will be positioned closer in energy to the orbital with the smaller magnitude of the product. This is the reason why, as shown in Figure 4.6, the DQI dip of metaN1 is closer to the LUMO and the DQI dip of metaN2 is closer to the HOMO. From Figure 4.10 we cannot apply the product rule because the right side of the HOMO is too small to assign a sign.

Figure 4.6 shows that there is in fact a DQI dip and since the HOMO product is small, the dip lies closer to the HOMO.

The above results that the magic number theory predicts the shifting of these DQI dips, even though both π_z or π_y orbitals are present in the pairs of carbon atoms within the linkers. To check if this is generally true, we change the linker between the central benzene and the anchor group into just four carbon atoms (ie two triple bonds in each linker) and repeat the above analysis. The new set of molecules are shown in Figure 4.12. In these molecules the carbon atoms in the linkers each possess both π_z or π_y orbitals, as shown in Figure 4.13.

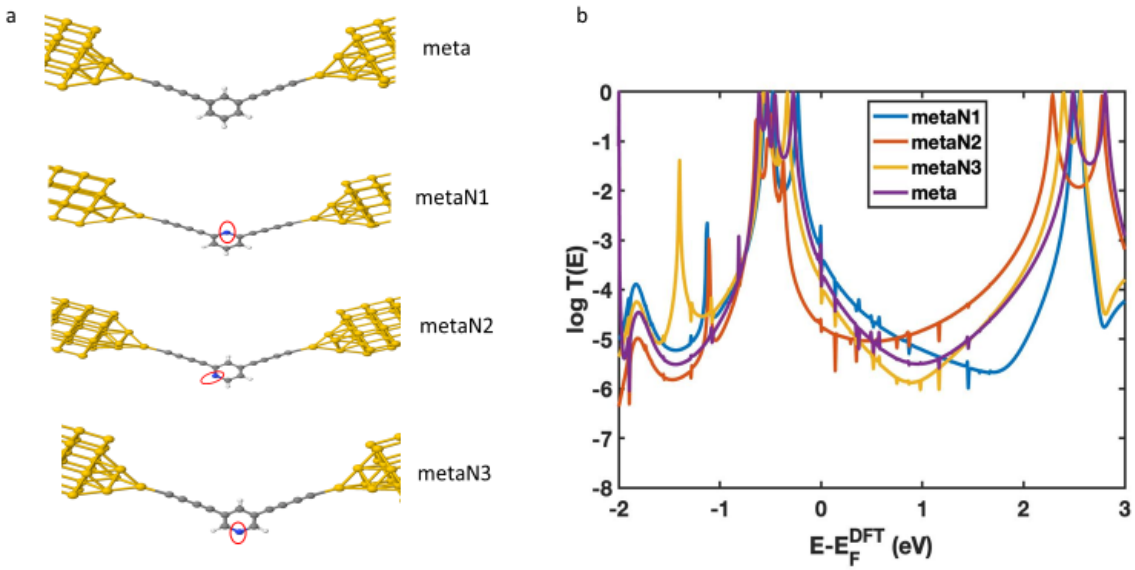

Figure 4.12: DFT-based transmission functions for benzene (one phenyl ring) with linkers composed of 4 carbon atoms (ie two triple bonds) and meta connectivity. The N atom is indicated by red circles.

Comparing the DFT-based transmission curves in Figure 4.12, with those of Figure 4.6, we see that this change in the linkers has caused the DQI dips to disappear. Our task now is to understand the origin of this disappearance. As a first step, I computed the frontier orbitals of these molecules and present them in section 4.11.

4.10 Examples of conjugated π_Z and π_Y systems

In what follows, I shall explore the occurrence of DQI and CQI in a variety of conjugated π_z and π_y systems. Examples of such systems are shown below.

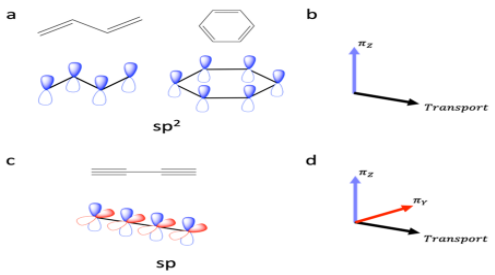

Figure 4.13: A comparison between molecules with a π_z system (a) and a molecule (c) with two π systems, i.e. π_z and π_y.

4.11 Wave functions for meta, metaN1, metaN2 and metaN3 with triple bombs of the benzene

To implement the orbital product rule, the frontier orbitals of the above molecules are shown below.

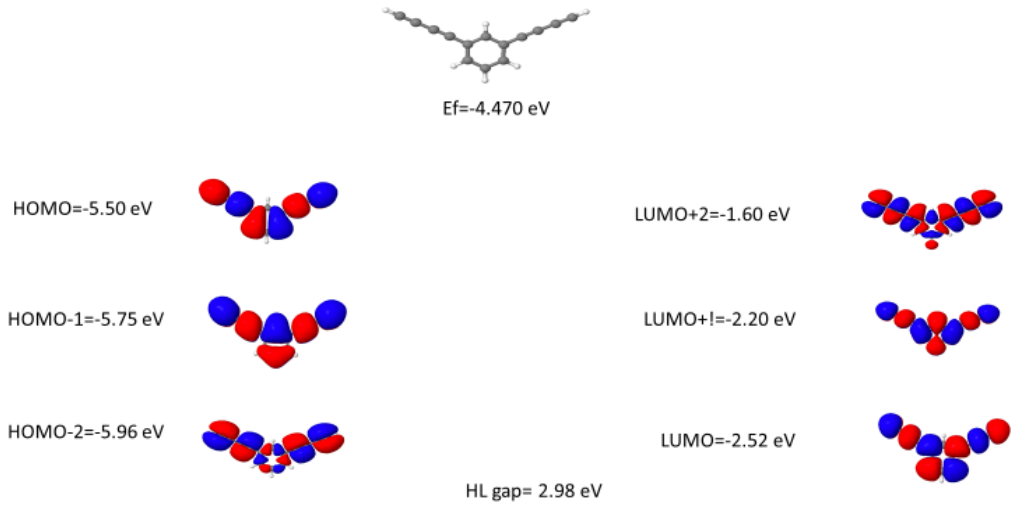

Figure 4.14: Frontier molecular orbitals of a meta-studied molecule with its eigenvalues obtained from DFT, where red represents positive and blue indicates negative regions of the wave functions

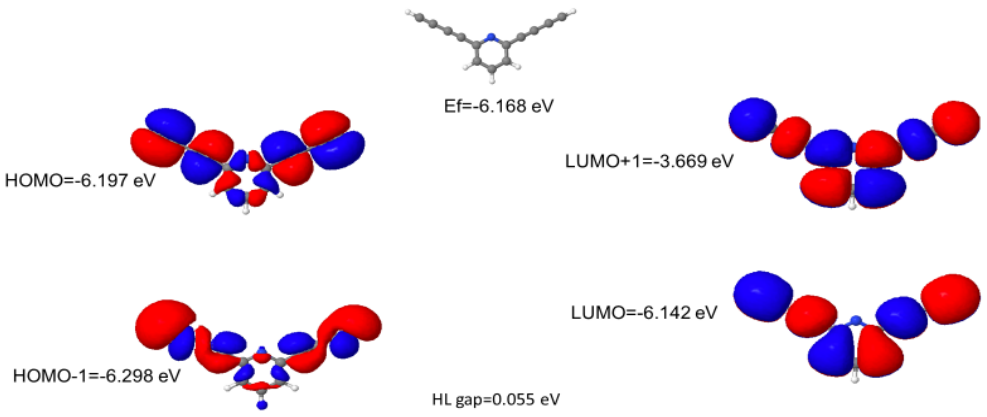

Figure 4.15 Frontier molecular orbitals of metaN1 studied molecule with its eigenvalues obtained from DFT, where red represents positive and blue indicates negative regions of the wave functions

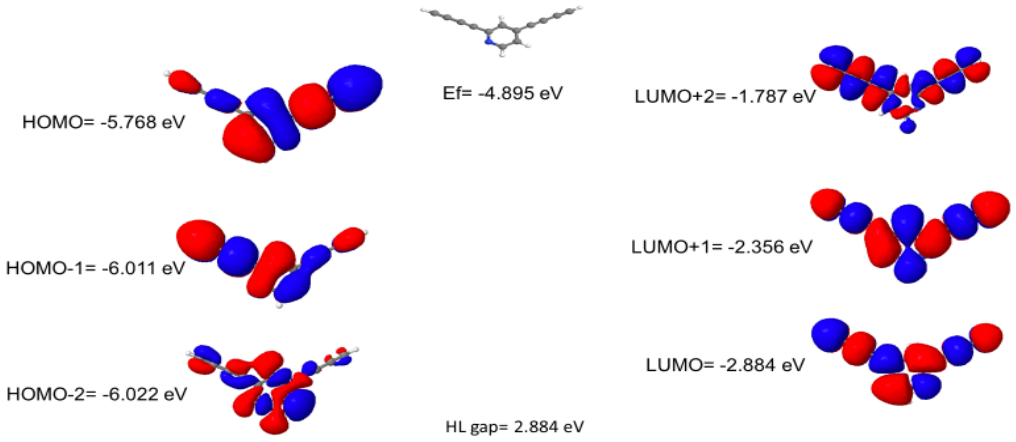

Figure 4.16 Frontier molecular orbitals of metaN2 studied molecule with its eigenvalues obtained from DFT, where red represents positive and blue indicates negative regions of the wave functions

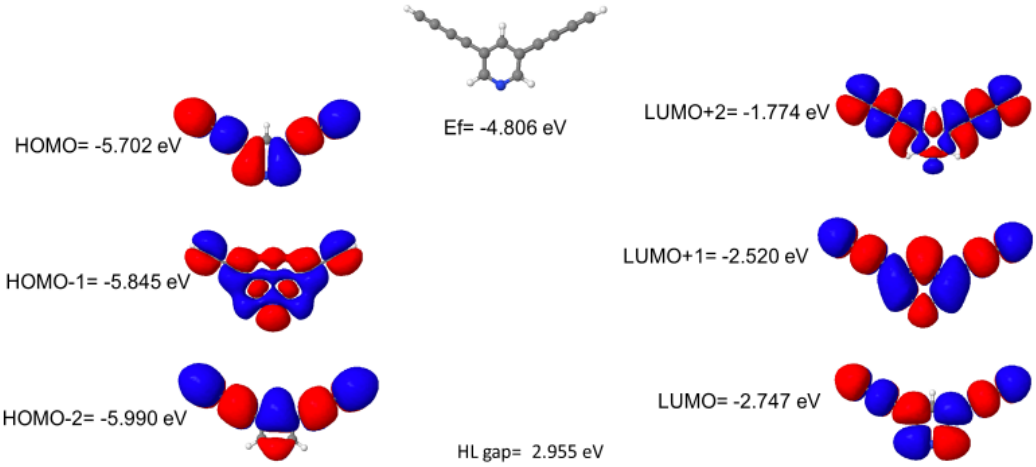

Figure 4.17: Frontier molecular orbitals of metaN3 studied molecule with its eigenvalues obtained from DFT, where red represents positive and blue indicates negative regions of the wave functions

In all cases of Figure 4.14,4.15,4.16 and 4.17, the HOMO and LUMO orbital products have the same sign and therefore the orbital product rule predicts DQI, in contrast with the absence of DQI dips in Figure 4.12.

To understand why the second π system in the triple bonds cause the DQI dips to disappear, we speculate that the π_y system will couple to the sigma orbitals in the central benzene ring. and facilitate the transmission of electrons through the sigma orbitals of the benzene ring. So, even if the π_z system shows DQI and does not transmit any electrons, the sigma orbitals can couple to the π_y system of the triple bonds and still allow electrons to be transmitted. Consequently, the total transmission function does not exhibit a DQI dip, even though the π_z system is subject to DQI. Typically, sigma bonds do not transmit electrons very well at all, but for the benzene ring, it is small but not zero and becomes the dominant transmission mechanism when transmission

through the π_z system is absent. Transmission through the sigma system of a molecular core is expected to decay rapidly as the size of the core (or distance between the contacts to the core) increases.

So, if we increase the size of the central core, those sigma orbitals would not be able to transmit electrons at all. To test this hypothesis, we increase the number of rings in the central core, by replacing the benzene by either naphthalene (two rings) or anthracene (three rings). If the hypothesis is correct, then the sigma systems of naphthalene and anthracene should be much worse at transmitting electrons than the sigma system of benzene and the effect of the π_y of the triple bonds should become negligible, thereby causing the DQI dip to appear.

4.12 An example of connectivity table (C) and the magic number theory table (M) of naphthalene rings

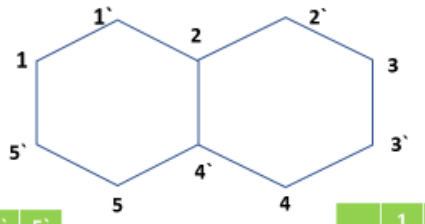

C =

	1	2	3	4	5	1`	2`	3`	4`	5`
1	0	0	0	0	0	1	0	0	0	1
2	0	0	0	0	0	1	1	0	1	0
3	0	0	0	0	0	0	1	1	0	0
4	0	0	0	0	0	0	0	1	1	0
5	0	0	0	0	0	0	0	0	1	1
1`	1	1	0	0	0	0	0	0	0	0
2`	0	1	1	0	0	0	0	0	0	0
3`	0	0	1	1	0	0	0	0	0	0
4`	0	1	0	1	1	0	0	0	0	0
5`	1	0	0	0	1	0	0	0	0	0

M =

	1	2	3	4	5	1`	2`	3`	4`	5`
1	0	0	0	0	0	-2	1	-1	1	-1
2	0	0	0	0	0	-1	-1	1	-1	1
3	0	0	0	0	0	1	-2	-1	1	-1
4	0	0	0	0	0	-1	2	-2	-1	1
5	0	0	0	0	0	2	-1	1	-1	-2
1`	-2	-1	1	-1	2	0	0	0	0	0
2`	1	-1	-2	2	-1	0	0	0	0	0
3`	-1	1	-1	-2	1	0	0	0	0	0
4`	1	-1	1	-1	-1	0	0	0	0	0
5`	-1	1	-1	1	-2	0	0	0	0	0

Table 4.2. The connectivity table C and magic number table M of naphthalene.

Table 4.2 shows the connectivity table and magic number table of naphthalene. The zeros in the latter show that mid-gap DQI is expected of the labels i and j of the site which connect to the linkers are either both odd or both even.

To test the above hypothesis, I calculated the transmission functions of the parent naphthalene and a selection of heteroatom-substituted daughters, when the labels i and j of the site which connect to the linkers are both odd. I shall refer to this as meta connectivity. First, I chose the linkers to contain a benzene ring and two carbon atoms, as shown in Figure 4.18. The resulting DFT-based transmission curves are shown in Figure 4.18 and the corresponding TBM-based curves are shown in Figure 4.19.

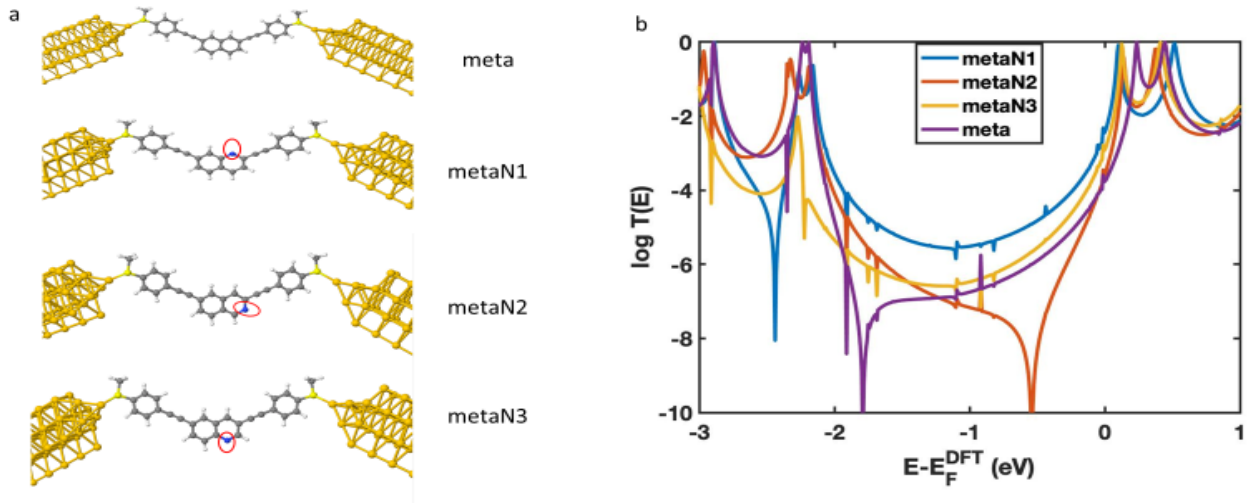

Figure 4.18: DFT-based transmission functions for naphthalene (two phenyl rings) connected to the gold via SMe-anchor at meta connectivity. The N atom is indicated by red circles.

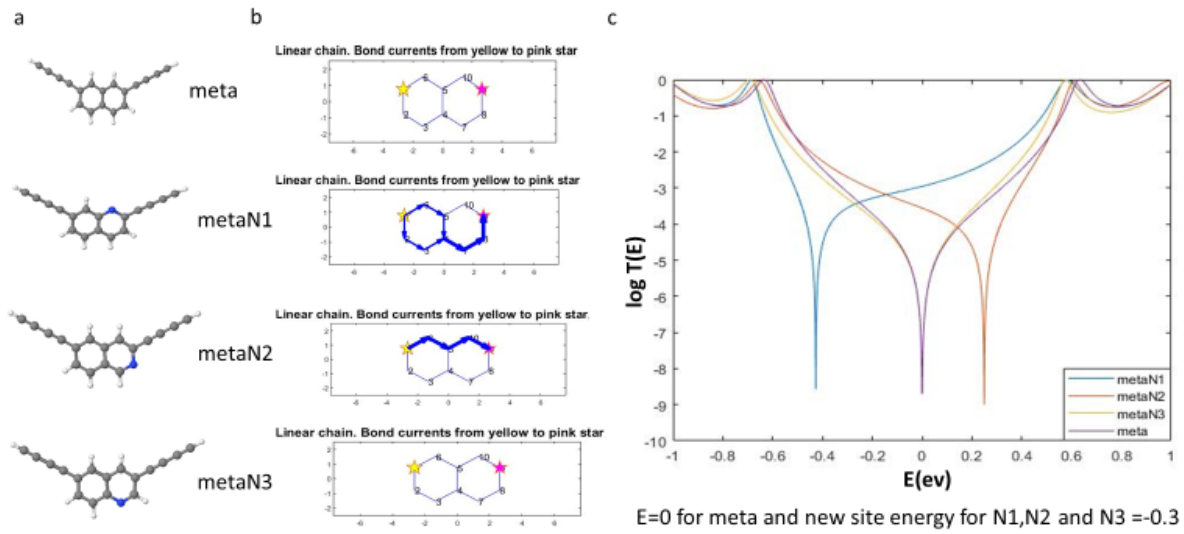

Figure 4.19: Tight binding model result for naphthalene.

For this meta connectivity, within the TBM, we expect the parent naphthalene to exhibit mid-gap DQI and mid-gap DQI to persist for metaN3, because the heteroatom is placed on an odd numbered site. In contrast, for metaN2 and meta N1, where the heteroatom is place on an even numbered site, Dyson's equation predicts that the mid-gap DQI will be alleviated and the dip will shift away from the mid-gap. Figure 4.19 agrees with these predictions.

In Figure 4.19, we find that the tight binding model predicts DQI dips within the gap for meta, meta N1, metaN2 and meta N3. In contrast, the DFT calculations in Figure 4.18 shows clear dips within the gap for meta and metaN2, but not obviously for metaN1 and metaN3. In fact, there are narrow DQI dips for metaN1 and metaN3 close to the HOMO resonance, so in this sense there is qualitative agreement between the TBM and DFT.

4.13 Wave functions for meta, metaN1, metaN2 and metaN3 with anchor groups of naphthalene

To implement the orbital product rule, the following figures show the frontier orbitals.

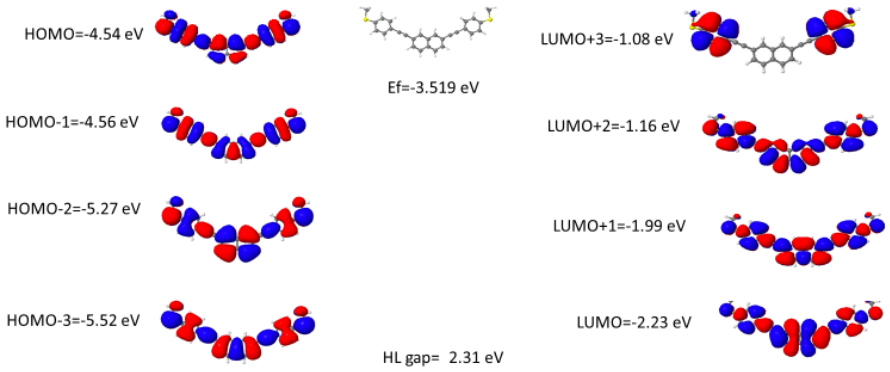

Figure 4.20: Frontier molecular orbitals of a meta-studied molecule with its eigenvalues obtained from DFT, where red represents positive and blue indicates negative regions of the wave functions

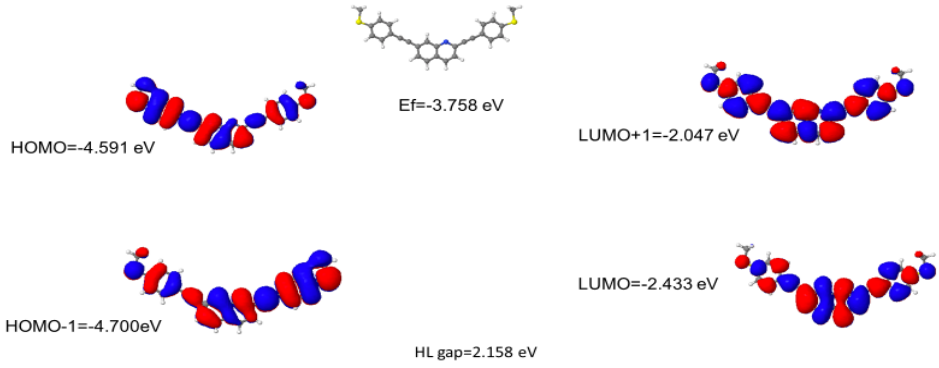

Figure 4.21: Frontier molecular orbitals of metaN1 studied molecule with its eigenvalues obtained from DFT, where red represents positive and blue indicates negative regions of the wave functions

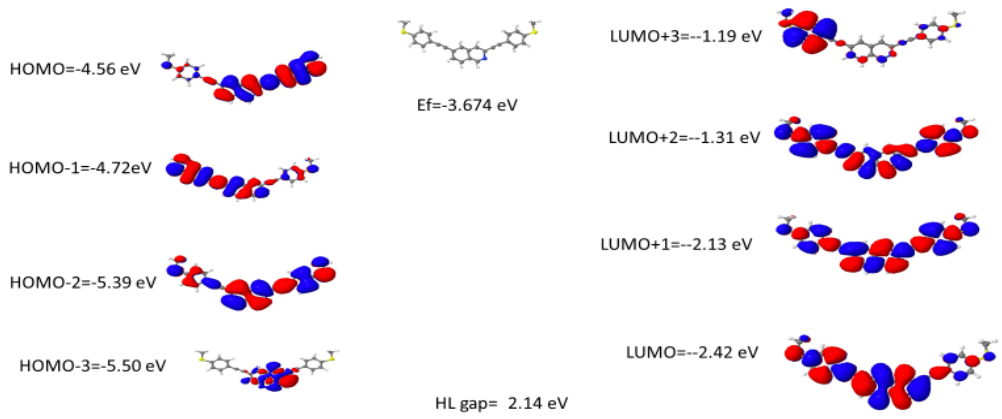

Figure 4.22: Frontier molecular orbitals of metaN2 studied molecule with its eigenvalues obtained from DFT, where red represents positive and blue indicates negative regions of the wave functions

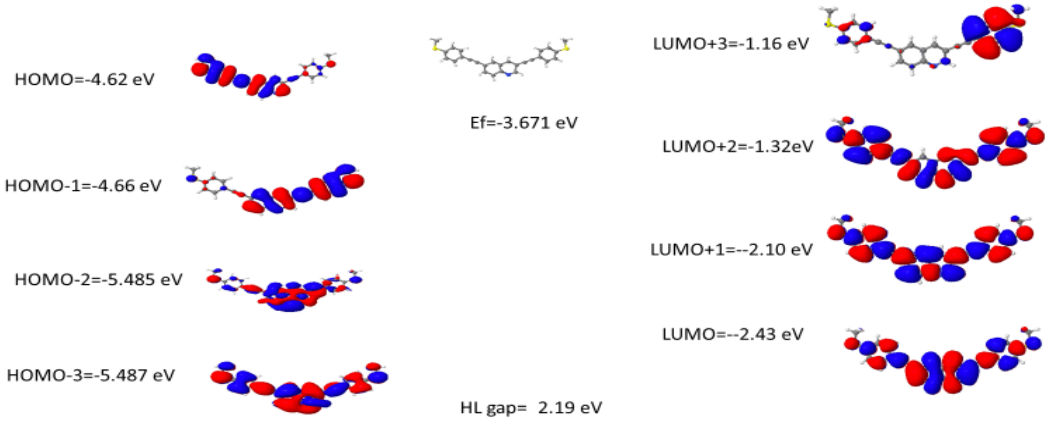

Figure 4.23: Frontier molecular orbitals of metaN3 studied molecule with its eigenvalues obtained from DFT, where red represents positive and blue indicates negative regions of the wave functions.

The HOMO and LUMO products of meta in Figure 4.20 have the same sign and therefore DQI is predicted.

The HOMO and LUMO products of metaN1 in Figure 4.21 have the opposite signs and therefore CQI is predicted, in agreement with the DFT calculations. The orbital product rule cannot be applied in the other cases (Figures 4.22 and 4.23), because the HOMO amplitude is too small at one end of the molecules.

To test the above hypothesis, I now repeat these calculations with linker formed from two triple bonds (ie each with four carbon atoms). The molecules and their DFT-based transmission curves are shown in Figure 4.24.

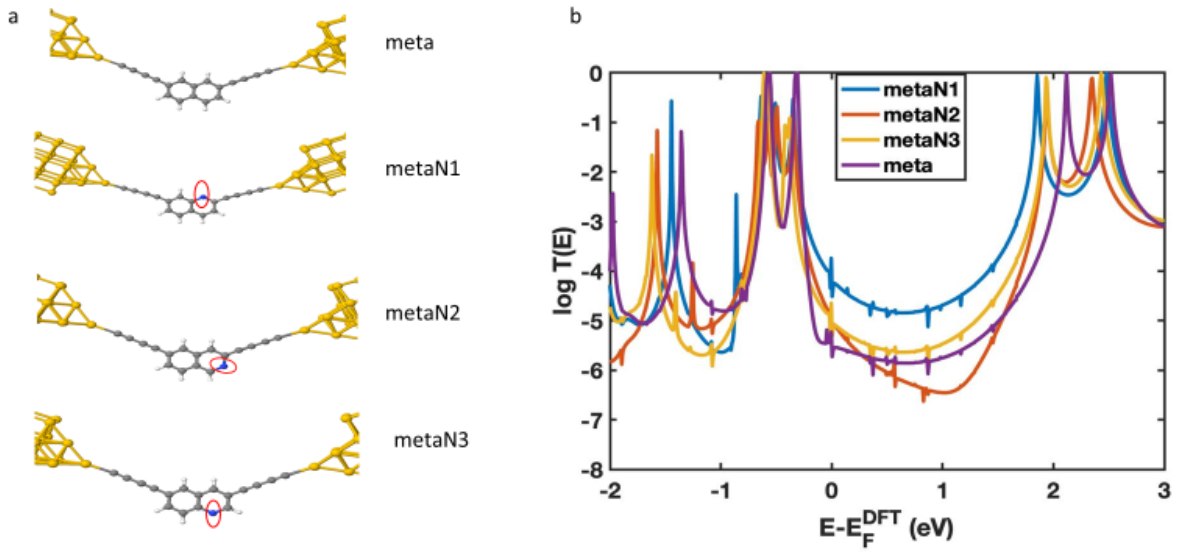

Figure 4.24: DFT-based transmission functions for naphthalene (two phenyl rings) with triple bonds at meta connectivity. The N atom is indicated by red circles.

Compared with Figure 4.18, Figure 4.24 shows that the change in linker has caused the DQI dips of the meta and metaN2 molecules to disappear. This is a consequence of the presence of both the π_z and the π_y systems in the triple bonds, with the latter coupling to the sigma system of the core to provide a parallel conductance path which hide the DQI dip in the π_z system of the core.

4.14 Wave functions for meta, metaN1, metaN2 and metaN3 with triple bombs of naphthalene

To implement the orbital product rule, the frontier orbitals of the above molecules are shown below.

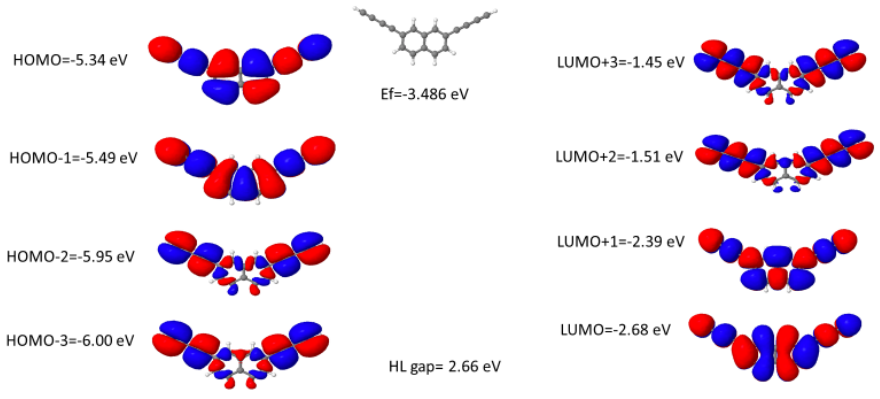

Figure 4.25: Frontier molecular orbitals of a meta-studied molecule with its eigenvalues obtained from DFT, where red represents positive and blue indicates negative regions of the wave functions

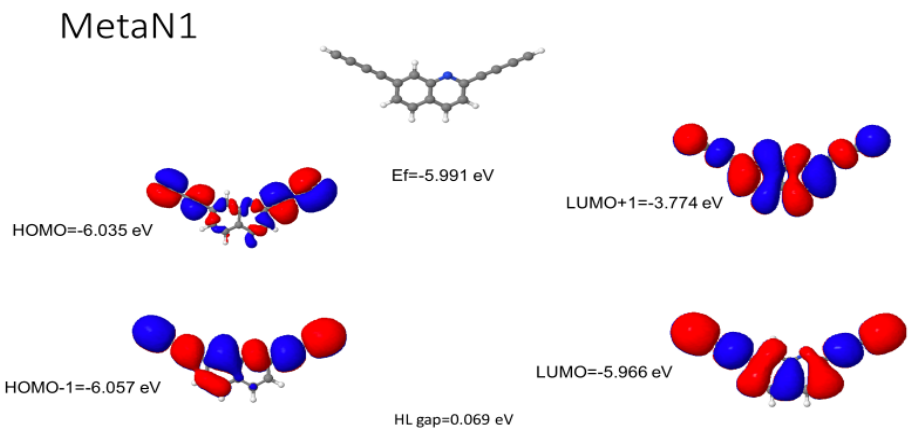

Figure 4.26: Frontier molecular orbitals of metaN1 studied molecule with its eigenvalues obtained from DFT, where red represents positive and blue indicates negative regions of the wave functions

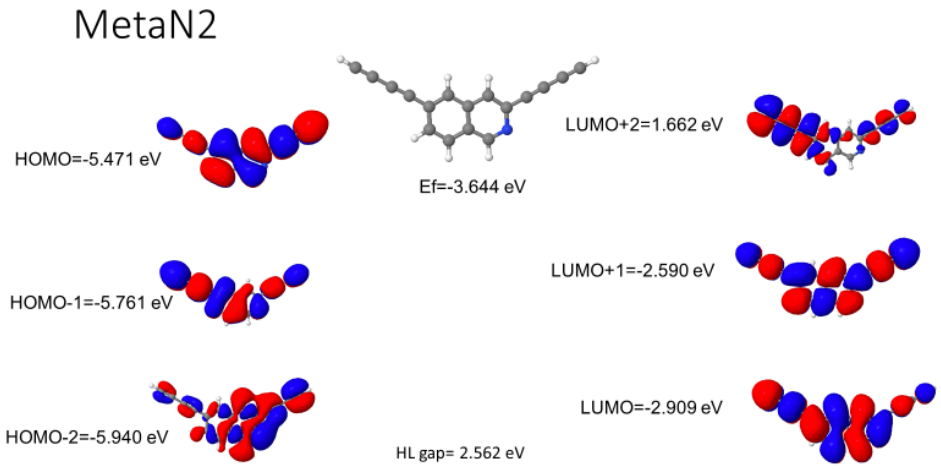

Figure4.27: Frontier molecular orbitals of metaN2 studied molecule with its eigenvalues obtained from DFT, where red represents positive and blue indicates negative regions of the wave functions

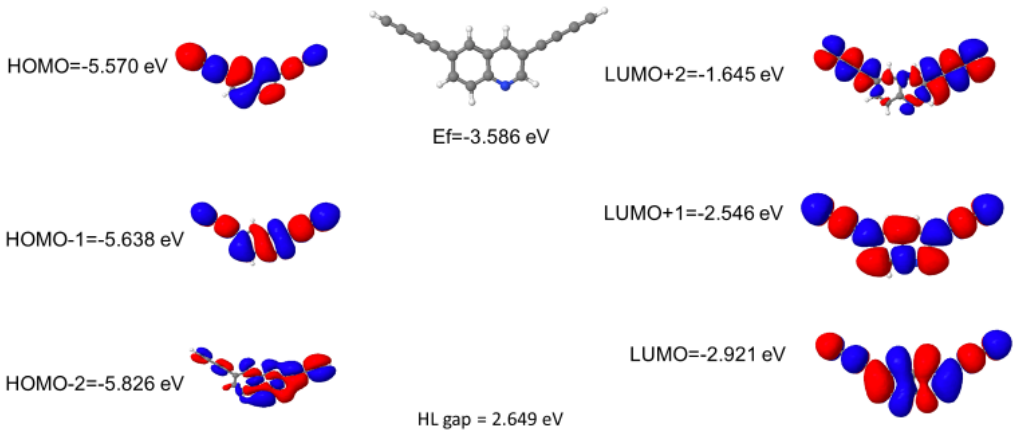

Figure 4.28: Frontier molecular orbitals of metaN3 studied molecule with its eigenvalues obtained from DFT, where red represents positive and blue indicates negative regions of the wave functions

Again, the HOMO and LUMO products of meta in Figure 4.25 have the same sign and therefore DQI is predicted, whereas the HOMO and LUMO products of metaN1in Figure 4.26 have the opposite signs and therefore CQI is predicted. For the other molecules (Figures 4.27 and 4,28), the HOMO and LUMO products have the same sign and therefore DQI is predicted. However, no clear DQI dips are displayed by the DFT-based transmission curves in Figure 4.24.

To test the above hypothesis, I shall now increase the size of the core to anthracene, with three rings. If the hypothesis is correct, then transmission by the sigma system should be diminished, thereby allowing the DQI dips to become apparent. The new molecules are shown in Figure 4.29, along with their DFT-based transmission curves. Their corresponding TBM curves are shown in Figure 4.30 and are in excellent agreement with the DFT results. The DQI dips are now obvious, because although the π_y systems in the triple bonds can couple to the sigma system of the core, the increase in size of the core has supressed transmission through the sigma system.

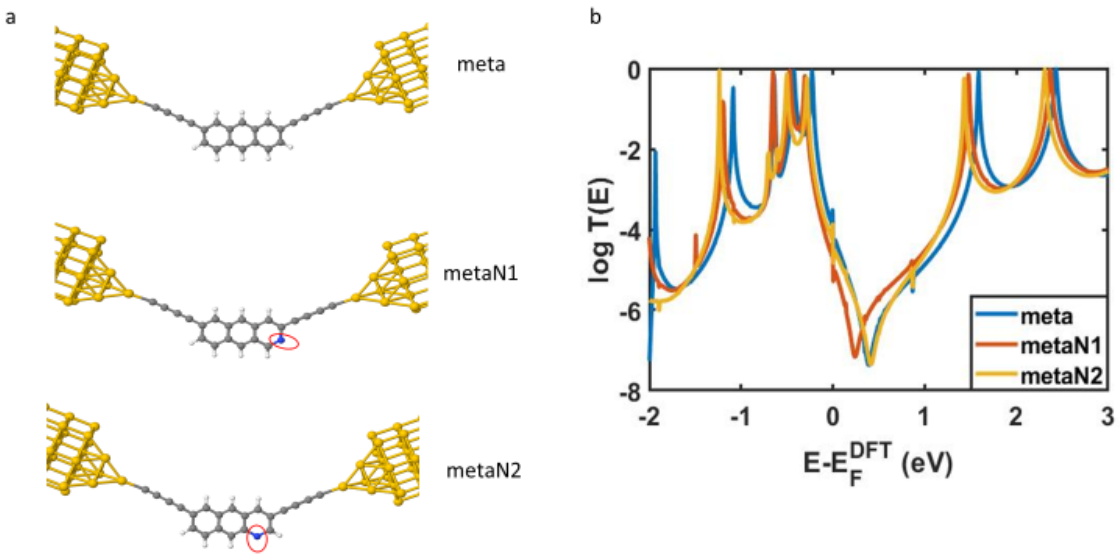

Fig 4.29: DFT-based transmission functions for anthracene (three phenyl rings) with triple bonds at meta connectivity. The N atom is indicated by red circles.

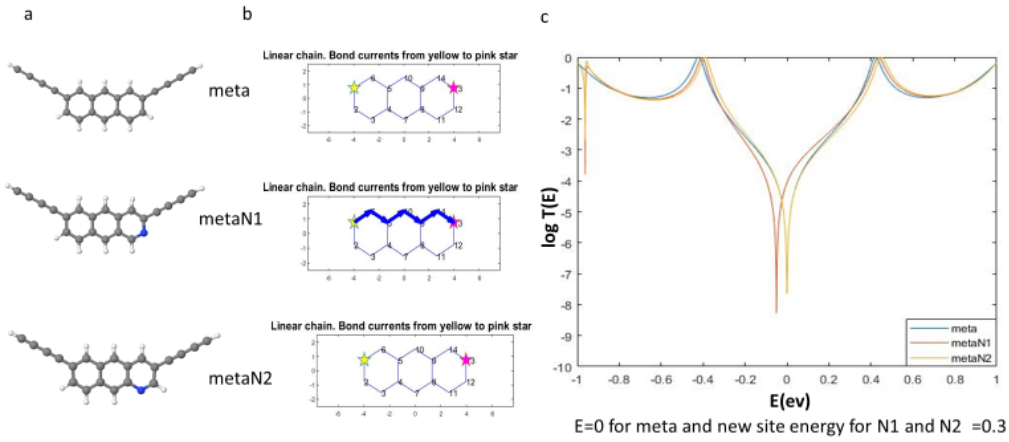

Figure 4.30: Tight binding model result for anthracene.

4.15 Wave functions for meta, metaN1 and metaN2 with triple bombs of anthracene

To explore the predictions of the orbital product rule, the frontier orbitals of the above three molecules are shown below.

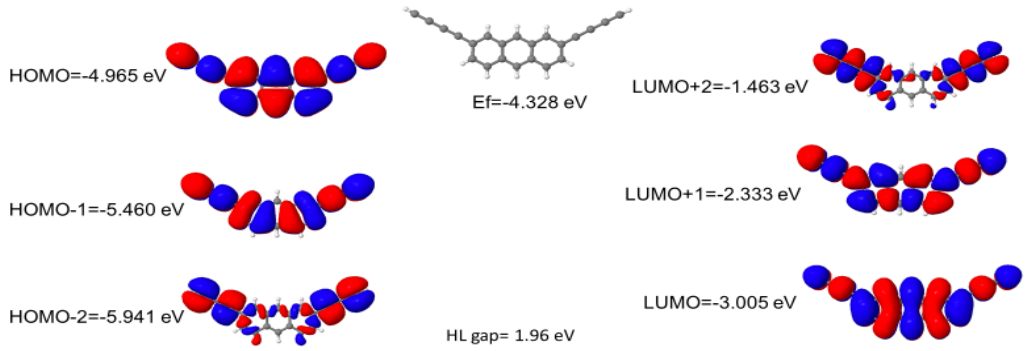

Figure 4.31: Frontier molecular orbitals of a meta-studied molecule with its eigenvalues obtained from DFT, where red represents positive and blue indicates negative regions of the wave functions

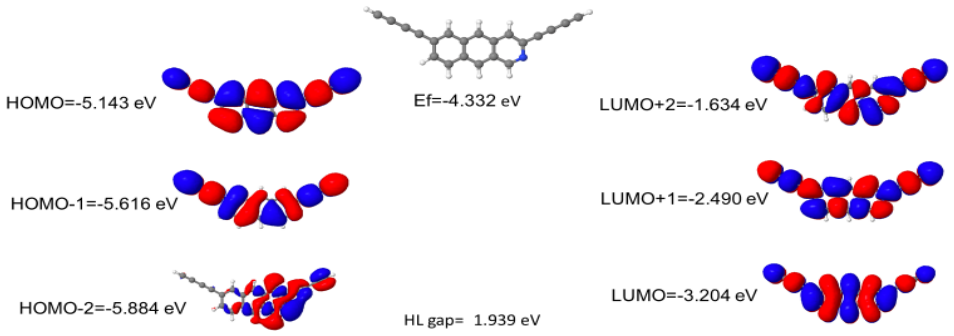

Figure 4.32 Frontier molecular orbitals of metaN1 studied molecule with its eigenvalues obtained from DFT, where red represents positive and blue indicates negative regions of the wave functions

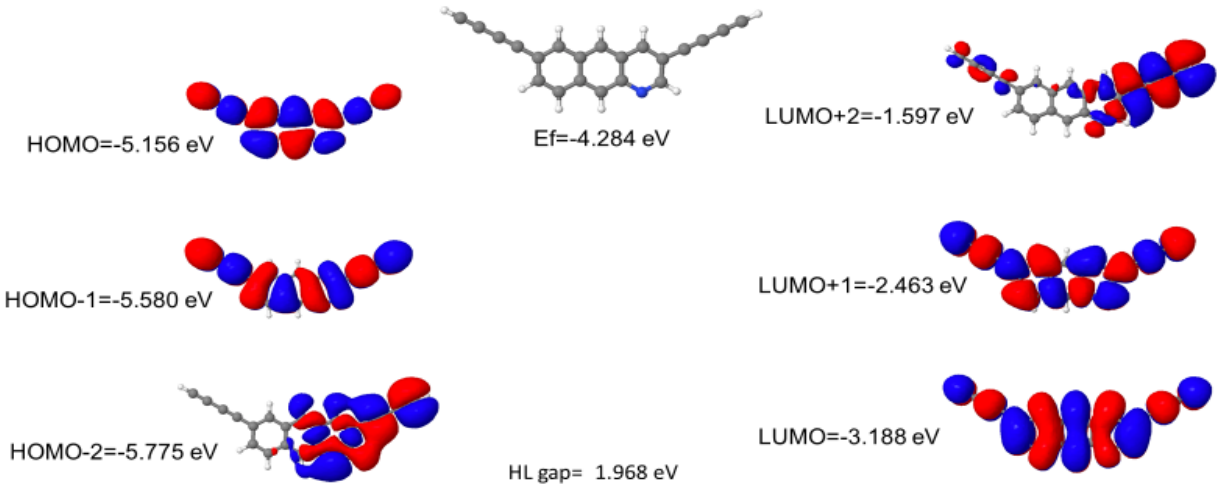

Figure 4.33: Frontier molecular orbitals of metaN2 studied molecule with its eigenvalues obtained from DFT, where red represents positive and blue indicates negative regions of the wave functions

In all cases in Figures (4.31,4.32 and 4.33), the HOMO and LUMO orbital products are of the same sign and therefore DQI is predicted, in agreement with the DFT and TBM transmission curves.

4.16 Summary

In this chapter, I studied charge transport through molecular junctions with gold electrodes connected to molecular cores by linkers with conjugated π systems formed from both π_z and π_y orbitals. I found that DQI dips in transport though the π_z system can be hidden, because the π_y orbitals of the linkers can couple to the sigma system of the core and create a parallel conductance channel. Although this channel makes only a small contribution, it becomes dominate when DQI suppresses transport through the π_z system. This mechanism was demonstrated by increasing the size of the core from benzene to naphthalene and then anthracene, which successively suppress transport through the sigma system and for the largest core allows the DQI transport dips to become visible. This points to an important design principle for future molecular electronic devices, since if one plans to use DQI to control transport through molecules, it would be wise to avoid links with more than one π system.

4.17 Bibliography

[1] Chemical principles of single-molecule electronics. T. A. Su, M. Neupane, M. L. Steigerwald, L. Venkataraman, and C. Nuckolls, *Nature Reviews Materials*, 1, 16002, Mar. 2016

[2] Perspective: Thermal and thermoelectric transport in molecular junctions. L. Cui, R. Miao, C. Jiang, E. Meyhofer, and P. Reddy, *The Journal of Chemical Physics*, 146(9), 092201, Mar. 2017

[3] Phase coherent electronics: A molecular switch based on quantum interference. R. Baer and D. Neuhauser, *American Chemical Society*, 124(16), 4200–4201, Apr. 2002

[4] Controlling quantum transport through a single molecule. D. M. Cardamone, C. A. Stafford, and S. Mazumdar, *Nano Letters*, 6(11), 2422–2426, 2006

[5] Observation of quantum interference in molecular charge transport. C. M. Guédon, H. Valkenier, T. Markussen, K. S. Thygesen, J. C. Hummelen, and S. J. Van Der Molen, *Nature Nanotechnology*, 7(5), 305–309, May 2012

[6] Quantum interference effects in charge transport through single-molecule junctions: Detection, manipulation, and application. J. Liu, X. Huang, F. Wang, and W. Hong, *Accounts of Chemical Research*, 52(1), 151–160, 2018

[7] Exploring quantum interference in heteroatom-substituted graphene-like molecules. S. Sangtarash, H. Sadeghi, and C. J. Lambert, *Nanoscale*, 8, 13199–13205, 2016

[8] Signatures of room-temperature quantum interference in molecular junctions. S.-X. Liu, A. Ismael, A. Al-Jobory, and C. J. Lambert, *Accounts of Chemical Research*, 56(3), 322–331, 2023

[9] Magic ratios for connectivity-driven electrical conductance of graphene-like molecules. Y. Geng, S. Sangtarash, C. Huang, H. Sadeghi, Y. Fu, W. Hong, T. Wandlowski, S. Decurtins, C. J. Lambert, and S.-X. Liu, *Journal of the American Chemical Society*, 137(13), 4469–4476, 2015

[10] Magic number theory of superconducting proximity effects and Wigner delay times in graphene-like molecules. P. Rakyta, A. Alanazy, A. Kormányos, Z. Tajkov, G. Kukucska, J. Koltai, S. Sangtarash, H. Sadeghi, J. Cserti, and C. J. Lambert, *Journal of Physical Chemistry C*, 123, 6812, 2019

[11] On the resilience of magic number theory for conductance ratios of aromatic molecules. L. Ulčakar, T. Rejec, J. Kokalj, S. Sangtarash, H. Sadeghi, A. Ramšak, J. H. Jefferson, and C. J. Lambert, *Scientific Reports*, 9, 3478, 2019

Chapter 5

Single-Molecule Conductance Enhancement in a Stable Diradical

5.1 Introduction

Stable organic radicals have half-filled orbitals at the Fermi energy, making them promising candidates for electrical devices. Due to the possibility that all-organic conjugated radical species with unpaired electrons would give rise to new quantum phenomena, these species have generated a great deal of interest in single-molecule electronics research. Additionally, organic radicals can improve electrical conductivity [1-2]. Therefore, studies of charge transfer in single-molecule junctions with radical species are of great importance for future functional electronic devices, such as spintronic and, recently, thermoelectric devices [3-12]. Extensive research has been done to improve charge transport properties in single molecules through changes in structure, environment, anchoring groups, external stimuli, and quantum interference (QI) [13-19]. In this chapter, the effects of diradicals on the charge transport have been investigated including the effects of CQI and DQI.

5.2 Studied molecules

The following molecules will be investigated. As indicated in the figure, these form series of related molecules, which may exhibit either DQI or CQI and which may be either neutral molecules or radicals.

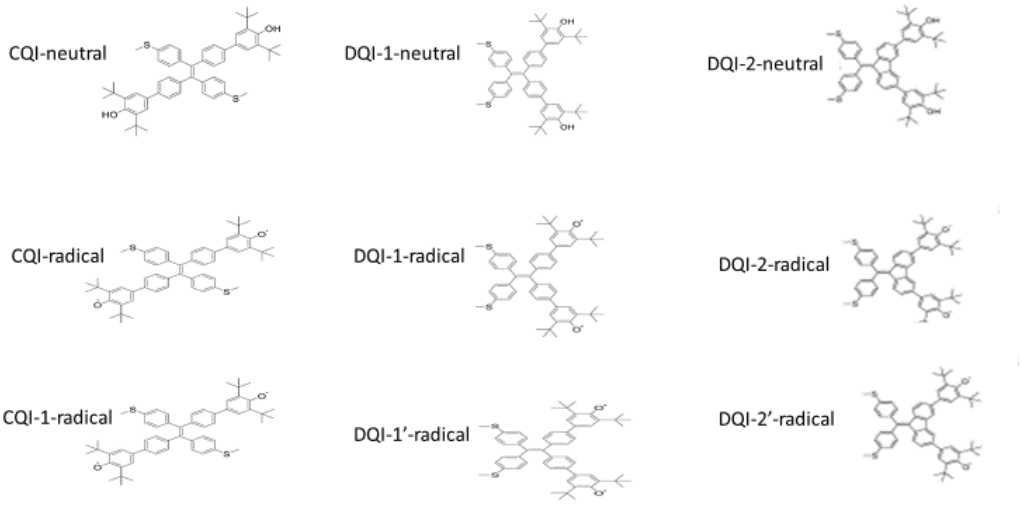

Figure 5.1: Studied diradical molecules and their corresponding neutral molecules.

The spin occupancies for the diradicals are shown below:

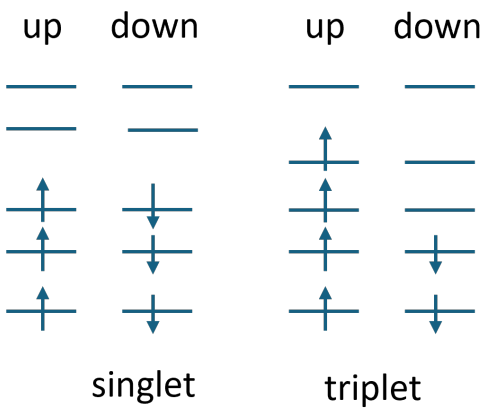

Figure 5.2: Schematic shows two spin states for diradical molecules.

5.3 Results and discussion

5.3.1 CQI case

As shown in Figure 5.5, the HOMO and LUMO products of CQI-neutral have different signs and therefore CQI is predicted. This is further confirmed by my transmission calculation where no dip appears in the HOMO-LUMO gap as indicated by the blue curve in Figure 5.3. In terms of its diradical counterpart, the two unpaired electrons sitting on the two oxygen atoms can have the same spin or different spins, namely, they can be singlets or triplets as shown in Figure 5.2. These two cases are therefore considered in this chapter. The transmission coefficient of the singlet case is plotted in Figure 5.3b, with spin up and spin down channels almost identical due to the symmetric character of this molecule. The two peaks near the Fermi level correspond to the SOMO (singly occupied molecular orbital) and the SUMO (singly unoccupied molecular orbital) respectively. The room temperature conductance is plotted in Figure 5.3 c, which shows an increased conductance compared with its neutral counterpart near the Fermi energy. I further carried on the calculation with a triplet spin state and plot the transmission curves in Figure 5.4. The two unpaired electrons on oxygens occupy the two energy levels indicated by the two red peaks below Fermi energy. A bigger enhancement is observed due to more resonances near Fermi energy.

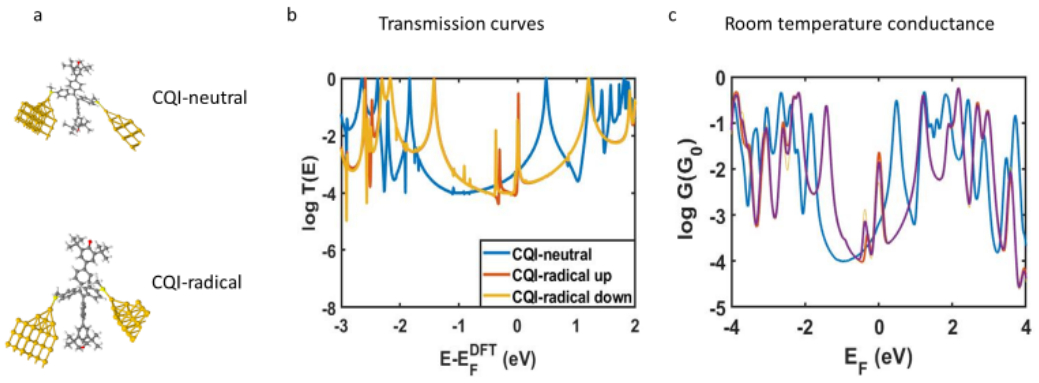

Figure 5.3: (a) the geometries of CQI-neutral and CQI-radical within junction. (b)their transmission curves (c)the room temperature conductance for stable radical where the purple one is the average of spin up and spin down transmission.

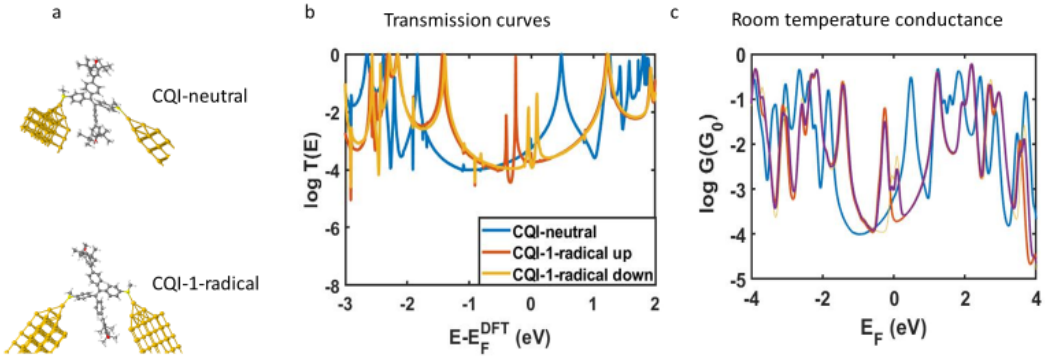

Figure 5.4: (a) the geometries of CQI-neutral and CQI-1-radical within junction. (b)their transmission curves (c)the room temperature conductance for stable radical where the purple one is the average of spin up and spin down transmission.

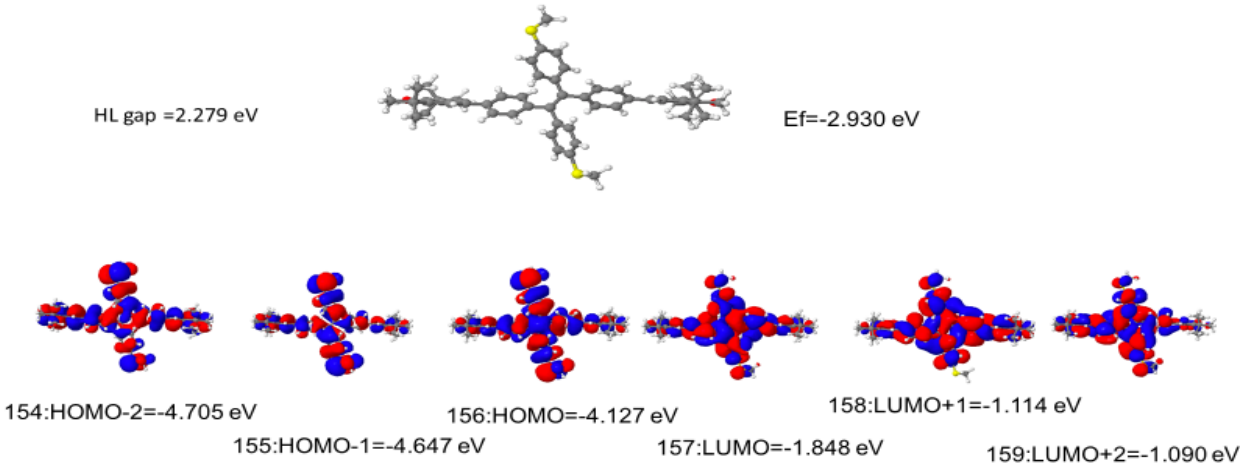

Figure 5.5: Frontier molecular orbitals of CQI-neutral studied molecule with its eigenvalues obtained from DFT, where red represents positive and blue indicates negative regions of the wave functions.

The two ends of the above HOMOs and LUMOs have different signs and therefore the product rule predicts CQI.

I choose to end up with HOMO -2 and LUMO +2 foe this case and the following cases because they are the highest level.

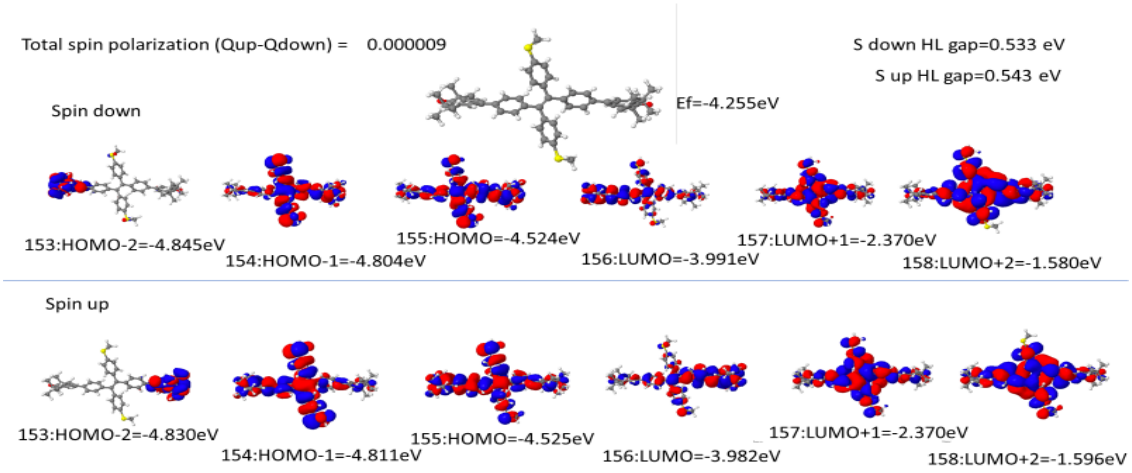

Figure 5.6: Frontier molecular orbitals of CQI-radical studied molecule with its eigenvalues obtained from DFT, where red represents positive and blue indicates negative regions of the wave functions

The two ends of the above HOMOs and LUMOs have different signs and therefore the product rule again predicts CQI.

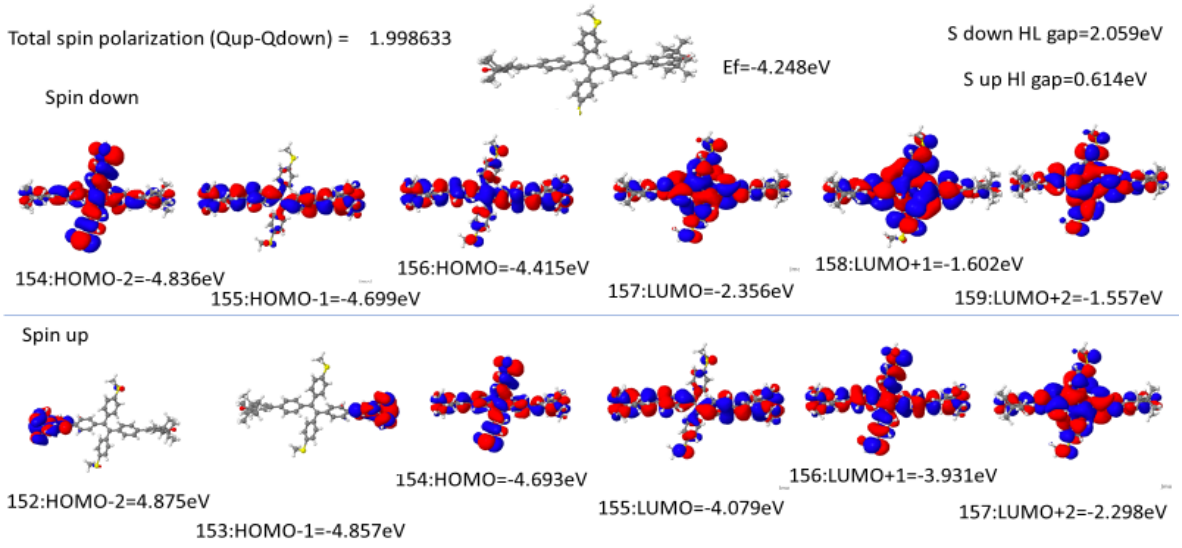

Figure 5.7: Frontier molecular orbitals of CQI-1-radical studied molecule with its eigenvalues obtained from DFT, where red represents positive and blue indicates negative regions of the wave functions

The two ends of the above HOMOs and LUMOs have different signs and therefore the product rule predicts CQI

5.3.2 The DQI 1 case

As shown in Figure 5.10, the HOMO and LUMO products of the DQI-1-neutral have the same sign and therefore DQI is predicted. This is further confirmed by my transmission calculation, where the dip appears in the HOMO-LUMO gap as indicated by the blue curve in Figure 5.8. In terms of its diradical counterpart, the two unpaired electrons sitting on the two oxygen atoms can again have the same spin or different spin, leading to either singlet or triplet states, as shown in Figure 5.2. The transmission coefficient of the singlet case is plotted in Figure 5.8b, with spin up and spin down channels almost identical due to the symmetric character of this molecule. The room temperature conductance is plotted in

Figure 5.8 c, which reveals an increased conductance compared with its neutral counterpart near the Fermi energy. I further carried on the calculation with a triplet spin state and plot the transmission curves in Figure 5.9.

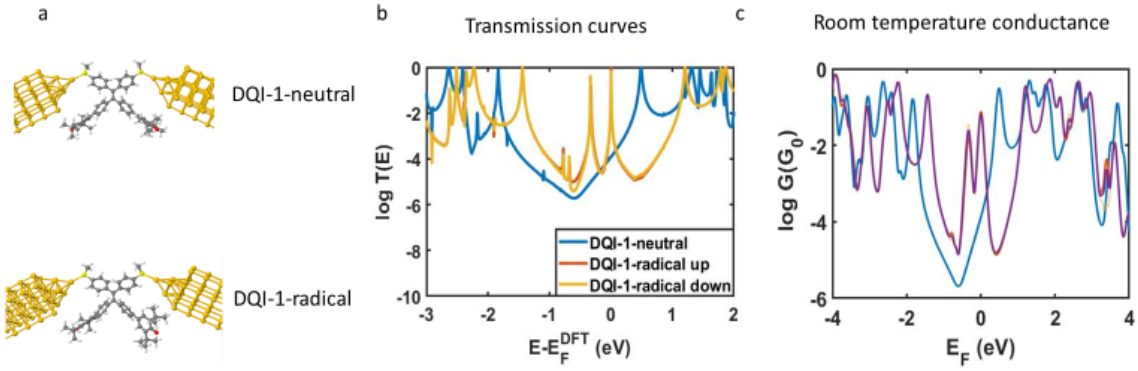

Figure 5.8: (a) the geometries of DQI-1-neutral and DQI-1-radical within junction. (b)their transmission curves (c)the room temperature conductance for stable radical where the purple one is the average of spin up and spin down transmission

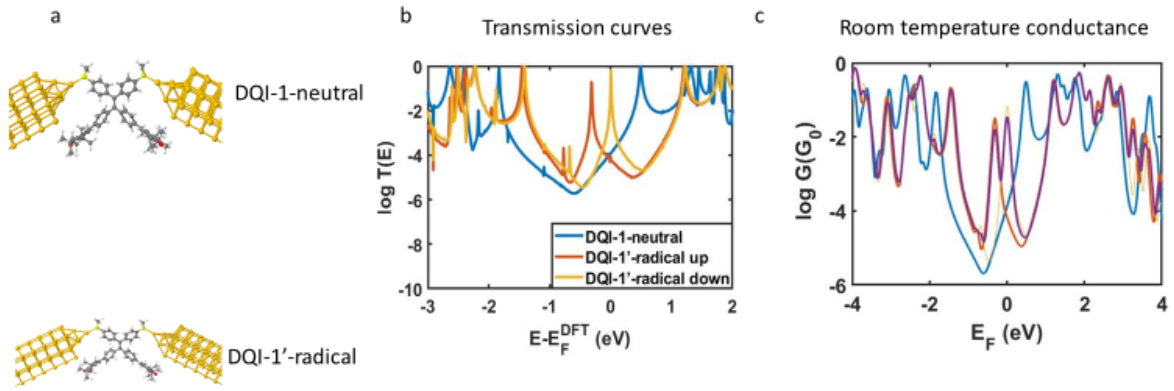

Figure 5.9: (a) the geometries of DQI-1-neutral and DQI-1'-radical within junction. (b)their transmission curves (c)the room temperature conductance for stable radical where the purple one is the average of spin up and spin down transmission

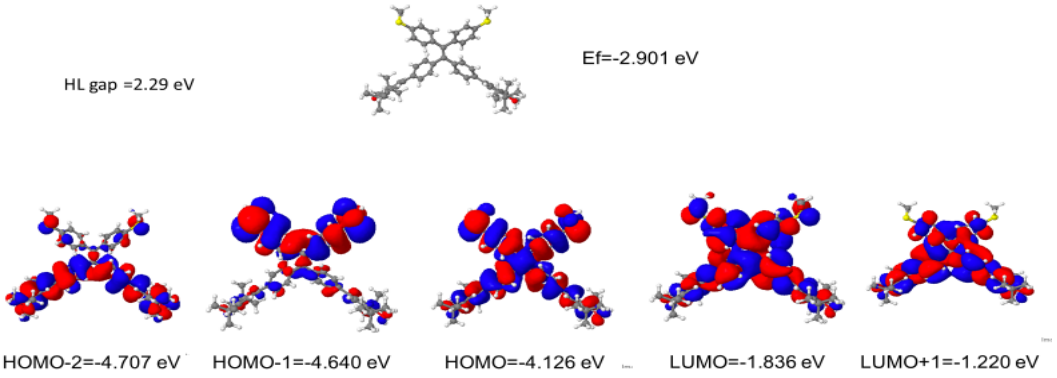

Figure 5.10: Frontier molecular orbitals of DQI-1-neutral studied molecule with its eigenvalues obtained from DFT, where red represents positive and blue indicates negative regions of the wave functions.

The two ends of the above HOMOs and LUMOs have the same signs and therefore the product rule predicts DQI.

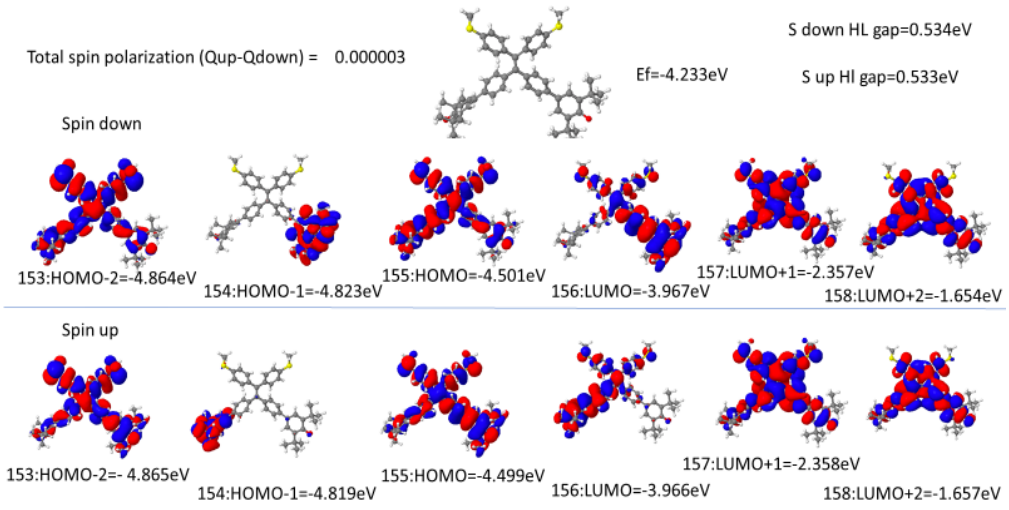

Figure 5.11: Frontier molecular orbitals of DQI-1-radical studied molecule with its eigenvalues obtained from DFT, where red represents positive and blue indicates negative regions of the wave functions

In this case, we cannot apply the product rule, because one side of LUMOs is negligibly small.

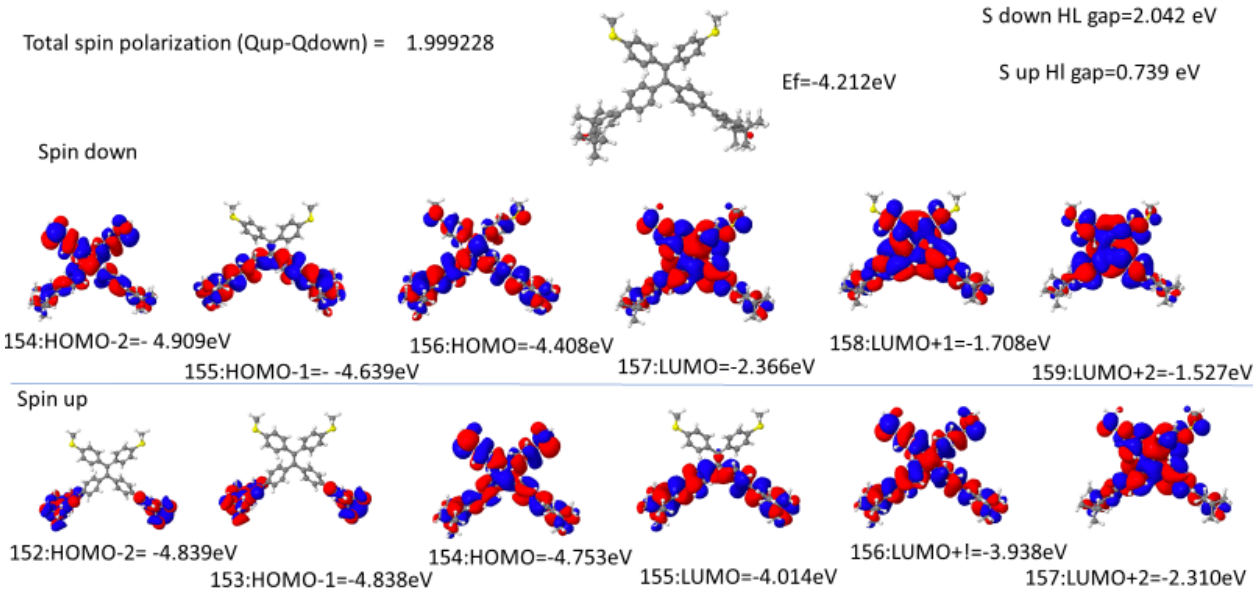

Figure 5.12: Frontier molecular orbitals of DQI-1'-radical studied molecule with its eigenvalues obtained from DFT, where red represents positive and blue indicates negative regions of the wave functions

The two ends of the above HOMOs and LUMOs have the same signs and therefore the product rule predicts DQI. However, for spin up, we cannot apply the product rule because one side of LUMO is negligibly small.

5.3.3 The DQI 2 case

As shown in Figure 5.15, the HOMO and LUMO products of DQI-2-neutral have the same sign and therefore DQI is predicted. This is further confirmed by my transmission calculation, where a dip appears in the HOMO-LUMO gap as indicated by the blue curve in Figure 5.13. The transmission coefficient of the singlet case is plotted in Figure 5.13b, with spin up and spin down channels almost identical due to the

symmetric character of this molecule. The room temperature conductance is plotted in Figure 5.13 c indicating an increased conductance compared with its neutral counterpart near the Fermi energy. I further carried on the calculation with a triplet spin state and plot the transmission curves in Figure 5.14.

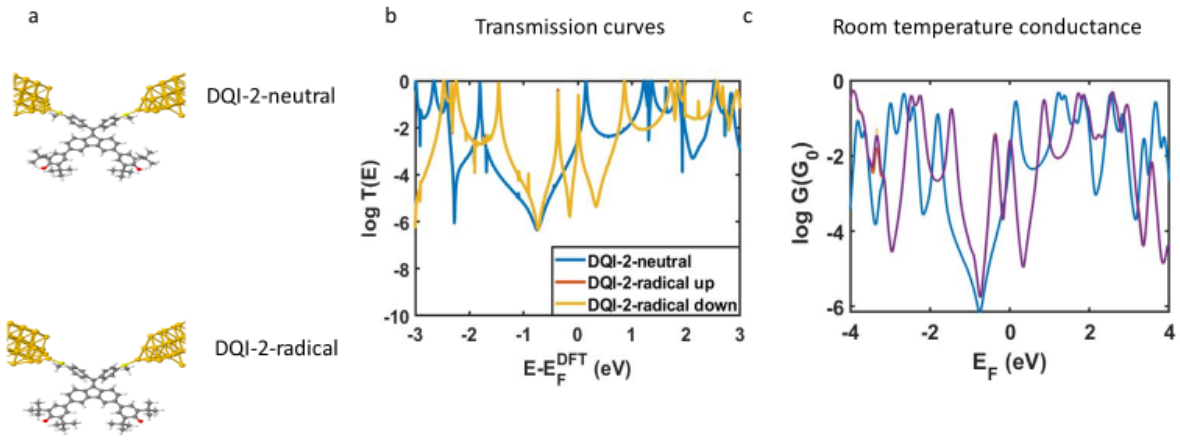

Figure 5.13: : (a) the geometries of DQI-2-neutral and DQI-2-radical within junction. (b)their transmission curves (c)the room temperature conductance for stable radical where the purple one is the average of spin up and spin down transmission

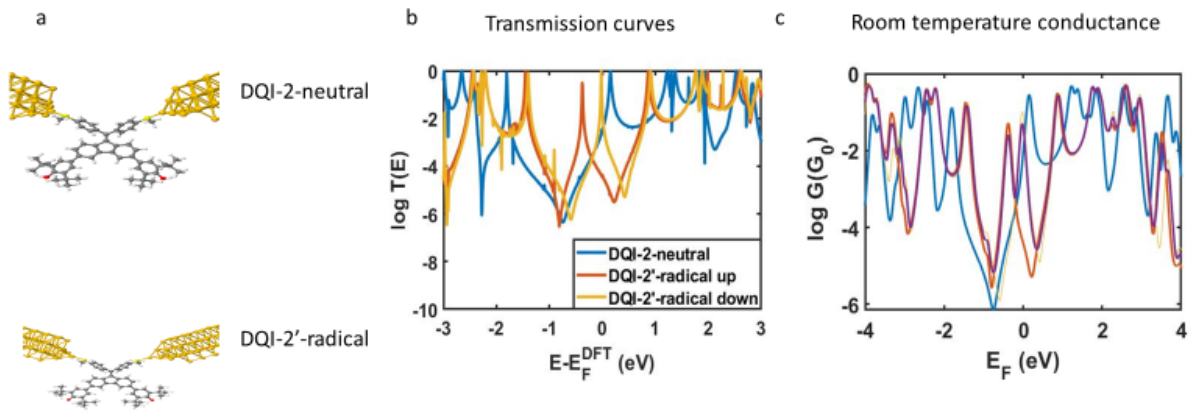

Figure 5.14: : (a) the geometries of DQI-2-neutral and DQI-2'-radical within junction. (b)their transmission curves (c)the room temperature conductance for stable radical where the purple one is the average of spin up and spin down transmission

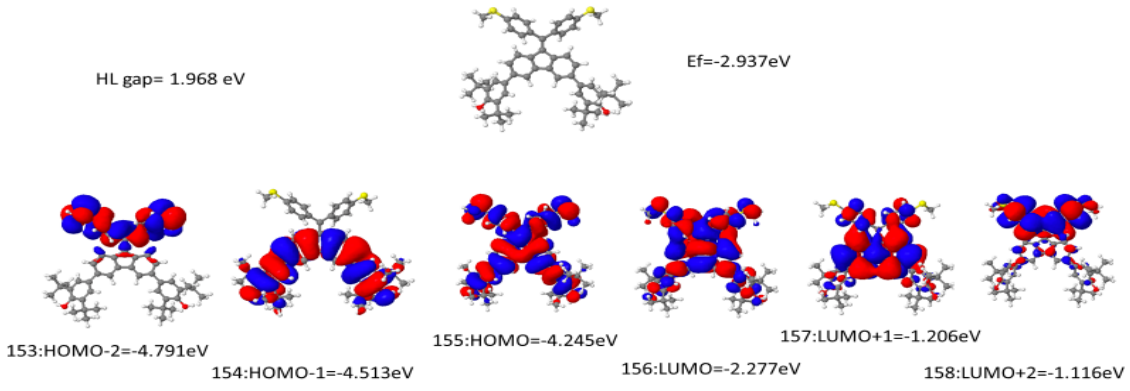

Figure 5.15: Frontier molecular orbitals of DQI-2-neutral studied molecule with its eigenvalues obtained from DFT, where red represents positive and blue indicates negative regions of the wave functions

The two ends of the above HOMOs and LUMOs have the same signs and therefore the product rule predicts DQI.

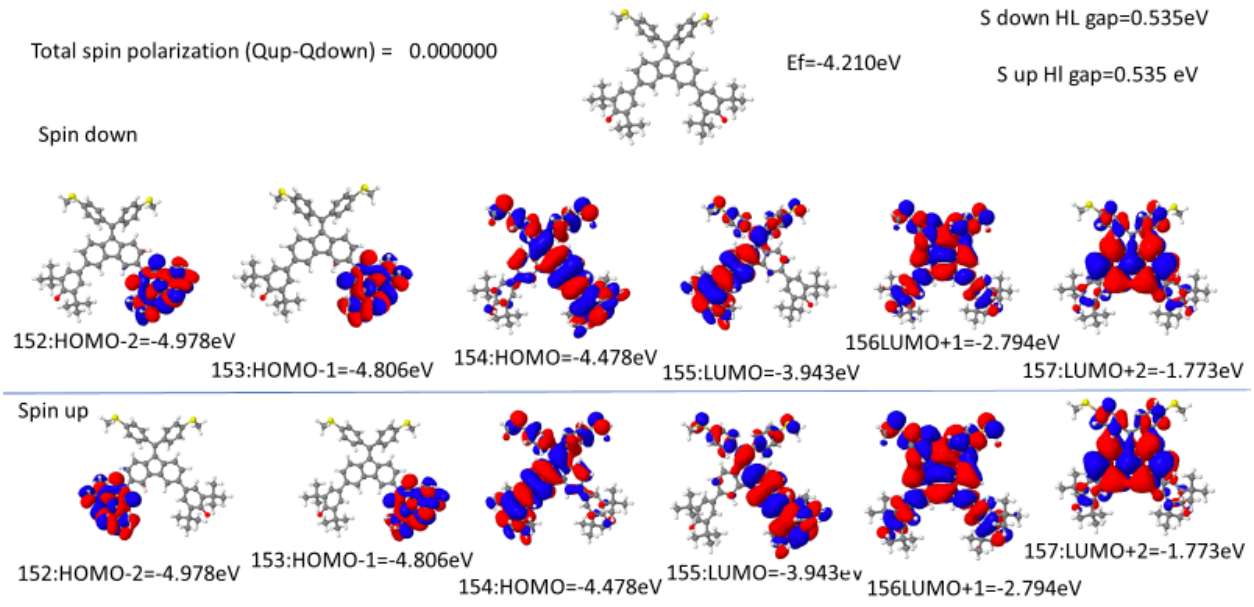

Figure 5.16: Frontier molecular orbitals of DQI-2-radical studied molecule with its eigenvalues obtained from DFT, where red represents positive and blue indicates negative regions of the wave function

From this figure, we cannot apply the product rule because the two sides of HOMOs and LUMOs are negligibly small.

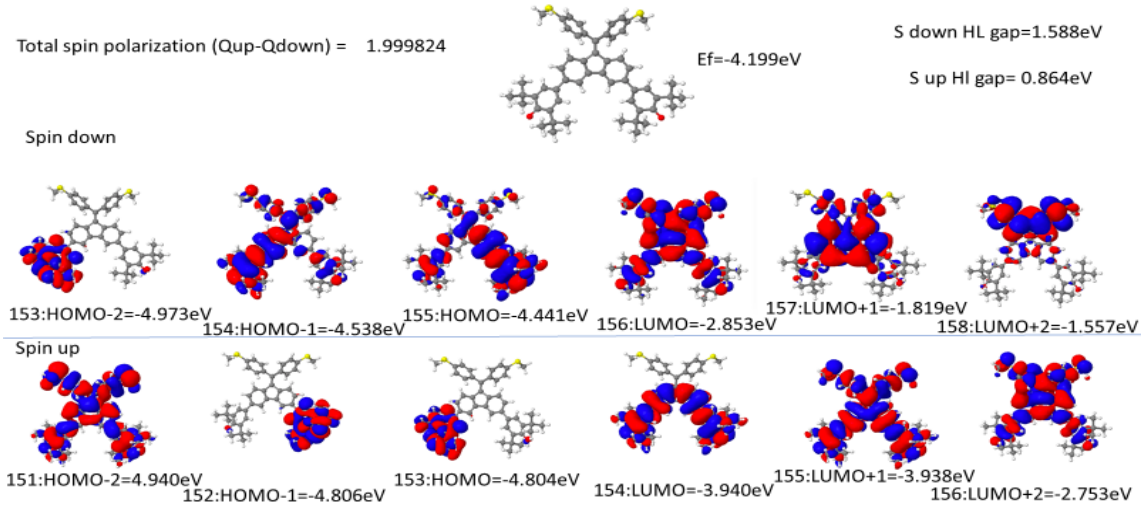

Figure 5.17: Frontier molecular orbitals of DQI-2'-radical studied molecule with its eigenvalues obtained from DFT, where red represents positive and blue indicates negative regions of the wave functions

The two ends of the above HOMOs and LUMOs have the same signs and therefore the product rule predicts DQI.

For spin-up, we cannot apply the product rule because the two sides of HOMOs and LUMOs are negligibly small.

From the above transmission and conductance properties of these molecules, we found that the conductance of the radical is greater than that of the neutral molecule in both cases of CQI and DQI.

5.4 Summary

This chapter emphasizes that stable organic diradicals have the potential for enhanced conductance compared to their closed-shell counterparts. Specifically, the triplet spin state case provides more enhancement than the singlet spin state. The influence of diradical based on CQI and DQI neutral molecules is also studied. Generally, we observe a bigger enhancement for a DQI system than that on a CQI system.

5.5 References

[1] Redox-addressable single-molecule junctions incorporating a persistent organic radical. S. Naghibi, S. Sangtarash, V. J. Kumar, J.-Z. Wu, M. M. Judd, X. Qiao, E. Gorenskaia, S. J. Higgins, N. Cox, R. J. Nichols, H. Sadeghi, P. J. Low, and A. Vezzoli, *Angewandte Chemie International Edition*, 61, e202116985, 2022

[2] Radical-enhanced charge transport in single-molecule phenothiazine electrical junctions. J. Liu, X. Zhao, Q. Al-Galiby, X. Huang, J. Zheng, R. Li, C. Huang, Y. Yang, J. Shi, D. Z. Manrique, C. J. Lambert, M. R. Bryce, and W. Hong, *Angewandte Chemie*, 129, 13241–13245, 2017

[3] Concepts in the design and engineering of single-molecule electronic devices. N. Xin, J. Guan, C. Zhou, X. Chen, C. Gu, Y. Li, M. A. Ratner, A. Nitzan, J. F. Stoddart, and X. Guo, *Nature Reviews Physics*, 1, 211–230, 2019

[4] Remarkable multichannel conductance of novel single-molecule wires built on through-space conjugated hexaphenylbenzene. S. Zhen, J.-C. Mao, L. Chen, S. Ding, W. Luo, X.-S. Zhou, A. Qin, Z. Zhao, and B. Z. Tang, *Nano Letters*, 18, 4200–4205, 2018

[5] Controlling formation of single-molecule junctions by electrochemical reduction of diazonium terminal groups. T. Hines, I. Díez-Pérez, H. Nakamura, T. Shimazaki, Y. Asai, and N. Tao, *Journal of the American Chemical Society*, 135, 3319–3322, 2013

[6] Achieving efficient multichannel conductance in through-space conjugated single-molecule parallel circuits. P. Shen, M. Huang, J. Qian, J. Li, S. Ding, X.-S. Zhou, B. Xu, Z. Zhao, and B. Z. Tang, *Angewandte Chemie*, 132, 4611–4618, 2020

[7] Towards molecular spintronics. A. R. Rocha, V. M. García-Suárez, S. W. Bailey, C. J. Lambert, J. Ferrer, and S. Sanvito, *Nature Materials*, 4, 335–339, 2005

[8] Complete mapping of the thermoelectric properties of a single molecule. P. Gehring, J. K. Sowa, C. Hsu, J. de Bruijckere, M. van der Star, J. J. Le Roy, L. Bogani, E. M. Gauger, and H. S. J. van der Zant, *Nature Nanotechnology*, 16, 426–430, 2021

[9] Normal and reversed spin mobility in a diradical by electron-vibration coupling. Y. Shen, G. Xue, Y. Dai, S. M. Quintero, H. Chen, D. Wang, F. Miao, F. Negri, Y. Zheng, and J. Casado, *Nature Communications*, 12, 6262, 2021

[10] Single-molecule calorimeter and free energy landscape. Y. Wang, Z. Tang, H.-Y. Chen, W. Wang, N. Tao, and H. Wang, *Proceedings of the National Academy of Sciences*, 118, e2104598118, 2021

[11] Thermoelectric enhancement in single organic radical molecules. J. Hurtado-Gallego, S. Sangtarash, R. Davidson, L. Rincón-García, A. Daaoub, G. Rubio-Bollinger, C. J. Lambert, V. S. Oganesyan, M. R. Bryce, N. Agraït, and H. Sadeghi, *Nano Letters*, 22, 948–953, 2022

[12] Thermoelectric properties of 2,7-dipyridylfluorene derivatives in single-molecule junctions. G. Yzambart, L. Rincón-García, A. A. Al-Jobory, A. K. Ismael, G. Rubio-Bollinger, C. J. Lambert, N. Agraït, and M. R. Bryce, *Journal of Physical Chemistry C*, 122, 27198–27204, 2018

[13] Quantum interference-enhanced chemical responsivity in single-molecule dithienoborepin junctions. M. Baghernejad, C. Van Dyck, J. Bergfield, D. R. Levine, A. Gubicza, J. D. Tovar, M. Calame, P. Broekmann, and W. Hong, *Chemistry – A European Journal*, 25, 15141–15146, 2019

[14] Covalently bonded single-molecule junctions with stable and reversible photoswitched conductivity. C. Jia, A. Migliore, N. Xin, S. Huang, J. Wang, Q. Yang, S. Wang, H. Chen, D. Wang, B. Feng, Z. Liu, G. Zhang, D.-H. Qu, H. Tian, M. A. Ratner, H. Q. Xu, A. Nitzan, and X. Guo, *Science*, 352, 1443–1445, 2016

[15] Direct single-molecule dynamic detection of chemical reactions. J. Guan, C. Jia, Y. Li, Z. Liu, J. Wang, Z. Yang, C. Gu, D. Su, K. N. Houk, D. Zhang, and X. Guo, *Science Advances*, 4, eaar2177, 2018

[16] Effect of anchoring groups on single-molecule charge transport through porphyrins. Z. Li, M. Smeu, M. A. Ratner, and E. Borguet, *Journal of Physical Chemistry C*, 117, 14890–14898, 2013

[17] Single-molecule field effect and conductance switching driven by electric field and proton transfer. Z. Yan, X. Li, Y. Li, C. Jia, N. Xin, P. Li, L. Meng, M. Zhang, L. Chen, J. Yang, R. Wang, and X. Guo, *Science Advances*, 8, eabm3541, 2022

[18] Voltage-induced single-molecule junction planarization. Y. Zang, E.-D. Fung, T. Fu, S. Ray, M. H. Garner, A. Borges, M. L. Steigerwald, S. Patil, G. Solomon, and L. Venkataraman, *Nano Letters*, 21, 673–679, 2020

[19] The drive force of electrical breakdown of large-area molecular tunnel junctions. L. Yuan, L. Jiang, and C. A. Nijhuis, *Advanced Functional Materials*, 28, 1801710, 2018

Chapter 6

Conclusion and Future Work

6.1 Conclusion

In conclusion, I have explained the fundamental equations and tools that support my work, including the Schrödinger equation, density functional theory (DFT), and the DFT-based SIESTA program. Additionally, I have discussed single-electron transport theory and given some examples about how it might be used. These concepts are explained in chapters 2 and 3, respectively.

In chapter 4, I studied charge transport through molecular cores connected to electrodes by linkers with conjugated π systems are formed from both π_z and π_y orbitals. I found that DQI dips in transport though the π_z system can be hidden, because the π_y orbitals of the linkers can couple to the sigma system of the core and create a parallel conductance channel. To explore this issue, I introduced magic number theory, an orbital product rule and made use of Dyson's equation to describe the effect of heteroatom substitution. I found that although the sigma channel usually makes only a small contribution, it becomes dominant when DQI suppresses transport through the π_z system. This mechanism was demonstrated by increasing the size of the core from benzene to naphthalene and then anthracene, which successively suppresses transport through the sigma system and for the largest core allows the DQI transport dips to become visible.

Chapter 5 discussed the impact of diradicals on electron transport properties. I found that the conductance of the diradical is enhanced in both the CQI and DQI cases.

6.2. Future work

During the period of my research, I investigated the electrical conductance of several different molecules that were connected to gold electrodes. To continue the work done in Chapter 4 where one C atom is substituted by atom N, the effect of substituted by more N atoms and other type of atoms will be studied. In this thesis, I have mainly focussed on electrical conductance. For the future, it would be of interest to examine thermoelectric effects and thermal transport, to determine if heteroatom substitution and diradicals can be utilised to increase the thermoelectric efficiency of organic molecules.

Appendices

Appendix 1: Correction for Basis Set Superposition Error (BSSE) and Counterpoise Correction (CP)

Basis Set Superposition Error Correction (BSSE) is a critical component that affects the precision of energy interaction calculations with incomplete bases. It is typically understood in conjunction with intermolecular interactions, especially in systems with weak intermolecular interactions. The SIESTA implementation of DFT used in this thesis means that the BSSE begins to use the linear combination of the atomic orbital formalism, which consists of a final nuclei-focusing basis when atoms are close enough to overlap their basis functions. This may artificially reinforce the atomic bond, shorten atomic distances, and therefore change the overall system energy. Boys and Bernardi proposed a method for lowering BSSE in molecular complexes in 1970 that used a so-called counterpoise-correction scheme with two geometrical configurations. Consider the molecular systems A and B, which are separated by a distance R. The interaction energy can be explained in.

$$\Delta E_{inter}^{AB}(R) = E^{AB}(R) - E^{A} - E^{B} \quad (1)$$

The overall energy of the supersystem is represented as ΔE_{inter} AB, while $E^{A}$and E^{B} represent the energies of the isolated subsystems.

Figure 1: shows counterpoise correction for dimers A and B.

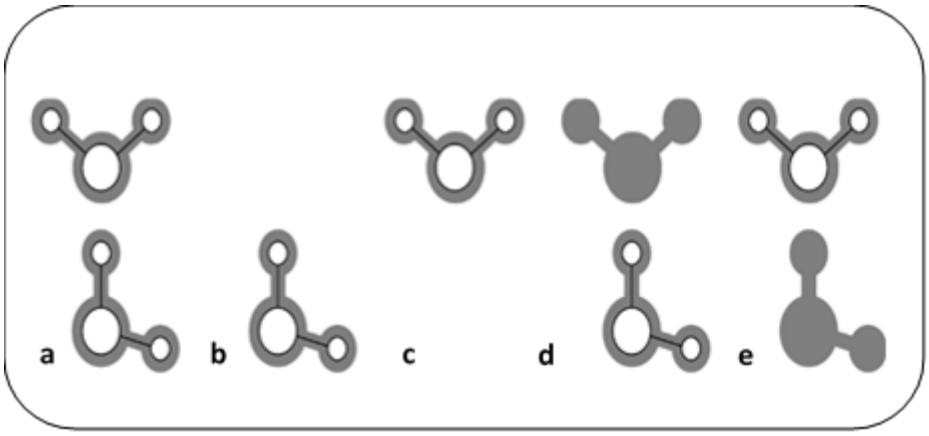

Figure 1: shows the Counterpoise method for calculating binding energy. (a) illustrates the basis functions for a whole system, with the atoms in white and the basis functions in grey. (b) and (c) represent the basis function for individual monomers, whereas (d) and (e) show the counterpoise correction. In (a), each molecule can be evaluated using the same basis function as the overall system.

Figure 1 a, b, and c illustrate the two isolated molecules and their corresponding basis functions, whereas the shaded grey atoms in figures 1, d and e show the ghost states (basis set functions without electrons or protons). The Basis Set Superposition Error Correction (BSSE) is obtained by recalculating the binding energy E_{Bin} using the mixed basis sets produced by introducing ghost orbitals and then decreasing the error from the uncorrected energy.

$$E_{Bin} = E_a - (E_d + E_e) \tag{2}$$

In figure 1, E_a, E_d and E_e represent the total energy of the systems (a), (d), and (e), respectively. This is an important idea, which has been effectively used in many systems to provide dependable and realistic energies.

Appendix 2: The coefficients of thermoelectricity S

At the turn of the nineteenth century, Seebeck, Peltier, and Thompson discovered the connection between heat, current, temperature, and voltage. The Seebeck effect describes the generation of electrical current as a result of a temperature difference, whereas the Thompson and Peltier effects describe the cooling or heating of a current-carrying conductor. A deeper mechanism can be envisaged in which the differential temperature (ΔT) and a theoretical drop in value (ΔV) occur in the system, causing heat and charge variations. In order to obtain the thermoelectric coefficients of a device that has two terminals, the usual Landauer-Buttiker formulas can be generalised to account for heat (Q) and charge (I) currents under the linear base and temperature scheme. The structure of the system consists of a scattering area connected to two leads that are connected to two electron reservoirs. The construction of these reservoirs depends on the use of the chemical potentials μ_L and μ_R, temperatures $\mathcal{T}_L$ and $\mathcal{T}_R$, and the Fermi distribution function.

$$f_i\,(E) = \left(1 + e^{\frac{E-\mu_i}{k_B \mathcal{T}_i}}\right)^{-1} \qquad (1)$$

The right moving charge current of an individual k-state coming from the left reservoir may be calculated using the number of electrons per unit length n, Fermi distribution f_L , group velocity v_g , and the scattering region's transmission coefficient T(E).

$$I_k^+ = nev_g(E(k))\,T\big(E(k)\big)\;f_L(E(k)) \qquad (2)$$

Therefore, it is possible to get the total charge from right moving states by adding up all positive k states and then integrating them into an integral form;

where $n = 1/L$ for the electron density.

And, $v_g = \frac{1}{\hbar}\frac{\partial E(k)}{\partial k}$.

$$I_k^+ = \sum_k e\,\frac{1}{L}\,\frac{1}{\hbar}\,\frac{\partial E(k)}{\partial k}\,T(E(k))\,f_L(E(k)) = \int_{-\infty}^{+\infty}\frac{2e}{h}\,T(E)\,f_L(E)\,dE \qquad (3)$$

So, for the states that move to the left, we get:

$$I_k^- = \int_{-\infty}^{+\infty}\frac{2e}{h}\,T(E)\,f_R(E)\,dE \qquad (4)$$

Thus, the total right-moving current may be expressed as follows:

$$I = I^+ - I^- = \frac{2e}{h}\int_{-\infty}^{+\infty} T(E)\,(f_L(E) - f_R(E))\,dE \qquad (5)$$

Equation 7 is the formula that represents Landauer-Büttiker. A similar derivation can be done for the heat current (or energy current) of the same system, beginning with the connection $Q = Env_g$ rather than $I = nev_g$. The result is similar to the previous one, but it has two new terms:

$$\begin{pmatrix} I \\ \dot{Q} \end{pmatrix} = \begin{pmatrix} G & L \\ M & K \end{pmatrix} \begin{pmatrix} \Delta V \\ \Delta \mathcal{T} \end{pmatrix} \quad (6)$$

The Onsager relation describes the relationship between the thermoelectric coefficients L and M in the absence of a magnetic field:

$$M = -L\mathcal{T} \quad (7)$$

T represents the temperature. The present relationships can be described using the following observable thermoelectric coefficients, electrical resistance (R) = 1/G,

thermopower (S) = -ΔV/ΔT, the Peltier coefficient Π, and the thermal constant (k):

$$\begin{pmatrix} \Delta V \\ \dot{Q} \end{pmatrix} = \begin{pmatrix} \frac{1}{G} & -\frac{L}{G} \\ \frac{M}{G} & K - \frac{LM}{G} \end{pmatrix} \begin{pmatrix} 1 \\ \Delta \mathcal{T} \end{pmatrix} = \begin{pmatrix} R & S \\ \Pi & -K \end{pmatrix} \begin{pmatrix} 1 \\ \Delta \mathcal{T} \end{pmatrix} \quad (8)$$

It is possible to define the thermopower S as the potential drop that occurs as a result of a temperature differential when there is no electrical current present:

$$S = -\begin{pmatrix} \Delta V \\ \Delta \mathcal{T} \end{pmatrix}_{I=0} = \frac{L}{G\prime} \quad (9)$$

The heat transfer only caused by the charge current in the absence of a temperature differential is called the Peltier coefficient Π.

$$\Pi = \left(\frac{\dot{\mathrm{Q}}}{\mathrm{I}}\right)_{\Delta \mathcal{T}=0} = \frac{\mathrm{M}}{\mathrm{G}} = -S\mathcal{T} \quad (10)$$

Finally, in the absence of an electric current, the heat current generated by a temperature drop is defined as the thermal conductance k:

$$k = -\left(\frac{\dot{Q}}{\Delta \mathcal{T}}\right)_{I=0} = -\left(1 + \frac{S^2 G \mathcal{T}}{k}\right) \tag{11}$$

Of course, the assessment of S or Π indicates the device's potential as a current-driven cooling device or as a heat-driven current generator.

The following observable thermoelectric coefficients can also be used to define the thermoelectric figure of merit, ZT:

$$Z\mathcal{T} = \frac{S^2 G \mathcal{T}}{k} \tag{12}$$

The ZT is determined in classical electronics by finding the highest induced temperature difference when Joule heating is present, which is caused by an applied electrical current. Assume that the current-carrying conductor is positioned between two heat baths which are $\mathcal{T}_L$ and $\mathcal{T}_R$,and two electrical potentials which are V_L and V_R.

The thermoelectric figure of merit is calculated by determining the maximum induced temperature differential in a conductor due to an electrical current. Using equation 3.14, we may define (Q̇) as the heat gain from bath L to R.

$$\dot{Q} = \Pi\, I - k\Delta\mathcal{T} \tag{13}$$

Heat transfer causes the left bath to cool and the right bath to heat, resulting in an increase in ΔT. The Joule heating amount is proportional to the electrical resistance and the square of the current

and is represented as $\dot{Q}_J = RI^2$. In the steady state case, this Joule heating will also change the temperature difference caused by the heat transfer.

$$\Pi\, I - k\Delta\mathcal{T} = \frac{R\, I^2}{2} \tag{14}$$

whereas R/2 represents the sum of two parallel resistances (internal and external). After reorganising this, the temperature difference is as the following:

$$\Delta\mathcal{T} = \frac{1}{k}\left(\Pi\, I - \frac{R\, I^2}{2}\right) \tag{15}$$

This expression illustrates the dependence of the temperature differential on the current. To obtain the greatest temperature difference, the derivative of equation 17 with respect to the electric current is used:

$$\frac{\partial\Delta\mathcal{T}}{\partial I} = \frac{\Pi - IR}{k} = 0 \tag{16}$$

Lastly, we may find the maximum temperature difference by rewriting I=Π /R and putting equation 12 into equation 18, and we can get:

$$(\Delta\mathcal{T})_{max} = \frac{\Pi^2}{2kR} = \frac{S^2\mathcal{T}^2G}{2k} \tag{17}$$

$$\frac{(\Delta\mathcal{T})_{max}}{\mathcal{T}} = \frac{S^2G\mathcal{T}}{2k} = \frac{1}{2}Z\mathcal{T} \tag{18}$$

A dimensionless number that may be used to express the "efficiency" of a molecular device.